UNIVERSITY OF SOUTHAMPTON

NOVEL RARE-EARTH-DOPED PLANAR WAVEGUIDE LASERS

Tajamal Bhutta

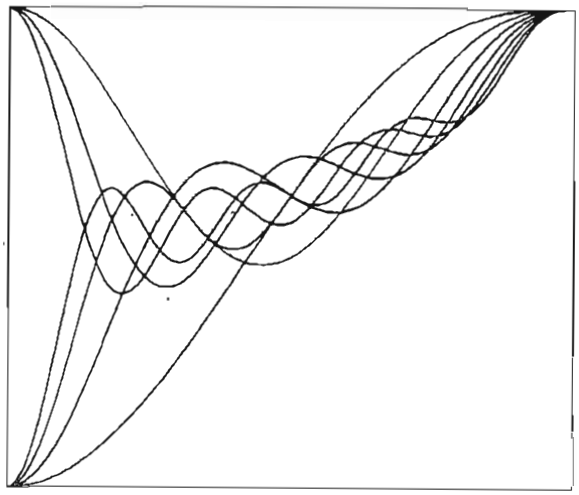

Submitted for the degree of Doctor of Philosophy

FACULTY OF SCIENCE
PHYSICS

September 2002

UNIVERSITY OF SOUTHAMPTON

ABSTRACT

FACULTY OF SCIENCE
PHYSICS

Doctor of Philosophy

NOVEL RARE-EARTH-DOPED PLANAR WAVEGUIDE LASERS

by Tajamal Bhutta

The planar guided-wave geometry is compatible with a wide range of materials, waveguide architectures and fabrication techniques. This thesis reports a series of studies of rare-earth-doped planar waveguide lasers, exploiting and extending the diverse range of possibilities that can be applied to planar technology. The areas investigated include the characterisation of guided-wave lasers produced by novel fabrication techniques, the design and implementation of new channel and planar waveguide structures and the demonstration of compact diode-bar pumped planar waveguide lasers.

Laser operation of buried planar waveguides fabricated by a novel solid-state ion-exchange technique based on direct bonding is reported. The fabrication process allows buried waveguide structures to be fabricated by a single-step process, and the resulting guides are shown to have optical losses of < 0.4 dB/cm. Direct UV writing is utilised to fabricate multiple channel sources on this buried platform, and absorbed pump power thresholds as low as 3 mW are demonstrated. These structures offer a new and versatile route to the large-scale production of low-loss components for glass integrated-optics.

Lanthanum fluoride thin-films fabricated by molecular beam epitaxy are investigated. The first laser action from a dielectric waveguide fabricated by molecular beam epitaxy is demonstrated using Nd-doped LaF_3 thin films grown on CaF_2 substrates. Channel waveguide lasers are designed and fabricated on these thin films by two techniques; ion-beam etching and a novel technique that employs a photo-definable polymer. These structures have a maximum phonon-energy of 380 cm^{-1}, which constitutes the lowest phonon energy dielectric to show laser waveguide emission to date, offering the potential for developing compact mid-infrared sources based on this technology.

The use of planar waveguides for very compact high-power sources is considered. Proximity coupling - the direct coupling of the diode-bar pump radiation is demonstrated for the first time and is used to realise a very compact and rugged laser system. Double-clad planar waveguide structures are utilised for spatial mode-control in the guided axis of the waveguide. To be compatible with planar fabrication techniques, and also due to the desire to retain a compact system, a double-clad design with large multimode core region is used. The theory of fundamental mode selection through confined doping for such structures is developed. This theory is applied to design the first double-clad planar waveguide and diffraction-limited performance in the guided axis is demonstrated from an Yb^{3+} doped device.

"No, Mr Bond; I expect you to die"

Goldfinger

CONTENTS

Chapter 1

INTRODUCTION

1.1 Overview

This thesis describes the results of research into novel rare-earth (RE) doped planar waveguide lasers, and can be divided into three broadly definable areas; RE-doped glass waveguides, fluoride waveguide lasers and planar waveguides for high-power laser operation. This introduction briefly discusses the RE transitions and dielectric materials used in this work, and techniques of waveguide fabrication in these materials. The main body of this thesis is organised in five further chapters. Chapter 2 introduces the basic theory of light propagation in optical waveguides and laser action in RE-doped dielectrics. Chapter 3 reports the investigation of novel buried planar waveguide lasers in borosilicate glass. Buried structures are important for applications in glass integrated-optics because they minimise surface scattering and fibre-optic coupling loss; the characterisation of buried ion-exchanged planar structures fabricated by a new single-step technique based on direct-bonding is reported. Also reported is the laser operation of buried channel waveguide lasers produced on these thin films by direct UV-writing in a step towards developing integrated optical components. Chapter 4 reports the characterisation of lanthanum fluoride crystal thin films; the first dielectric waveguides lasers fabricated by molecular beam epitaxy and the design and fabrication of channel waveguide lasers on these films. These structures constitute the lowest phonon energy dielectric material to show waveguide laser emission to date, and so offer the potential for developing compact mid-infrared waveguide sources. Chapter 5 reports the design and development of high power diode-pumped waveguide lasers. Proximity coupling (the direct coupling of diode-bar pump radiation without any intervening optics) is used to realise a very compact laser system, and the design and demonstration of the first double-clad planar waveguide laser is reported. The final chapter, chapter 6, collectively summarises the experimental work and discusses some current developments and future work.

1.2 RE-doped waveguide lasers

1.2.1 Guided-wave devices

Since the first demonstration of laser action from a RE-doped thin film in the early seventies [1] a great deal of research has centred on the development of planar waveguide lasers. Total internal reflection at the waveguide boundary confines the light so that, unlike free-space resonators, the light does not diverge; thus the cavity mode volume is smaller, and the pump power required to reach threshold is reduced. Waveguides also provide inherently rugged and compact devices that are immune to effects such as cavity misalignment. The benefits of guided-wave geometries have most clearly been demonstrated in glass optical fibres. The very first laser action in glass made use of a multimode fibre [2] consisting of a RE-doped core rod encased in a cladding of lower refractive index, and the optical confinement of the waveguide was used to overcome the poor quality of the glass available at the time. Modern glass silica fibres have exceptionally low propagation losses (0.1 dB/km) and can be designed to only support a single spatial mode at the laser wavelength for diffraction-limited output [3]. The single mode core can be combined with double clad designs and long device lengths to effectively couple high-power diode pump sources, and these devices can now provide over a 100 W of output power in a diffraction-limited beam [4]. More recent has been the development of 'soft glass' technology, in particular fluoride based ZBLAN fibre lasers [5]. These have the advantage that the cut–off for their vibrational spectra is at lower energies than silica and has allowed the development of fibre sources that operate at longer wavelengths in the 2-4 μm region [6-9].

Although planar waveguides devices have not reached the same level of maturity, they are potentially more versatile than optical fibres. The planar geometry can combine the benefits of a guided-wave resonator with a more compact monolithic format that is directly compatible with the techniques and concepts of integrated optics [10-12]. The fabrication techniques for realising these devices are diverse and not limited to just glasses; laser waveguides can be produced using crystals with large non-linear coefficients such as $LiNbO_3$ [13-16] or high gain materials such as Nd:YAG [17-21]. Laser operation of planar waveguides fabricated in Ti-sapphire [22,23] have also recently been reported, which should allow the development of miniature tuneable sources. And, as reported here, fluoride crystal waveguide lasers with lower phonon energies than ZBLAN fibres can be produced in a planar geometry. The advantages of planar waveguides are not limited to the development of low-power integrated optics; the slab geometry is well known to have improved thermal limitations over cylindrical geometries [24,25]. The shape of a planar waveguide is also well suited to the emission of high-power diode-bar pump sources so that simple pump coupling with the minimum of optics can be used, or, as demonstrated here pump delivery can be achieved with no optics whatsoever to realise very compact laser systems suitable for high power operation.

1.2.2 Active materials

The planar waveguide laser devices reported here were produced by fabricating a waveguide in, or from, a RE-doped dielectric material. The RE hosts considered in this work are glass, lanthanum fluoride and the garnets YAG and GGG. The use of glass substrates for integrated optics is of interest for applications such as telecommunications due to their high availability, relatively low cost and their natural refractive index match to silica optical fibres [11]. The key feature of the lanthanum fluoride crystal is the maximum phonon energy of the host (350-400 cm^{-1}) [26], which compares favourably with that of ZBLAN (520 cm^{-1}) and offers the potential for developing planar mid-infrared technology.

Of the oxide garnets [27] YAG has established a place of dominance due to its exceptional mechanical strength, high thermal conductivity, good optical properties and high damage threshold. Consequently, incorporating RE-doped YAG in a waveguide is desirable for the development of high power planar lasers. The garnet GGG is also a well-known laser material and shares many of the properties of YAG. Although YAG has slightly better thermal and optical properties, GGG possesses a higher refractive index. Both garnets share a cubic crystal structure with similar lattice spacing, which allows the two to be combined by epitaxially growing RE-doped GGG thin films on undoped YAG substrates to form planar waveguides suitable for high power operation. Both RE-doped YAG and RE-doped GGG core waveguides are considered.

Much of the work reported in this thesis details the characterisation of the first laser waveguides of their kind. For these initial demonstrations and test of the suitability of these waveguide structures the $^4F_{3/2}$-$^4I_{11/2}$ transition of the neodymium (Nd^{3+}) RE ion is used. The general energy level scheme for Nd^{3+} is shown in figure 1.2.1, each of the free-ion energy states have a host induced stark-splitting, however, the position of these energy levels does not vary much between different hosts due the shielding of the 4f electronic energy states by the outer electrons.

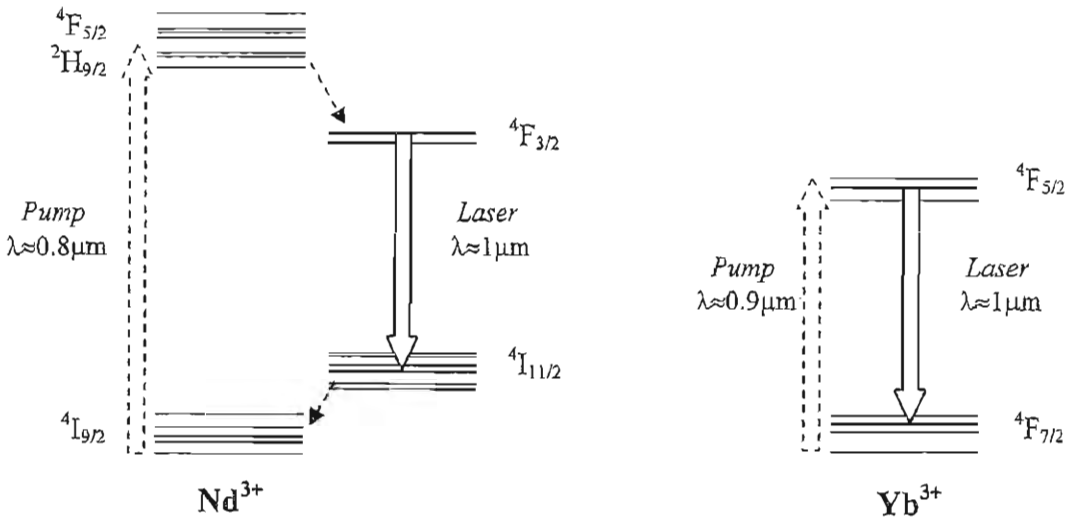

Figure 1.2.1 Schematic representation of RE laser transitions used in this work.

The laser transition is optically pumped at a wavelength around 0.8 μm to a high lying manifold from which it decays non-radiatively to the long-lived $^4F_{3/2}$ manifold. Laser action at a wavelength (λ) of around 1 μm occurs between a stark level of this manifold and one of the $^4I_{11/2}$ manifold. The terminating stark level for the laser transition is high above the ground-state (~2000 cm^{-1}) and so has no thermal population at room temperature. The $^4F_{3/2}$-$^4I_{11/2}$ transition is a four-level system and one that displays high gain in most host materials, making it relatively easy to achieve laser action on. This transition is used for the initial investigation of glass and LaF_3 planar waveguides reported in chapters 3 and 4.

In chapter 5, the $^2F_{5/2}$ -$^2F_{7/2}$ transition of the ytterbium (Yb^{3+}) ion is used for the first demonstration of a double-clad planar waveguide laser. This transition is illustrated in figure 1.2.1 and has attracted interest over the last decade for the development of efficient high power lasers [28,29]. The advantages of this transition derive from the simple electronic energy level structure of the dopant ion. Yb^{3+} has only two active manifolds, the $^2F_{5/2}$ pump manifold, which contains the upper laser level and the $^2F_{7/2}$ ground manifold containing lower laser level. As the lower laser level is thermally populated, the laser transition is quasi-three level leading to an increased threshold when compared to Nd-doped systems. However for high-power operation, the very small energy mismatch between the pump (λ≈0.9μm) and laser photons (λ≈1μm) results in a very efficient system with a low thermal load [30]. The absence of intermediate or higher lying energy levels also means that excited state absorption and concentration dependent ion-ion energy transfer effects that lead to well known concentration quenching in Nd^{3+} systems [31] are not present.

1.3 Waveguide structures and fabrication

1.3.1 Planar waveguides

Planar waveguides can be fabricated by creating a region of high refractive index on a suitable substrate. This can be achieved by either modifying the refractive index of the surface of the planar substrate or by depositing a material of higher refractive index on the substrate surface. Index modification generally results in a gradually varying refractive index profile, whereas thin film deposition is better suited to the production of a more abrupt, step index profile. The basic planar waveguide geometries and refractive index profiles are illustrated in figure 1.3.1. In general, the buried planar geometry is preferred as this minimises scattering loss at the guide-air interface and provides a more symmetric optical mode. The two key parameters in designing laser waveguide structures are the size of the light guiding core and the refractive index difference between this and the substrate. As discussed in chapter 2, these parameters govern the number of propagating modes and their physical size at a given optical wavelength, both of which are critical to the laser performance of such guides. These parameters are also important when coupling pump light into the guide as they govern the physical size and divergence of the pump beam that can be accommodated by the structure. The numerical aperture (NA) and core depth requirements for diode pumping via proximity coupling are discussed in more detail in chapter 5.

The number of techniques that have been demonstrated separately or in combination to fabricate planar waveguides is now vast and continues to grow; the brief discussion here will concentrate on those techniques relevant to the work reported in subsequent chapters

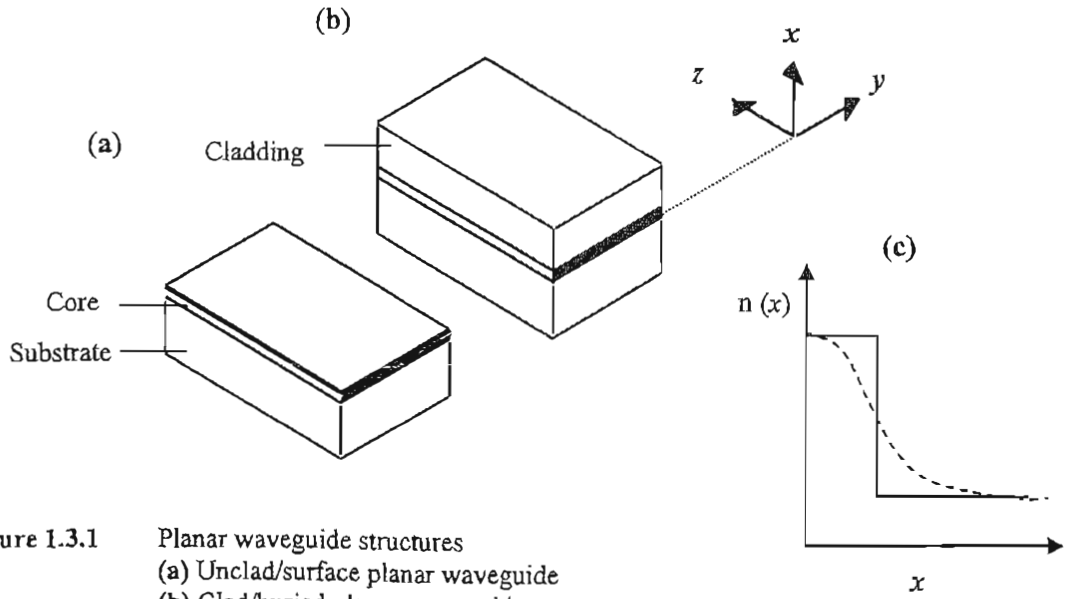

Figure 1.3.1 Planar waveguide structures
(a) Unclad/surface planar waveguide
(b) Clad/buried planar waveguide
(c) Possible refractive index profiles for both surface and buried planar waveguides: step index (solid line) and graded index (dotted line).

Ion-exchange is one of the most widely used waveguide fabrication technique for glasses [11,32,33]. This process relies on replacing an ion in the glass by an ion of larger size or polarisability to locally increase the refractive index. A purely thermal process can be used, or this can be combined with electric fields to give better control over exchange speed and refractive index profile. Typically, the ions are introduced into the glass from a molten salt bath, the apparatus used for the common K^+-Na^+ thermal ion exchange process is illustrated in figure 1.3.2 (a). The glass substrate is submerged in a melt of KNO_3 salt, and the K^+ ions of the molten salt replace the Na^+ in the glass at the substrate surface, locally increasing the refractive index and thus creating a waveguide region. Buried structures can be created by a secondary heat [34], electric field [35] or exchange process [33]. Waveguides fabricated using a novel solid-state source for K^+-Na^+ ion-exchange are investigated in chapter 3.

Similar chemical surface treatments have been applied to some crystals. Proton exchange is a classic technique for lithium niobate integrated optics [13,14]. Waveguides have also been fabricated in lithium niobate by indiffusion [15,16], a process where metal ions evaporated onto the substrate surface are diffused into the substrate using a heat treatment. Recently, indiffusion has also been used to incorporate titanium into sapphire substrates to fabricate Ti-sapphire waveguide lasers [22]. These chemical surface treatments, however, are not generally applicable to all crystals, and have not as yet been used successfully for garnets such as YAG and GGG. The technique of ion-implantation is certainly a more generally applicable process of index modification. This method uses high-energy ions to bombard the planar substrate to create sub-surface damage, and has been applied to a variety of glasses [36] and crystals, including garnets [17,37], to fabricate waveguides. Unfortunately, the propagation losses of these structures are quite high (typically >1dB/cm), which compromises their use as lasers.

The most common technique for planar waveguide fabrication for crystal YAG and GGG is epitaxial thin film growth. Several techniques exist for the epitaxial deposition. The thin-film growth of garnet crystals by liquid phase epitaxy (LPE), growth from supersaturated solutions, has been studied for a number of decades and has proved particularly effective for the production of YAG and GGG devices [1,19]. The optical losses of current LPE RE-doped YAG on YAG guides is 0.05 dB/cm, which is very close to the value of the scattering loss of bulk crystals, and an NA of 0.2 has been achieved by incorporating Ga ions into the active layer to increase refractive index [18]. More recently, LPE has also been extended to the growth of other materials [19] including the first fluoride (Nd:YLF) crystal laser [38]. LPE remains a relatively cheap technique for the production of these crystal devices, however the growth of new systems is limited by the need to find suitable flux constituents for the growth solution. Waveguide engineering is also restricted as LPE provides poor control over the morphology of very thin layers and the NA achievable with homo-epitaxial deposition is limited. For higher NAs, techniques that are capable of combining different active layer and substrate materials are required.

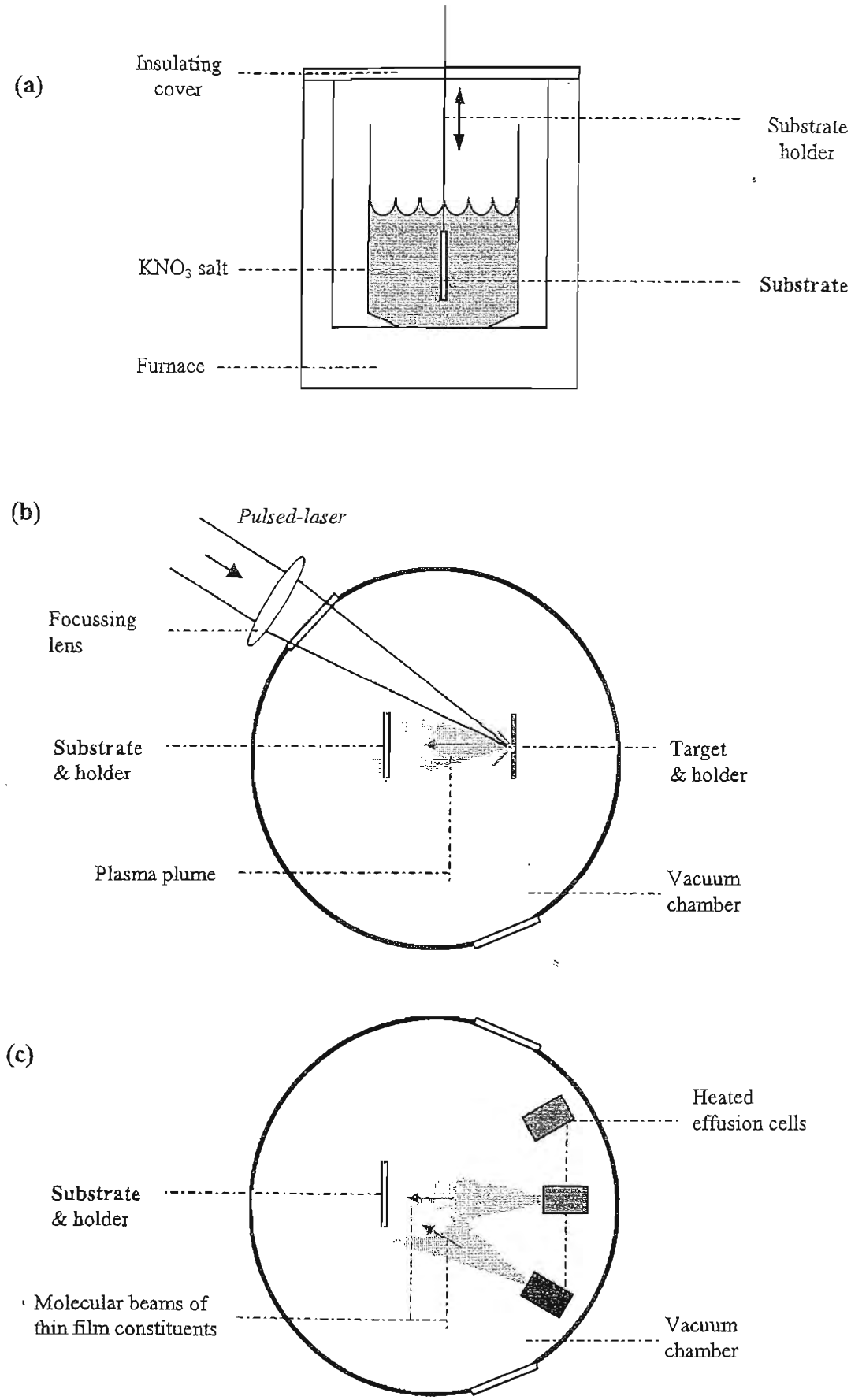

Figure 1.3.2 Examples of planar waveguide fabrication techniques
(a) Thermal ion exchange (b) Pulsed-laser assisted deposition (c) Molecular beam epitaxy

Deposition from vapour sources is inherently better suited to accurate process control; source switching and shuttering can be applied while the growth can be monitored and optimised throughout the deposition. The two techniques considered in this work are pulsed-laser-assisted deposition and molecular beam epitaxy. Both are suitable for the deposition of very thin layers (<10 μm) and hetero-epitaxial growth for high NAs.

Pulsed-laser-assisted deposition (PLD) is a particularly attractive technique; it combines accurate control with exceptionally quick deposition times and inexpensive hardware. The basic elements of the apparatus used to fabricate waveguides by PLD are illustrated in figure 1.3.2(b). The pulsed-laser is used to ablate the target material, which is then deposited as a thin film on the substrate. This technique has recently been applied to the growth of RE-doped GGG on YAG to form high NA (0.75) waveguides with optical losses as low as 0.5 dB/cm [39,40] and also low-loss Ti-sapphire waveguide lasers [23]. PLD has one major drawback; the formation of macroscopic particles in the grown layer. These particulates are, at least in part, due to imperfect ablation of the target material [41], and the effect of particulate density on device performance for Nd:GGG/YAG waveguides is discussed in chapter 5.

Molecular beam epitaxy (MBE), in which growth is carried out in ultra-high vacuum (UHV) using thermally generated molecular beams, provides exceptional control over the grown layer. An MBE growth system is shown schematically in figure 1.3.2(c). A large number of cells can be used to deposit the constituents of the growing film, which, for example, allows separate cells to be used to generate the RE-dopant and dielectric-host molecular beams, so that the doping level can easily be controlled by varying the relative molecular beam fluxes. The thin-film deposition can be monitored throughout the growth by x-ray diffraction techniques, and slow deposition rates can be used to provide mono-atomic control over the growing layer. Although the need for strict process control and UHV makes the hardware expensive, MBE allows exceptional waveguide engineering on the atomic scale, as demonstrated by the success of MBE semiconductor quantum well lasers. The fabrication of dielectric devices by MBE is however still in its infancy. MBE is best suited to the fabrication of fluoride rather than oxide dielectrics, as these have higher energies for molecule dissociation [42]. A number of groups have studied the growth of RE-doped fluoride thin films [43-46], RE-doped ZnF_2, PbF_2, CaF_2, and LaF_3 have all been grown with various substrate materials, including GaAs and Si, however no laser action had been reported. The first laser action from dielectric waveguide devices fabricated by MBE is reported in chapter 4.

Evidently there is a desire to develop more generally applicable techniques that do not require a lattice-match. Direct bonding (also referred to as optical or thermal bonding) has emerged as a particularly versatile technique, involving simply contacting of surfaces that have been polished to an optical finish and then chemically cleaned. In the low temperature version of this process, Van der Waals forces hold the surfaces together, and chemically and structurally dissimilar materials can be bonded, provided the thermal expansion co-efficients of the substrate and waveguide layers are

compatible. Once bonded, the bond is strong enough to allow mechanical thinning of the active layer by polishing, and buried structures can then be constructed in a second bonding step. Composite direct-bonded waveguides have exactly the same spectral properties as the original bulk crystals, optical losses are as low as 0.2 dB/cm [21] and demonstrated NAs range from 0.06 (Nd:YAG/YAG) to 0.8 (Nd:YAG/glass) [20]. Although the process is labour intensive, the versatility of the direct bonding process is unmatched by epitaxial techniques and this is the technique used for the fabrication of the high power YAG/sapphire waveguides (NA=0.46) reported in chapter 5. Direct bonding is also an integral part of the new ion-exchange process used to fabricate the glass waveguides reported in chapter 3.

1.3.2 Channel waveguides

Channel waveguides structures are the basic components of low-power integrated optics and allow the production of multiple sources on a single planar substrate. The lateral confinement of the laser and pump radiation can also markedly reduce laser threshold and provides an optical mode better suited to coupling to fibre-optic components. Channel waveguide structures can be created by selectively processing a small area of a planar substrate. The most widely used techniques rely on photo-lithographic pattern transfer, in which a master pattern is defined in a sacrificial imaging layer (resist) by exposure to UV light through a contact printing mask. Development of the photo-resist leaves a mask on the thin film, which can be combined with deposition, etching or index modification processes to transfer the pattern into the waveguide material.

Channel waveguides can be formed directly on a planar substrate by an index modification process combined with photolithographic masking. For example, ion-exchange glass channels can be fabricated by depositing an aluminium thin film on the substrate, which is then etched through a negative relief of the channel created by photolithography to leave a negative metal mask [11]. By placing the prepared substrate in the melt of KNO_3 salt, ion exchange only occurs in the exposed regions of the substrate and thus a channel waveguide is created. Indiffused channels can be fabricated by creating a photo-resist mask prior to depositing the metal to be diffused; the metal is thus only deposited on the exposed regions of the substrate providing a patterned source for indiffusion resulting in a channel as opposed to planar structure. These processes generally result in a graded-index channel of the type shown schematically in figure 1.3.3(a). However, the limited applicability of index modification process to crystals means that alternative techniques are required for many applications, in which a thin film slab waveguide is formed first and then is structured. The rib waveguide (figure 1.33(b)) can be defined by applying a photo-resist mask to an unclad thin film and then etching using an ion beam [47].

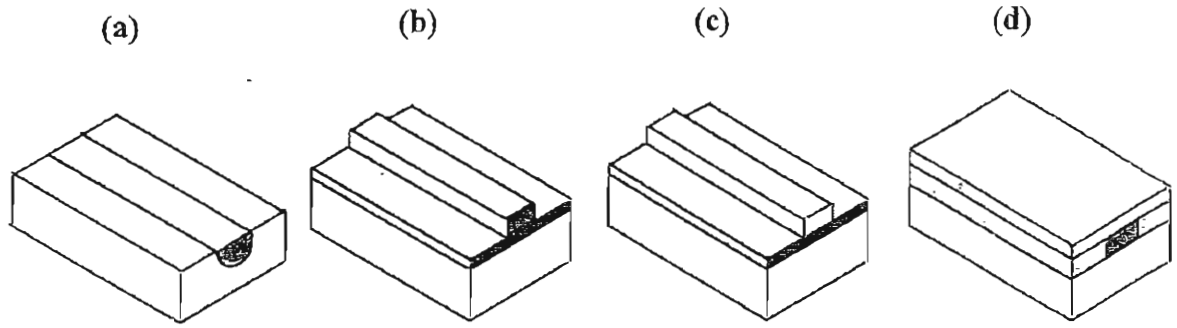

Figure 1.3.3 Examples of channel waveguide structures
(a) Ion-exchange/Indiffused channel (b) Rib Channel
(c) Slab-loaded channel (d) Buried channel (e.g UV writing)

It is, however, not always necessary to structure the core layer directly, the channel pattern can be formed in a clad waveguide by structuring the top layer to produce a loading slab as illustrated in figure 1.3.3(c). Slab-loaded structures provide lateral confinement of the thin film mode by interaction with the evanescent field, and so provide a non-invasive technique for confining optical radiation, which is useful for core materials that may be susceptible to etch-damage. Slab-loaded structures also add a greater degree of versatility; the cladding material can be amorphous and can be chosen with respect to how easy it is to process. These types of structures are investigated in chapter 4 and a particularly versatile technique based on a photosensitive BCB polymer stripe-cladding that can be processed using photolithographic techniques alone is developed.

A new technique for channel waveguide fabrication that does not rely on the inflexible technology of photo-lithographic masking is direct UV writing [48]. This process can be applied to photosensitive glasses (usually those that contain germanium) in which a focussed UV laser beam is used to induce a refractive index change. The beam can be focussed through a cladding layer to produce buried channel waveguides such as the one illustrated in figure 1.3.3 (d), and virtually any waveguide pattern can be written using computer control [49]. This technique has many desirable features; the ability to produce buried structures, flexibility, and compatibility with automated waveguide fabrication. UV written channels in borosilicate glass are investigated in chapter 3.

1.4 References

[1] J.P. Ziel, W.A. Bonner, L. Kopf & L. Uitert, *"Coherent emission from Ho^{3+} ions in epitaxially grown thin film aluminium garnet thin films"*, Physics Letters, Vol. 42A, No. 1, p. 105-106, (1972).

[2] E. Snitzer, *"Optical maser action of Nd^{3+} in barium crown glass"*, Physical Review Letters, Vol. 7, No. 12, p. 444-446, (1961).

[3] D. Richardson, J. Minelly & D.C. Hanna, *"Fiber laser systems shine brightly"*, Laser Focus World, September 1997, p. 87-95, (1997).

[4] V. Dominic, S. MacCormack, R. Waarts, S. Sanders, S. Bicknese, R. Dohle, E. Wolak, P.S. Yeh & E. Zucker, *"110W fibre laser"*, Electronic Letters, Vol. 35, p. 1158-1160, (1999).

[5] P. France, *"Optical properties and applications"* in "*Flouride glasses*", A.E. Comyns (Ed.), John Wiley & Sons, (1989).

[6] J. Schneider, C. Carbonnier & U.B. Unrau, *"Characterisation of a Ho^{3+}-doped fluoride fibre laser with a 3.9μm emission wavelength"*, Applied Optics, Vol. 36, p. 85-95, (1997).

[7] B. Srinvasan, J. Tafoya, & R.K. Jain, *"High-power 'Watt-level' cw operation of diode-pumped 2.7μm lasers using efficient cross-relaxation and energy transfer mechanisms"*, Optics Express, Vol. 4, p. 493 (1999).

[8] S.D. Jackson, *"8.8 W diode-cladding-pumped Tm^{3+}, Ho^{3+}-doped fluoride fibre laser"*, Electronics Letters, Vol. 37, No. 13, p. 821-822, (2001).

[9] M. Pollnau & S.D. Jackson, "*Erbium 3-μm fiber lasers*", IEEE J. of Quantum Electronics, Vol. 7, No. 1, p. 30-40, (2001).

[10] P.K. Tien, *"Integrated optics and new wave phenomena in optical waveguides"*, Reviews of Modern Physics, Vol. 49, No. 2, p. 361-420, (1977).

[11] S.I. Najafi, *"Introduction to glass integrated optics"*, Artech House, (1992).

[12] R. Hunsperger, *"Integrated Optics: theory and technology"*, 4th edition, Springer-Verlag, (1995).

[13] J.L. Jackel, C. Rice & J. Veselka, *"Proton exchange for high-index waveguides in $LiNbO_3$"*, Applied Physics Letters, Vol. 41, No. 7, p. 607-608, (1982).

[14] D. Lee, *"Waveguide fabrication"*, Chapter 7 of *"Electromagnetic principles of integrated optics"*, Wiley; (1986).

[15] M. Hempstead, J.S. Wilkinson & L. Reekie, *"Waveguide lasers operating at 1084 nm in neodymium-diffused lithium niobate"*, IEEE Photonics Technology Letters, Vol. 4, No. 8, p. 852-855, (1992).

[16] R. Brinkman, W. Sohler & H. Suche, *" Continous-wave Erbium diffused $LiNbO_3$ wave-guide laser"*, Electronic Letters, Vol. 27, No. 5, p. 415-417, (1991).

[17] P.J. Chandler, S.J. Field, D.C. Hanna, D.P. Shepherd, P.D. Townsend, A.C. Tropper & L. Zhang, *"An Ion-Implanted Nd:YAG Planar waveguide Laser"*, Electronic Letters, Vol. 25, No. 15, p. 985-986, (1989).

[18] D.C. Hanna, A.C. Large, D.P. Shepherd, A.C. Tropper, I. Chartier, B. Ferrand, & D. Pelenc, *"Low Threshold quasi-three-level 946nm laser operation of an epitaxially grown Nd:YAG waveguide"*, Applied Physics Letters, Vol. 63, p.7-9, (1993).

[19] B. Ferrand, B. Chanbaz & M. Couchaud, *"Liquid phase epitaxy: A versatile technique for the development of miniature optical components in single crystal dielectric media"*, Optical Materials, Vol. 11, p. 101-114, (1999).

[20] C.T.A. Brown, C.L. Bonner, T.J. Warburton, D.P. Shepherd, A.C. Tropper, & D.C. Hanna, *"Thermally bonded planar waveguide lasers"*, Applied Physics Letters, Vol. 71, No. 9, p. 1139-1141, (1997).

[21] D.P. Shepherd, C.L. Bonner, C.T.A. Brown, W.A. Clarkson, A.C. Tropper, D.C. Hanna & H.E. Meissner, *"High-numerical-aperture, contact-bonded, planar waveguides for diode-bar-pumped lasers"*, Optics Communications, Vol. 160, p. 47-50, (1999).

[22] L.M.B. Hickey, A.A. Anderson & J.S. Wilkinson, *"Ti:sapphire channel waveguide laser by thermal diffusion of titanium into sapphire"*, ECIO '97, Stockholm Sweden 2-4 Apr PD6, (1997).

[23] A.A. Anderson, R.W. Eason, L.M.B. Hickey, M. Jelínek, C. Grivas, D.S. Gill, & N.A. Vainos, *"A Ti:sapphire planar waveguide laser grown by pulsed laser deposition"*, Optics Letters, Vol. 22, No. 20, p. 1556-1558, (1997).

[24] J.M. Eggleston, T.J. Kane, K. Kuhn, J. Unternahrer, & R.L. Byer, *"The slab geometry laser – part 1: theory"*, IEEE J. of Quantum Electronics, Vol. QE-20, p. 289-301, (1984).

[25] D.P. Shepherd, S.J. Hettrick, C. Li, J.I. Mackenzie, R.J. Beach, S.C. Mitchell & H.E. Meissner, *"High-power planar dielectric waveguide lasers"*, J. of Physics D: Applied Physics, Vol. 34, p. 2420-2432, (2001).

[26] W.M. Yen, W.C. Scott & A.L. Schawlow, *"Phonon-induced Relaxation in exited states of Trivalent Praseodymium in LaF_3"*, Physics Review, Vol. 136, No. 1A, p. A271, (1964).

[27] W. Koechnar, *"Properties of solid-state materials"*, Chapter 2 of *" Solid-state laser engineering"*, 4th edition, Springer-Verlag, (1996).

[28] P. Lacovara, H.K. Choi, C.A. Wang, R.L. Aggarwal & T.Y. Fan, *"Room temperature diode-pumped Yb:YAG laser"*, Optics Letters, Vol. 16, No. 14, p. 1089-1091, (1991).

[29] D. Sumida, A. Betin, H. Bruesselbach, R. Byren, S. Mathews, R. Reeder & M. Mangir, *" Diode-pumped Yb:YAG catches up with Nd:YAG"* Laser Focus World, June 1999, p. 63-70, (1999).

[30] T.Y. Fan, *"Heat generation in Nd:YAG and Yb:YAG"*, IEEE J. of Quantum Electronics, Vol. 29 , No. 6, p. 1457-1459, (1993).

[31] V. Lupie, A. Lupei, S. Georgescu & C. Ionescu, *"Energy transfer between Nd ions in YAG"*, Optics Communications, Vol. 60, No. 1-2, p. 59-63, (1986).

[32] R.V. Ramaswamy & R. Srivastava, *"Ion-exchanged glass waveguides: a review"*, J. of Lightwave Technology, Vol. 6, No. 6, p. 984-1002, (1988).

[33] N.V. Nikonorov & G.T. Petrovskii, *"Ion-exchange glasses in integrated optics; the current state of research and prospects (a review)"*, Glass Physics and Chemistry, Vol. 25, No. 1, p.16-55, (1999).

[34] T.G. Giallorenzi, E.J. West, R. Kirk, R. Ginther, & R.A. Andrews, *"Optical waveguides formed by thermal migration of ions in glass"*, Applied Optics, Vol. 12, No. 6, p. 1240-1245, (1973).

[35] P.G. Noutsios & G.L. Yip, *"Characterisation and modelling of planar surface and buried glass waveguides made by field-assisted K^+ ion exchange"*, Applied Optics, Vol. 31, No. 25, p. 5283-5291, (1992).

[36] D.P. Shepherd, D.J. Brinck, J. Wang, A.C. Tropper, D.C. Hanna, G. Kakarantzas & P.D. Townsend, *"1.9μm operation of a Tm:Lead germanate glass waveguide laser"*, Optics Letters, Vol. 19, p. 954-956, (1994).

[37] S.J. Field, D.C. Hanna, A.C. Large, D.P. Shepherd, A.C. Tropper, P.J. Chandler, P.D. Townsend & L. Zhang, *"An efficient, diode-pumping, ion-implanted Nd:GGG Planar waveguide laser"*, Optics Communications, Vol. 86, No. 2, p. 161-166, (1991).

[38] P. Rogin & J. Hulliger, *"Epitaxial Nd:YLF linear waveguide laser"*, Optics Letters, Vol. 22, p. 1701 (1997).

[39] D.S. Gill, R.W. Eason, J. Mendiola & P.J. Chandler, *"Growth of crystalline $Gd_3Ga_5O_{12}$ thin-film optical waveguides by pulsed laser deposition"*, Materials Letters, Vol. 25, p. 1-4, (1995).

[40] A.A. Anderson, C.L. Bonner, D.P. Shepherd, R.W. Eason, C. Grivas, D.S. Gill & N. Vainos, *"Low loss (0.5 dB/cm) Nd:$Gd_3Ga_5O_{12}$ waveguide layers grown by pulsed laser deposition"*, Optics Communications, Vol. 144, p. 183-186, (1997).

[41] S.J. Barrington, T. Bhutta, D.P. Shepherd & R.W. Eason, *"The effect of particulate density on performance of Nd:$Gd_3Ga_5O_{12}$ waveguide lasers grown by pulsed laser deposition"*, Optics Communications, Vol. 185, p. 145-152, (2000).

[42] T. Bhutta, A.M. Chardon, D.P. Shepherd, E. Daran, C. Serrano & A. Munoz-Yague *"Low phonon energy Nd:LaF_3 channel waveguide lasers fabricated by molecular beam epitaxy"*, IEEE J. of Quantum Electronics, Vol. 37, No. 11, p. 1469-1477, (2001).

[43] L.E. Bausa, C. Fontaine, E. Daran, & A. Munoz-Yague, *"Molecular beam epitaxy of Nd-doped CaF_2 and $CaSrF_2$ layers on Si and GaAs substrates"*, J. of Applied Physics, Vol. 72, p. 499-503, (1992).

[44] R.A. McFarlane, M. Lui, & D.Yap, *"Rare earth doped fluoride waveguides fabricated using molecular beam epitaxy"*, IEEE J. of Select. Topics Quantum Electronics, Vol. 1, No. 1, p. 82-91, (1995).

[45] J.M. Ko & T. Fukuda, *"Molecular beam epitaxy of $Ca_{1-x}R_xF_{2+x}$ (R=Nd,Er) layers: study of RHEED pattern and lattice mismatch"*, J. of Crystal Growth, Vol. 200, p. 490, (1999).

[46] E. Daran, D.P. Shepherd, T. Bhutta, & C. Serrano, *"Laser operation of Nd:LaF_3 thin film grown by molecular beam epitaxy"*, Electronic Letters, Vol. 35, No. 5, p. 398 (1999).

[47] R. Gerhardt, J. Kleine-Borger, L. Beilschmidt, M. Frommeyer, H. Dotsch, & B. Gather, *"Efficient channel-waveguide laser in Nd:GGG at 1.062μm wavelength,"* Applied Physics Letters, Vol. 75, p. 1210-1212, (1999).

[48] M. Svalgaard, C.V. Poulsen, A. Bjarklev, & O. Poulsen, *"Direct UV writing of buried singlemode channel waveguides in Ge-doped silica films"*, Electronics Letters, Vol. 30, No. 17, p. 1401-1403, (1994).

[49] M. Svalgaard, *"Optical waveguides and gratings made by UV-photogeneration"*, ECIO, p. 333-338, (1999).

Chapter 2

ELEMENTS OF LASER WAVEGUIDE THEORY

2.1 Introduction

This chapter describes the underlying theory of RE-doped dielectric planar waveguide lasers. Several textbooks give a detailed account of optical modes in waveguide geometries, for example Lee (1986)[1] or Snyder and Love (1983)[2], and only the simplest case of a symmetric three-layer dielectric slab is examined here. This theory is applicable to the crystal thin-film structures reported in the subsequent chapters and the straightforward analysis and analytical solutions that this geometry affords also offer good insight into the behaviour of the optical modes for more complex index profiles that require numerical analysis, such as the graded-index guides of chapter 3 and slab loaded channels of chapter 4. The theory is then extended to five layer symmetric slab structures in appendix A to calculate the optical modes of the waveguide structures reported in chapter 5.

Section 2.3 introduces the quasi-three level model of laser action developed by Fan [3] and Risk [4]. This model is based on a rate equation approach, in which the spatial variation of the waveguide modes is accounted for, and is applicable to Yb and Nd transitions reported in this work. The analysis is applied to end-pumped waveguides lasers in section 2.3.3 to derive approximate expressions for threshold and slope efficiency that are used throughout this work to characterise planar and channel waveguides. This analysis is also the basis for the theory and modelling of gain saturation and mode selection developed in chapter 5.

2.2 Waveguide modes

2.2.1 Review of electromagnetic theory

To determine characteristics of the optical fields in planar dielectric waveguides, we consider Maxwell's equations for a loss-less, isotropic charge-free medium. These have the following form in terms of the electric (**E**) and magnetic (**H**) field vectors.

$$\nabla \wedge \mathbf{E} = -\mu \frac{\partial}{\partial t}\mathbf{H} \qquad [2.2.1]$$

$$\nabla \wedge \mathbf{H} = \varepsilon \frac{\partial}{\partial t}\mathbf{E} \qquad [2.2.2]$$

$$\nabla . \mathbf{E} = 0 \qquad [2.2.3]$$

$$\nabla . \mathbf{H} = 0 \qquad [2.2.4]$$

Where ∇ is the spatial vector operator $\nabla = \frac{\partial}{\partial x}\hat{\mathbf{x}} + \frac{\partial}{\partial y}\hat{\mathbf{y}} + \frac{\partial}{\partial z}\hat{\mathbf{z}}$, $\frac{\partial}{\partial t}$ is the differential with respect to time and, ε and μ, are the electric permittivity and magnetic permeability respectively. Maxwell's equations can be expressed in terms of just the **E** field by taking the curl of equation 2.2.1 and using the vector identity $\nabla \wedge (\nabla \wedge \mathbf{U}) = \nabla(\nabla . \mathbf{U}) - \nabla^2 \mathbf{U}$ (for any vector **U**) to produce the homogenous wave equation.

$$\nabla^2 \mathbf{E} + \varepsilon\mu \frac{\partial^2}{\partial t^2}\mathbf{E} = 0 \qquad (\nabla^2 \mathbf{H} + \varepsilon\mu \frac{\partial^2}{\partial t^2}\mathbf{H} = 0) \qquad [2.2.5a(b)]$$

(the wave equation in terms of **H** is generated by applying the same procedure to 2.2.2). For an electromagnetic wave travelling in the $+z$ direction with propagation constant β and angular frequency ω the wave equations have general solutions [5].

$$\mathbf{E} = (E_x(x,y)\,\hat{\mathbf{x}} + E_y(x,y)\,\hat{\mathbf{y}} + E_z(x,y)\,\hat{\mathbf{z}})e^{i(\omega t - \beta z)} \qquad [2.2.6a]$$

$$\mathbf{H} = (H_x(x,y)\,\hat{\mathbf{x}} + H_y(x,y)\,\hat{\mathbf{y}} + H_z(x,y)\,\hat{\mathbf{z}})e^{i(\omega t - \beta z)} \qquad [2.2.6b]$$

($\hat{\mathbf{x}}, \hat{\mathbf{y}}$ and $\hat{\mathbf{z}}$ being the unit vectors in the respective Cartesian co-ordinate directions)

The values of $E_{x,y,z}$ and $H_{x,y,z}$ have to be determined by finding the field solutions that are continuous across the boundaries of the waveguide structure. This analysis can be simplified by noting the high degree of symmetry of Maxwell's equations, if the substitutions -**H** for **E**, **E** for **H** are made and μ and ε are interchanged, we generate exactly the same set of equations [1]. Consequently by solving for one set of fields we can generate a second set of solutions by making these changes, and use of this fact is made in the following analysis.

2.2.2 Guided modes of symmetric planar waveguides

A planar waveguide is characterised by parallel planar boundaries with respect to one (x) direction, and is assumed to extend infinitely in lateral directions (y and z). The structure depicted below in figure 2.2.1 is considered, with core of depth D and refractive index n_2 and cladding and substrates with indices n_1, with $n_2 > n_1$ for guided wave propagation. This three-layer symmetric step index waveguide has uniform refractive index except for the abrupt discontinuity at $x = \pm D/2$. Using equations 2.2.6 for **E** and **H** in Maxwell's curl equations (2.2.1 and 2.2.2) and noting that for this structure $\partial/\partial y = 0$, reveals the two polarisation states for these structures- transverse electric, TE, ($E_z=0$, $H_z \neq 0$), or transverse magnetic, TM, ($H_z=0$, $E_z \neq 0$), and their non-zero field components (listed below).

	TE modes field components	*TM modes field components*
(i)	E_y	H_y
(ii)	$H_x = -\frac{\beta}{\omega\mu} E_y$	$E_x = \frac{\beta}{\omega\varepsilon} E_y$
(iii)	$H_z = -\frac{1}{i\omega\mu}\frac{\partial E_y}{\partial x}$	$E_z = \frac{1}{i\omega\varepsilon}\frac{\partial H_y}{\partial x}$
	[2.2.7a]	[2.2.7b]

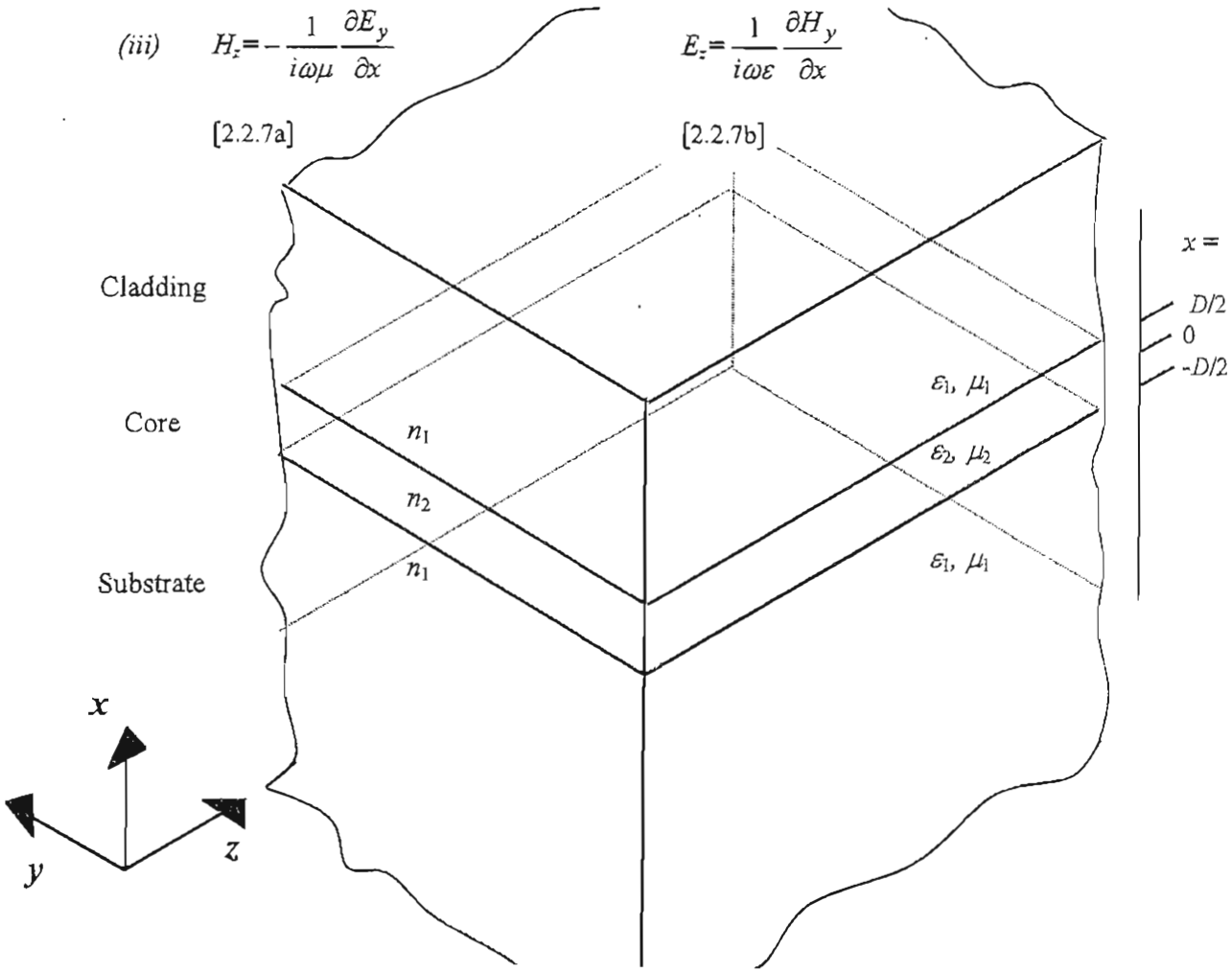

Figure 2.2.1- Three-layer symmetric dielectric slab waveguide

The conditions for $\mathbf{E}$ and $\mathbf{H}$ to be continuous across the waveguide boundaries for TE and the TM modes are different, and so each have to be considered separately. Starting with TE modes ($E_x=0$, $E_z=0$) we can write the electric field as

$$\mathbf{E}= E_y(x)e^{i(\omega t-\beta z)}\,\hat{\mathbf{y}} \qquad TE\ modes \qquad [2.2.8]$$

For guided modes the fields are expected to decay for $|x|>D/2$ (in the cladding or substrate) and to be oscillatory for $|x|<D/2$ (the core). The symmetry of the structure suggests that the field decay will be the same for substrate and cladding, and also that the modes will either be symmetric or anti-symmetric (even or odd) with respect to $x=0$, so solutions of the following form for the transverse variation of the electric field are assumed [1]

$$E_y(x)= E_{yo}\begin{bmatrix} Ae^{-\alpha x} & & x>D/2 \\ \begin{pmatrix}\cos(\kappa x)\\ \sin(\kappa x)\end{pmatrix} & \begin{matrix}even\\ odd\end{matrix} & -D/2<x>D/2 \\ \pm Ae^{\alpha x} & & x<-D/2 \end{bmatrix} \qquad [2.2.9]$$

E_{yo} is the maximum electric field amplitude, A is a relative amplitude coefficient for the substrate and cladding, κ is the transverse wavenumber for the core and α is the decay constant for the cladding and substrate. For 2.2.9 to satisfy the wave equation in the respective layers α and κ have to obey the following relationships.

$$\alpha^2=\beta^2-\omega^2\mu_1\varepsilon_1, \qquad \kappa^2=\omega^2\mu_2\varepsilon_2-\beta^2 \qquad [2.2.10a, b]$$

These can be combined in a single condition by noting that β, the longitudinal wavenumber, must be a constant for a given mode. So it follows that

$$\kappa^2+\alpha^2=\omega^2(\mu_2\varepsilon_2-\mu_1\varepsilon_1) \qquad wavenumber\ condition \qquad [2.2.11]$$

To determine the allowed optical modes we apply the condition that $\mathbf{E}$ and $\mathbf{H}$ must be continuous across the boundaries $x = \pm D/2$. We consider the two tangential components of the fields as this automatically satisfies the condition for the longitudinal component through Maxwell's equations. For a TE mode the tangential components are E_y and H_z (2.2.7a) and for our symmetric structure the boundary conditions at $x = D/2$ is the same as that at $x = -D/2$. Matching boundary conditions yields, for even solutions, for example

$$Ae^{-\alpha D/2} = \cos(\kappa D/2) \qquad [2.2.12]$$

For H_z we use 2.2.7 (a iii), and again consider $x = D/2$, resulting in

$$\frac{1}{\mu_1}\alpha Ae^{-\alpha D/2} = \frac{\kappa}{\mu_2}\sin(\kappa D/2) \qquad [2.2.13]$$

Taking the ratio of 2.2.12 and 2.2.13 eliminates the unknown A, and we are left with the following transcendental equation for the even modes.

$$\frac{\mu_2\alpha}{\mu_1\kappa} = \tan(\kappa D/2) \qquad \textit{TE even mode condition} \qquad [2.2.14]$$

Doing the same for the odd modes gives

$$\frac{\mu_2\alpha}{\mu_1\kappa} = \cot(\kappa D/2) \qquad \textit{TE odd mode condition} \qquad [2.2.15]$$

These two equations are often called the guidance conditions, and by graphically or numerically solving them in conjunction with 2.2.11 for a given waveguide structure, the allowed values of α and κ can be determined. Once these values have been determined they can be substituted into 2.2.12 to determine the relative amplitude coefficient A for the cladding and substrate, and substituted into 2.2.9 to determine the mode profile. In general there is more than one solution for both guidance conditions, each solution of 2.2.14 contributes to the total number of even modes and each solution of 2.2.15 to the total number of odd modes. The solutions are usually labelled as TE_m with m=0, 2, 4 for even modes and m=1, 3, 5 for the odd modes.

For TM modes the procedure of the analysis exactly parallels the one for the TE modes (2.2.8 to 2.2.16), except that we use 2.2.7 b for the field components. However rather than go through the whole procedure again we can make use of duality to generate the guidance condition for TM modes (interchanging ε for μ in 2.2.14 and 2.2.15)

$$\frac{\varepsilon_2\alpha}{\varepsilon_1\kappa} = \tan(\kappa D/2) \qquad \textit{TM even mode condition} \qquad [2.2.16]$$

$$\frac{\varepsilon_2\alpha}{\varepsilon_1\kappa} = \cot(\kappa D/2) \qquad \textit{TM odd mode condition} \qquad [2.2.17]$$

With the transverse TM field components being the counterparts of 2.2.8 and 2.2.9, such that

$$H_y(x) = H_{yo}\begin{bmatrix} Ae^{-\alpha x} & & x > D/2 \\ \begin{pmatrix}\cos(\kappa x)\\ \sin(\kappa x)\end{pmatrix} & \begin{matrix}even\\ odd\end{matrix} & -D/2 < x > D/2 \\ \pm Ae^{\alpha x} & & x < -D/2 \end{bmatrix} \qquad [2.2.18]$$

2.2.3 Properties of optical modes in laser waveguides

It is useful to recast the wavenumber, TE and TM guidance conditions in terms of the layer refractive index (n) and free space wavelength (λ_0) to discuss optical modes in terms of the properties of the waveguide laser. At optical wavelengths the magnetic permeability differs negligibly from its free space value (μ_0) and so we can set $\mu_1 = \mu_2 = \mu_0$, and by using the relations $\lambda_0 = 2\pi/\omega\sqrt{\varepsilon_o\mu_o}$ and $n = \sqrt{\varepsilon/\varepsilon_o}$ (ε_0 being the electric permittivity of free space) equations 2.2.11, and 2.2.14 to 2.2.17 become

$$\kappa^2 + \alpha^2 = \frac{2\pi}{\lambda_0}(n_2^2 - n_1^2) \qquad \textit{wavenumber condition} \qquad [2.2.19]$$

$$\frac{\alpha}{\kappa} = \tan(\kappa D/2) \qquad \frac{\alpha}{\kappa} = \cot(\kappa D/2) \qquad \textit{TE conditions} \qquad [2.2.20\ a\ \&\ b]$$

$$\frac{n_2^2\alpha}{n_1^2\kappa} = \tan(\kappa D/2) \qquad \frac{n_2^2\alpha}{n_1^2\kappa} = \cot(\kappa D/2) \qquad \textit{TM conditions} \qquad [2.2.21\ a\ \&\ b]$$

These forms of the mode conditions illustrate the important scaling factors that govern the transverse profiles of the modes in laser waveguides; the core depth, the optical wavelength and numerical aperture NA=$\sqrt{n_2^2 - n_1^2}$. In general, equations 2.2.19 to 2.2.21 have to be solved for a particular waveguide structure, however, it is worth examining a few solutions to illustrate some general properties important to laser design. Figure 2.2.2 shows how the TE mode intensity changes for the fundamental mode (m=0), and first even (m=1) mode with decreasing NA, for λ_0 = 1 μm and D = 3 μm. We could equally fix NA and decrease D, or fix both D and NA and increase λ_0 to achieve similar mode behaviour [1]. The profiles are normalised so that each contains the same total power.

For a high NA all the modes are well confined, with high intensities in the core and very little penetration into the cladding or substrate. As the NA is decreased the modes extend further and further into the cladding until the mode can no longer be supported by the structure or is 'cut-off' (true for all modes with m>0). The mode profile for the first odd (TE_1) mode near cut-off is shown in figure 2.2.2c, the wings of the mode extend far into the cladding and the overlap with the core region is very small.

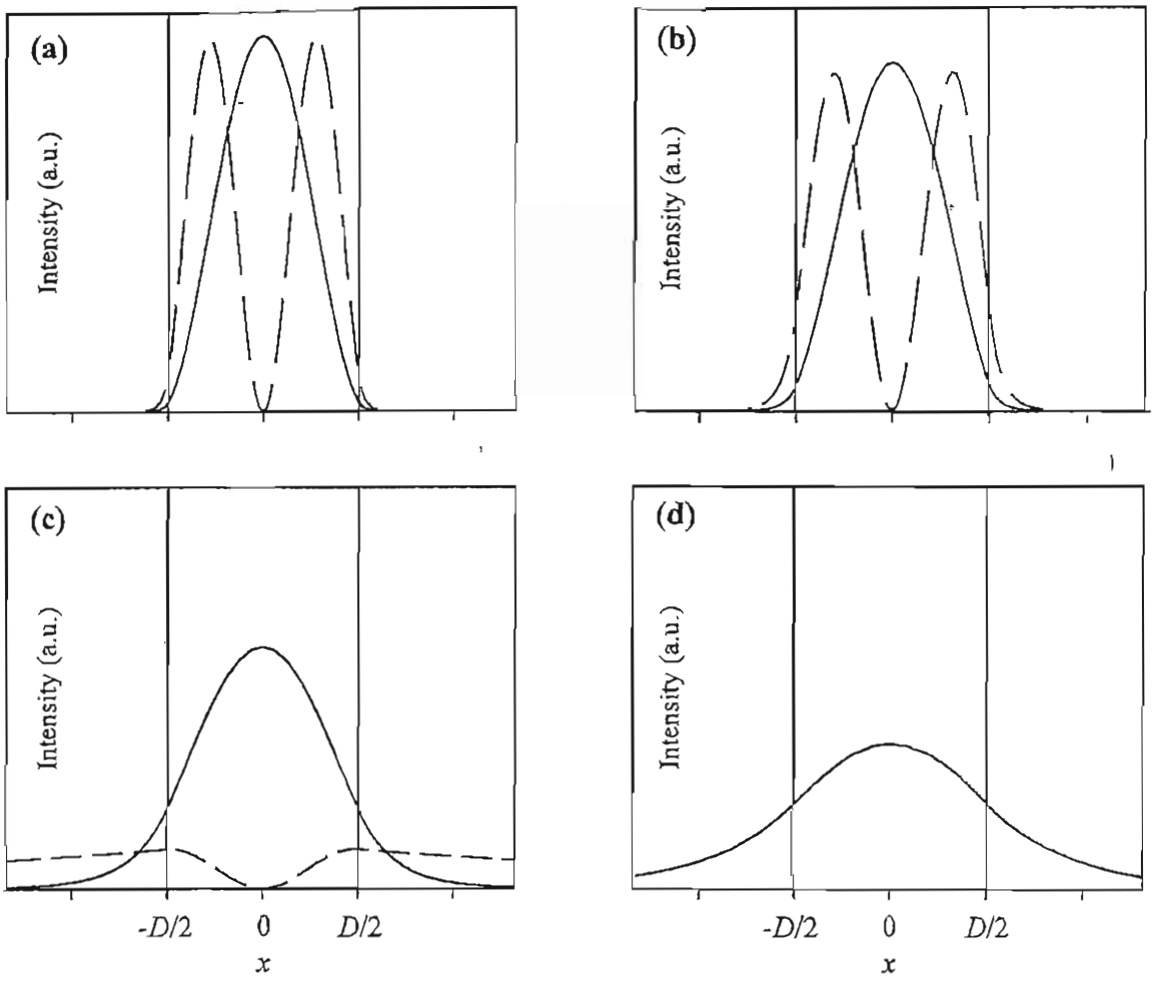

Figure 2.2.2- TE mode intensity for the fundamental mode (solid line), and first even mode (dotted line) for $\lambda_0 = 1$ μm and $D = 3$ μm.
(a) NA= 0.9 **(b)** NA= 0.5 **(c)** NA= 0.2 **(d)** NA= 0.1

The free-space divergence of a waveguide mode near cut-off is far from that of an ideal Gaussian beam, and as the mode gets closer and closer to cut-off the M^2 increases rapidly [6]. The fundamental mode of a symmetric waveguide is unusual in that it does not exhibit cut-off and always has a beam quality and mode profile very close to a diffraction limited Gaussian (M^2<1.1) [6]. However, for low NA (or small D/ long λ_0) the mode extends far into the cladding with a reduction in the peak intensity and a reduced overlap with the core region. Unlike the TE modes the transverse profiles of the TM modes do not scale rigorously with NA; the additional dependence on refractive index in the guidance condition (2.2.21) means that absolute values for the layer refractive indices should strictly be taken. However, the difference for TE and TM modes is very small over a wide range of indices and so figure 2.2.2 is also a good representation of TM mode profiles.

Although determining the specific properties of the waveguide modes requires solving the guidance conditions, a simple expression can be derived for the total number of propagating modes

(N_{modes}). For a guided mode solution α has to take a real positive value and consequently a particular mode will just be at cut-off when $\alpha=0$. The guidance conditions give that $\tan(\kappa D/2) = 0$ for even modes and $\cot(\kappa D/2) = 0$ for odd modes, which means that $\kappa D/2$ is equal to π or $\pi/2$ (odd or even) or an integer multiple of these at cut-off. Equation 2.2.19 shows that for $\alpha=0$, $\kappa = 2\pi NA/\lambda_0$ and so a particular mode (m) will be at cut off when $NA=m\lambda_0/2D$. The total number of propagating modes will then be given by $m+1$ (allowing for the $m=0$ mode), resulting in

$$N_{modes} \leq \frac{2\,NA\,D}{\lambda_0} + 1 \qquad [2.2.22]$$

Where the number of modes is always an integer and each value of N_{modes} actually corresponds to two possible polarisations (TE and TM). Equation 2.2.22 shows that the number of propagating modes decreases with wavelength, which can be a useful feature for the design of mid-IR waveguide lasers pumped at near IR wavelengths.

2.3 Laser theory

2.3.1 The quasi-three level model

Laser operation of RE-doped planar waveguides can be described using the quasi-three level model originally developed by Fan [3]. This model is generally applicable, it can be used to model four, three and quasi-three level transitions and allows for the spatial variation of the waveguide modes at the pump and laser wavelengths using a rate equation approach based on population inversion densities. The generalised energy level diagram for a quasi-three level transition is shown in figure 2.3.1a, the RE ion is pumped from the ground-state to either a high lying pump manifold from which there is fast non-radiative relaxation to the upper laser manifold, or, directly to one of the high lying stark levels of the upper manifold (in the case of the Yb transition, from the $^2F_{7/2}$ to $^2F_{5/2}$ manifolds). Laser action occurs between a lower lying level of this manifold (the upper laser level) and a high lying stark level of the ground-state (the lower laser level). Due to the rapid relaxation within each manifold, it is assumed that the populations within the manifolds are in 'quasi-thermal equilibrium' and can always be described by a Boltzmann distribution. The population density of the upper laser level is then $N_2=f_2N_U$, if N_U is the total population density of the upper manifold and f_2 is the fraction of N_U that resides in the appropriate stark level. Similarly, for the lower laser level $N_1=f_1N_L$, if f_1 is the fraction of N_L that resides in that level. The energy gap between the ground-state and upper manifold is assumed to be large so that in equilibrium (no pumping) the population densities of the manifolds and levels are $N_U^0 = N_2^0 = 0$, N_L^0 and $N_1^0 = f_1 N_L^0$ (where the "0" superscript is used to denote the equilibrium values of the populations). In the following analysis the effects of spatial hole burning are neglected and it is assumed that there is negligible depletion of the ground-state manifold, which is generally the case when $f_1/f_2<<1$ [3] (which holds for the 1.030 μm transition of Yb:YAG, with $f_1=0.05$ and $f_2=0.70$ [7]).

The application of the quasi-three level model to four level transitions [8] (e.g. the $^4F_{3/2}$ to $^4I_{11/2}$ transition at 1.06 μm of the Nd ion) is straightforward. The energy level diagram for a four level transition is shown in figure 2.3.1b. The ion is pumped from the ground-state to a high lying manifold from which it decays to the upper laser manifold. Laser action occurs from a stark level in this manifold to a level in the lower laser manifold, from which the ion then decays back to the ground-state. If the same assumption of negligible ground-state depletion is made and also that the non-radiative decay paths from pump to upper and lower to ground-state manifolds are rapid, then the results of the following analysis can be used with the lower laser populations set to zero, $N_L = N_1 = 0$.

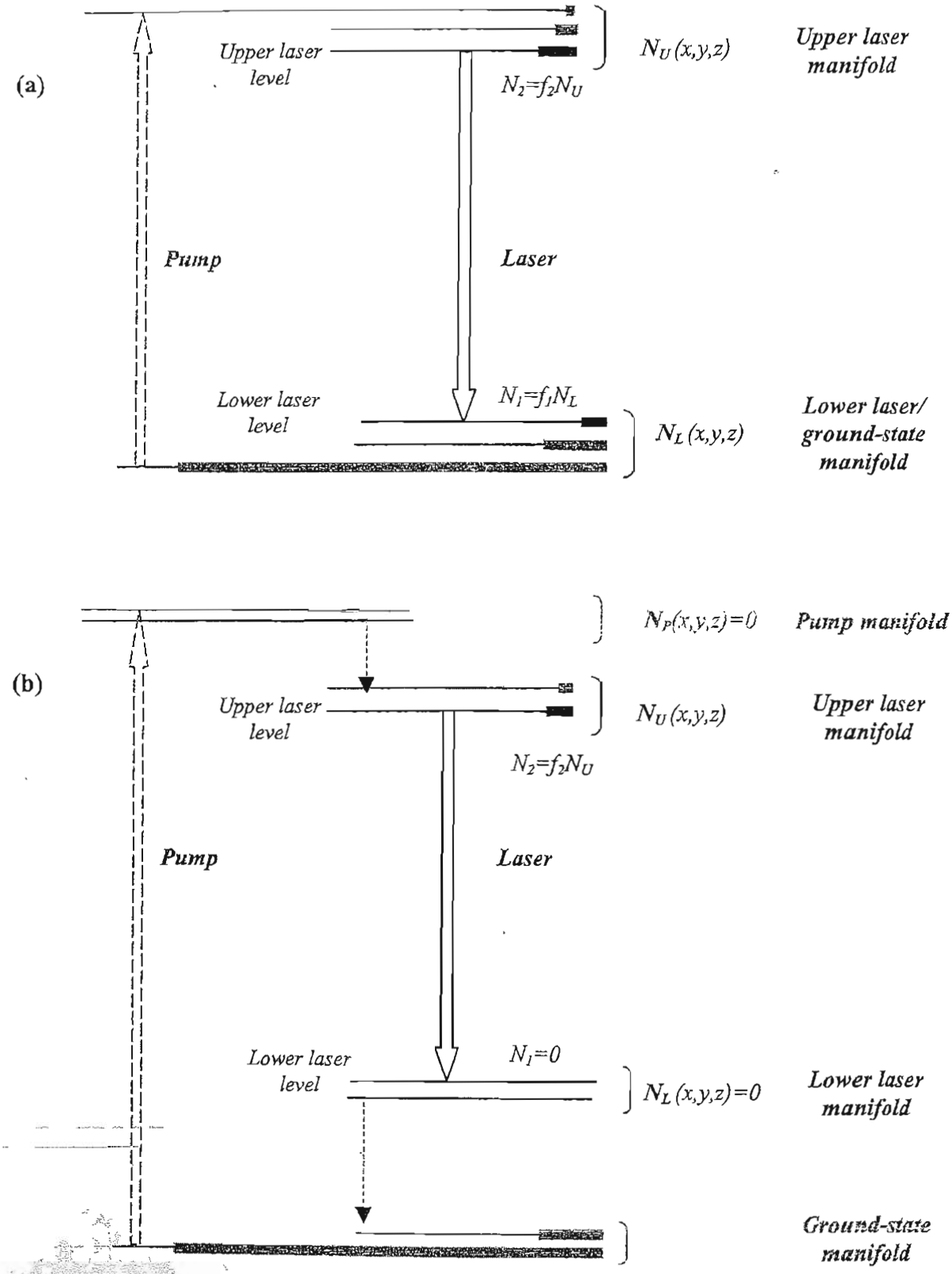

Figure 2.3.1- The quasi-three level model for
(a) a quasi-three level transition (b) a four level transition

(For clarity all the stark levels are not shown. The thick horizontal bars are intended to be representative of the population densities at steady-state. However, the spatial variation of pump and laser modes will means that these will vary across the cavity, and for the quasi-three level transition $N_1(x,y,z)$ can in fact be greater than $N_2(x,y,z)$ in the wings of a pump distribution, in which case the arrow in figure (a) should be reversed to indicate re-absorption loss).

2.3.2 Rate equations

We can write the steady-state rate equations for the population densities in the upper and lower laser manifolds in terms of the pump rate density $r(x,y,z)$ and laser photon density $\phi(x,y,z)$ (the pump rate and number of laser photons per unit volume respectively) as

$$\frac{\partial N_U(x,y,z)}{\partial t} = \eta_p\, r(x,y,z) - \frac{N_U(x,y,z)}{\tau} - c_n\sigma\left[N_2(x,y,z) - N_1(x,y,z)\right]\phi(x,y,z) = 0$$

$$\frac{\partial N_L(x,y,z)}{\partial t} = -\eta_p r(x,y,z) + \frac{N_U(x,y,z)}{\tau} + c_n\sigma\left[N_2(x,y,z) - N_1(x,y,z)\right]\phi(x,y,z) = 0$$

[2.3.1 a & b]

Where c_n is the speed of light in the waveguide for the laser radiation, τ is the upper manifold lifetime, σ is the gain cross-section and η_p is the pump quantum efficiency (the number of ions exited to the upper laser manifold for each absorbed pump photon). For our assumption of negligible ground state depletion $r(x,y,z)$ is independent of the lower laser manifold population and integrated over the laser waveguide is equal to the total pump rate R. Similarly, $\phi(x,y,z)$ integrated over the laser mode is equal to the total number of laser photons Φ,

$$\iiint_{cavity} r(x,y,z)\partial x\partial y\partial z = R \qquad \iiint_{cavity} \phi(x,y,z)\partial x\partial y\partial z = \Phi \qquad \text{[2.3.2a \& b]}$$

which are related to the absorbed pump power (P_p) and the average laser power inside the cavity in one direction (P_l) by

$$R = \frac{P_p}{h\upsilon_p} \qquad \Phi = \frac{2l_c P_l}{c_n h\nu_l} \qquad \text{[2.3.3a \& b]}$$

Where and l_c is the cavity length, h is Planck's constant and ν_p and ν_l are the pump and laser frequencies respectively. The factor of 2 appears in 2.3.3b because we are considering the power travelling in one direction inside the cavity and have defined Φ as the total number of laser photons (i.e the number of photons travelling in both directions). The steady state rate equation for the total number of laser photons inside the cavity is [3,4]

$$\frac{\partial\Phi}{\partial t} = c_n\sigma \iiint_{cavity} \Delta N(x,y,z)\ \phi(x,y,z)\partial x\partial y\partial z\ - \frac{\Phi}{\tau_c} = 0 \qquad \text{[2.3.4]}$$

Where $\Delta N(x,y,z) = N_2(x,y,z) - N_1(x,y,z)$, is the population inversion density and τ_c is the cold cavity photon lifetime, the time taken for Φ to fall to 1/e of its initial value in a passive cavity. If the roundtrip propagation loss is e^{-L} then the cold cavity lifetime is given by $\tau_c = 2l_c/c_n(L+T)$, where L is the roundtrip waveguide loss exponent and T is the output coupling (the negative natural logarithm of the mirror reflectivity, approximately equal to mirror transmission for small values of T). It is

convenient to express the pump rate and laser photon densities in terms of normalised spatial distributions r_p and ϕ_l, such that

$$r(x,y,z) \equiv R r_p(x,y,z)$$

$$\phi(x,y,z) \equiv \Phi \phi_l(x,y,z)$$

[2.3.5 a / b]

$$\iiint_{cavity} \phi_l(x,y,z) = \iiint_{cavity} r_p(x,y,z) = 1$$

[2.3.5 c]

If we define the roundtrip gain as e^{+G}, equation 2.3.4 can be re-arranged to give an expression for the roundtrip gain exponent,

$$G \equiv 2\sigma l_c \iiint_{cavity} \Delta N(x,y,z)\ \phi_l(x,y,z)\partial x \partial y \partial z = L + T \qquad [2.3.6]$$

which is simply a statement of the condition for laser oscillation, that the round trip gain averaged over the laser mode must equal the total roundtrip loss. To determine the inversion density the fractional population densities that reside in the upper and lower laser levels within the manifolds must be considered. For the upper laser level $\partial N_2/\partial x = f_2 \partial N_U/\partial x$, and $f_2 N_L = N_2$ and so from equation 2.3.1a and using the expressions for r and ϕ

$$\frac{\partial N_2(x,y,z)}{\partial t} = f_2 \eta_p R r_p(x,y,z) - \frac{N_2(x,y,z)}{\tau} - f_2 c_n \sigma \left[N_2(x,y,z) - N_1(x,y,z)\right] \Phi \phi_l(x,y,z) = 0$$

[2.3.7]

Similarly for the lower laser level $\partial N_l/\partial x = f_l \partial N_L/\partial x$. However to express N_U/τ in terms of N_l we make use of the fact that the total population density must be a constant, consequently $N_U + N_L = N_L^0$, and so it follows that $f_l N_U = f_l (N_L^0 - N_L) = N_1^0 - N_l$, giving

$$\frac{\partial N_1(x,y,z)}{\partial t} = -f_1 \eta_p R r_p(x,y,z) + \frac{N_1^0 - N_1(x,y,z)}{\tau} + f_1 c_n \sigma \left[N_2(x,y,z) - N_1(x,y,z)\right] \Phi \phi_l(x,y,z) = 0$$

[2.3.8]

Subtracting 2.3.8 and 2.3.7 and using $f = f_l + f_2$ for compactness, gives a single equation in terms of the inversion density $\Delta N = N_2 - N_l$,

$$\frac{\partial \Delta N(x,y,z)}{\partial t} = f \eta_p R r_p(x,y,z) - \frac{\Delta N(x,y,z) + N_1^0}{\tau} - f c_n \sigma \Delta N(x,y,z) \Phi \phi_l(x,y,z) = 0 \qquad [2.3.9]$$

Which can be re-arranged to give an expression for the population inversion density

$$\Delta N(x,y,z) = \frac{\tau f \eta_p R\, r_p(x,y,z) - N_1^0}{1 + fc_n \sigma \tau \Phi \phi_l(x,y,z)} \qquad [2.3.10]$$

that can now be substituted into equation 2.3.6

$$2\sigma l_c \int_0^l \int_{-\infty}^{\infty} \int_{-\infty}^{\infty} \frac{\tau f \eta_p R r_p(x,y,z) - N_1^0}{1 + fc_n \sigma \tau \Phi \phi_l(x,y,z)} \phi_l(x,y,z)\partial x \partial y \partial z = L + T \qquad [2.3.11]$$

This is the key equation that governs the behaviour of a quasi-three level waveguide laser at and above threshold and this equation is the starting point for the analysis carried out in chapter 5 for spatial mode-selection in multimode waveguide lasers. Equation 2.3.11 can also be re-expressed to relate absorbed pump power and laser output power ($P_{out}=TP_l$) by using equations 2.3.3 for R and Φ, and re-arranging to give

$$2\sigma l_c \int_0^l \int_{-\infty}^{\infty} \int_{-\infty}^{\infty} \left[\frac{\frac{\tau f \eta_p}{h\nu_p} P_p r_p(x,y,z) - N_1^0}{1 + \frac{2 l_c P_{out}}{T I_{sat}} \phi_l(x,y,z)} \right] \phi_l(x,y,z)\partial x \partial y \partial z = L + T \qquad [2.3.12]$$

Where the saturation intensity has been defined as $I_{sat}= f\sigma\tau/h\nu_l$ [4]. Equation 2.3.11 can now be evaluated at different pump or laser powers for arbitrary pump and laser distributions to determine input-output characteristics. In the following analysis Gaussian distributions are used as approximations for the fundamental waveguide modes to allow us to derive expressions for end-pumped waveguide lasers. In chapter 5, the solutions to the guidance conditions are considered to allow modelling of mode competition and spatially varying gain saturation in multimode waveguides.

2.3.3 End-pumped waveguide lasers

For an end-pumped waveguide laser, if we assume that the pump radiation is coupled to the fundamental mode of the waveguide and also that this mode is strongly confined to the doped core region (so that we can neglect any pump energy outside the core) the normalised distribution for the pump can be written as

$$r_p(x,y,z) = \frac{2\alpha_p}{\pi\, w_{py} w_{px}(1-e^{-\alpha_p l_c})} \exp\left(\frac{-2x^2}{w_{px}^2}\right)\exp\left(\frac{-2y^2}{w_{py}^2}\right)\exp(-\alpha_p z) \qquad [2.3.13]$$

Where w_{px} and w_{py} are the pump spot sizes in the x and y directions. The definition of spot size used throughout this thesis is the radius at which the intensity falls to $1/e^2$ of its peak value. The pump is assumed to make a single pass through the gain medium and α_p is the pump absorption co-efficient. If the waveguide laser operates on the fundamental mode then the normalised laser distribution is given by

$$\phi_l(x,y,z) = \frac{2}{\pi\, w_{ly} w_{lx} l_c} \exp\left(\frac{-2x^2}{w_{lx}^2}\right)\exp\left(\frac{-2y^2}{w_{ly}^2}\right) \qquad [2.3.14]$$

With w_{lx} *and* w_{px} being the spot sizes of the laser mode in the x and y directions. To determine the absorbed pump power required to reach threshold ($P_p=P_{th}$) we set the output power to zero, $P_{out}=0$ in equation 2.3.12, giving the following general expression for threshold,

$$\frac{2\sigma l_c \tau f \eta_p}{h\nu_p} P_{th} \int_0^l \int_{-\infty}^{\infty}\int_{-\infty}^{\infty} r_p(x,y,z)\phi_l(x,y,z)\; \partial x \partial y \partial z = L + T + 2\sigma N_1^0 l_c \qquad [2.3.15]$$

illustrating the general point that the pump power required to reach threshold is higher for transitions that exhibit re-absorption loss ($N_1^0>0$) than those that don't ($N_1^0 = 0$) (all other factors being equalroygbiv). Substituting in equations 2.3.13 and 2.3.14 results in the following expression for absorbed pump power threshold.

$$P_{th} = \frac{\pi h\nu_p}{4\sigma\tau f \eta_p}\sqrt{w_{px}^2 + w_{lx}^2}\sqrt{w_{py}^2 + w_{ly}^2}\,(L + T + 2\sigma N_1^0 l_c) \qquad [2.3.16]$$

Equation 2.3.16 illustrates that to minimise the threshold of an end-pumped waveguide both the pump and laser spot sizes should be made as small as possible, indicating that small core sizes combined with high NAs should be used. Consequently guided wave thresholds can be much lower than in a comparable bulk resonator in which divergence of the modes can significantly increase the effective mode volume [7]. The threshold is also directly proportional to the roundtrip loss and so the choice of fabrication technique has to be made carefully to minimise L. This is particularly important for laser operation on four level transitions in which roundtrip losses are dominated by L, but less critical for three-level transitions where re-absorption ($2\sigma N_1^0 l_c$) plays a significant role.

In general the slope efficiency (η_{SE}) has to be determined by numerically evaluating 2.3.12 using the expressions for r_p and ϕ_l at different values of P_{out} and P_P. However for the particular case of $N_1^0 = 0$ (a four level transition) a solution can be reached [9]

$$\eta_{SE} \equiv \frac{\partial P_{out}}{\partial P_p} = \frac{T}{(T+L)} \frac{\nu_l}{\nu_p} \eta_p \eta_{pl} \qquad [2.3.17]$$

The overall slope efficiency is a combination of the ratio of output coupling to total roundtrip cavity loss ($T/(L+T)$), the quantum defect of the laser transition (ν_l/ν_p), the pump quantum efficiency η_p and a factor η_{pl} that describes the spatial overlap of the pump and laser modes. For low power operation η_{pl} is given by [9]

$$\eta_{pl} = w_{lx} w_{ly} \frac{\sqrt{2w_{px}^2 + w_{lx}^2}\sqrt{2w_{py}^2 + w_{ly}^2}}{(w_{px}^2 + w_{lx}^2)(w_{py}^2 + w_{ly}^2)} \qquad [2.3.18]$$

One of the advantages of a waveguide geometry is that a good overlap is usually ensured as both the pump and laser modes are confined to approximately the same volume and for $w_{px} \approx w_{lx}$ and $w_{py} \approx w_{ly}$, $\eta_{pl} \approx 0.75$. This makes the roundtrip loss ratio the most significant resonator dependent factor in equation 2.3.17, indicating the need for low values of waveguide loss if high efficiency is to be achieved. In practice planar fabrication techniques result in L being greater for waveguides than bulk crystals, and so it may be necessary to use a higher value of output coupling (T) in a waveguide laser to achieve the same efficiency as a bulk resonator. An increase in T will increase the threshold (equation 2.3.16); however, as long as L is not too great, lower thresholds and comparable efficiencies can still be realised by moving from a bulk to a waveguide geometry.

Finally, in equations 2.3.13 and 2.3.14 we have assumed that the pump and laser modes do not diverge and so equations 2.3.16 to 2.3.18 are directly applicable to channel waveguide lasers. However, many of the devices investigated in the subsequent chapters are planar, either as a first step towards the fabrication of channels (chapters 3 and 4) or for compatibility with high power diode-pumping (chapter 5), in which case divergence in the unguided (y) axis must be considered. For these devices, the approximation of an average spot size is used for the unguided axis [8,10] and this is discussed in more detail in the following chapter when it is first used.

2.4 References

[1] D. Lee, *"Electromagnetic principles of integrated optics"*, Wiley, (1986).

[2] A.W. Snyder & J.D. Love, *"Optical waveguide theory"*, Chapman & Hall, (1983).

[3] T. Fan & R. Byer, *"Modelling and CW operation of a quasi-three level 946 nm Nd:YAG laser"*, IEEE J. of Quantum Electronics, Vol. QE-23 , p. 605-612, (1987).

[4] W. Risk, *" Modelling of longitudinally pumped solid-state lasers exhibiting re-absorption loss"*, J. of Optical Society of America B, Vol. 5, No. 7, p. 1412-1423, (1988).

[5] D. Franklin, *"Electromagnetic theory"*, Prentice Hall, (1986).

[6] A. Tropper, *"Fibre & waveguide lasers"*, in *"Advances in lasers and applications"*, Proceedings of the 52nd Scottish universities summer school in physics, D.M. Finlayson, B.D. Sinclair (Eds), p. 39-59, (1998).

[7] T. Taira, W. Tulloch & R. Byer *"Modelling of quasi-three level lasers and operation of CW Yb:YAG lasers"*, Applied Optics, Vol. 36, No 9, pp 1867-1874, (1997).

[8] M. Digonnet & C. Gaeta, *"Theoretical analysis of optical fiber laser amplifiers and oscillators"* Applied Optics, Vol. 24, No. 3, p. 333-342, (1985).

[9] W. Clarkson & D. Hanna *"Effects of transverse-mode profile on slope efficiency and relaxation oscillations in a longitudinally pumped laser"*, J. of Modern Optics, Vol. 36, No. 4, p. 483-489, (1989).

[10] K. Kubodera & K Otsuka, *"Single transverse-mode $LiNdP_4O_{12}$ slab waveguide laser"*, J. of Applied Physics, Vol. 50, No. 2, p. 653-659, (1979).

Chapter 3

BOROSILICATE GLASS WAVEGUIDE LASERS

3.1 Introduction

This chapter describes the optical characterisation of novel laser waveguide structures in borosilicate glasses. Planar structures fabricated by a new method of ion-exchange (IE) in glasses are investigated. The ion-exchange process is based on the direct-bonding (DB) technique that allows the fabrication of deeply buried waveguides by a single-step process and the resulting guides are shown to have optical losses of < 0.4 dB/cm. These structures are then combined with direct UV writing for the production of buried channel waveguide lasers. Absorbed pump power thresholds as low as 2.7 mW in structures that are suitable for integrated optical applications are demonstrated.

3.2 DB-IE Planar waveguide lasers

3.2.1 Buried DB-IE structures

The production of ion-exchanged integrated optical devices in glass requires that losses associated with surface waveguides must be minimised. Such problems are due to light scattering from imperfections at the guide-air interface and the asymmetric mode profile of the waveguide structure, which can prove inefficient for coupling into optical fibres [1]. Fabrication of a buried waveguide by ion exchange is generally achieved in two stages, an initial ion-exchange process to create a surface waveguide, followed by a secondary process where the exchange ions are diffused further into the substrate by a subsequent heat [2] or electric field treatment [3], or by means of a second ion-exchange process to lower the refractive index at the guide surface [4]. A more recently applied method is that of attaching a cladding layer by direct bonding to an ion-exchanged substrate to bury the waveguide completely [5].

In contrast to all these processes, a new ion exchange process was developed by Corin Gawith at Southampton University that combines direct bonding and ion exchange in a single-step process (DB-IE) for buried waveguide devices [6]. The key to the DB-IE process is the bonding of glass substrates with opposing chemical gradients so that the substrate can act as both a source for ion-exchange and a cladding layer. The DB-IE process has the advantage that by using glass (a previously unexplored source for ion-exchange) the hostile environment of a molten salt bath can be avoided and a buried waveguide can be produced in a single step. The DB-IE process is also less labour intensive (and consequently cheaper) than using DB alone for waveguide fabrication, as only a single bonding step is required as opposed to first bonding the core material, then polishing it to the required thickness and then adding a cladding layer in a second bonding step. The process used for the initial characterisation and feasibility study for DB-IE glass waveguides is shown below.

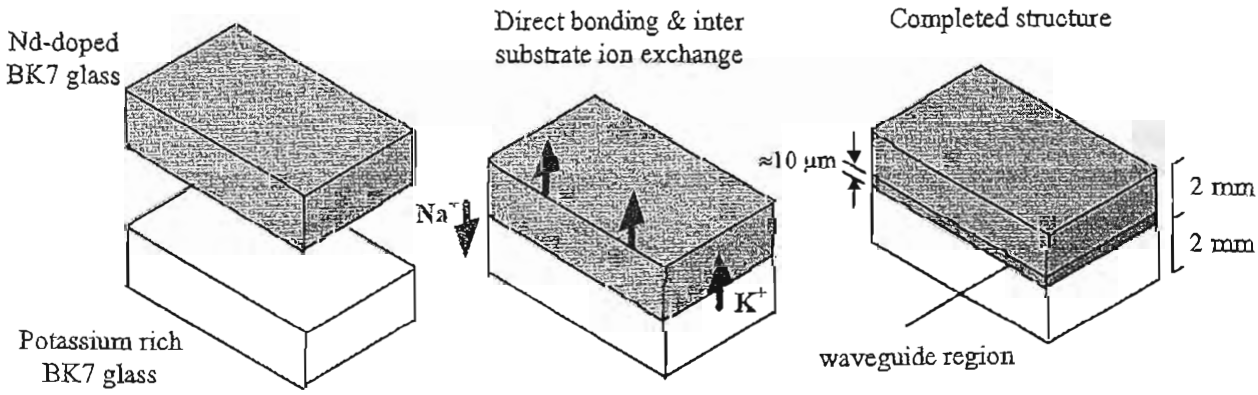

Figure 3.2.1- Fabrication of DB-IE waveguide lasers

The active superstrate was prepared from a melt of commercially available borosilicate glass (BK7 from Schott) with additional 2 wt % of Nd. The composition of the undoped substrate was also based on a commercially available BK7 glass, however in this case to facilitate ion-exchange an additional 4 wt% of K_2O was added by removing an equal amount of Na_2O. Upon direct bonding and annealing at 350°C for six hours the offset in glass composition between substrate and superstrate results in internal K^+ - Na^+ ion exchange and the formation of buried waveguides at the DB interface. Further details of this process and glass composition can be found in Gawith (1999) [6].

3.2.2 Lasing of DB-IE Nd:BK7 planar waveguides

Characterisation of the spectroscopy and laser performance of the DB-IE planar BK7 guide was carried out using a 5.8 mm long device as illustrated in figure 3.2.2(a). A Ti-sapphire pump laser was end-launched into the waveguide using a x10 microscope objective to focus to a spot size of approximately 3 μm at the front face of the guide, and optimisation of the pump-launch was achieved by maintaining a maximum fluorescence signal while both aligning the guide and tuning the pump wavelength. For the direct-bonded ion-exchanged structures it was necessary to isolate the fluorescence signal of the core from that of the doped superstrate. This was achieved by using a x 10 microscope objective to image just the guided-wave fluorescence through a mask onto a silicon detector. By this method it was possible to couple 76 % of the incident pump power into the guide, with 68 % of the launched power being absorbed at a wavelength of 808 nm in the 5.8 mm long device. These launch and absorption efficiencies (η_L = 0.76 and η_A = 0.68, respectively) were estimated by measuring the guided wave pump-transmission at 808 nm and comparing it to the pump-transmission of the doped superstrate and undoped substrate.

The fluorescence lifetime of Nd^{3+} $^4F_{3/2}$ level was measured in the guide by chopping the pump and monitoring the fluorescence decay using a digital oscilloscope, and the measured lifetime of 470 μs (1/e of the maximum intensity) is typical of neodymium ions in borosilicate and silicate glasses [7]. The emission spectrum was obtained by observing the fluorescence using an optical spectrum analyser. A typical spectrum from the guide is shown in figure 3.2.2(c) and is identical to that obtained from the bulk superstrate and is also typical of borosilicate glasses [7].

Laser action on the $^4F_{3/2}$-$^4I_{11/2}$ Nd^{3+} transition was achieved by butting plane dielectric mirrors to the guide end-faces using a small drop of fluorinated liquid for adhesion. For two highly-reflecting (HR) mirrors (at the laser wavelength of 1.06 μm) a pump power threshold of 42 mW incident on the input objective was achieved, which accounting for the launch and absorption efficiencies and objective and input mirror transmission corresponds to an absorbed pump power threshold of 21 mW. The output mirror was changed to one with a 3% transmission and the output power as a function of absorbed pump power is shown in figure 3.2.3(c).

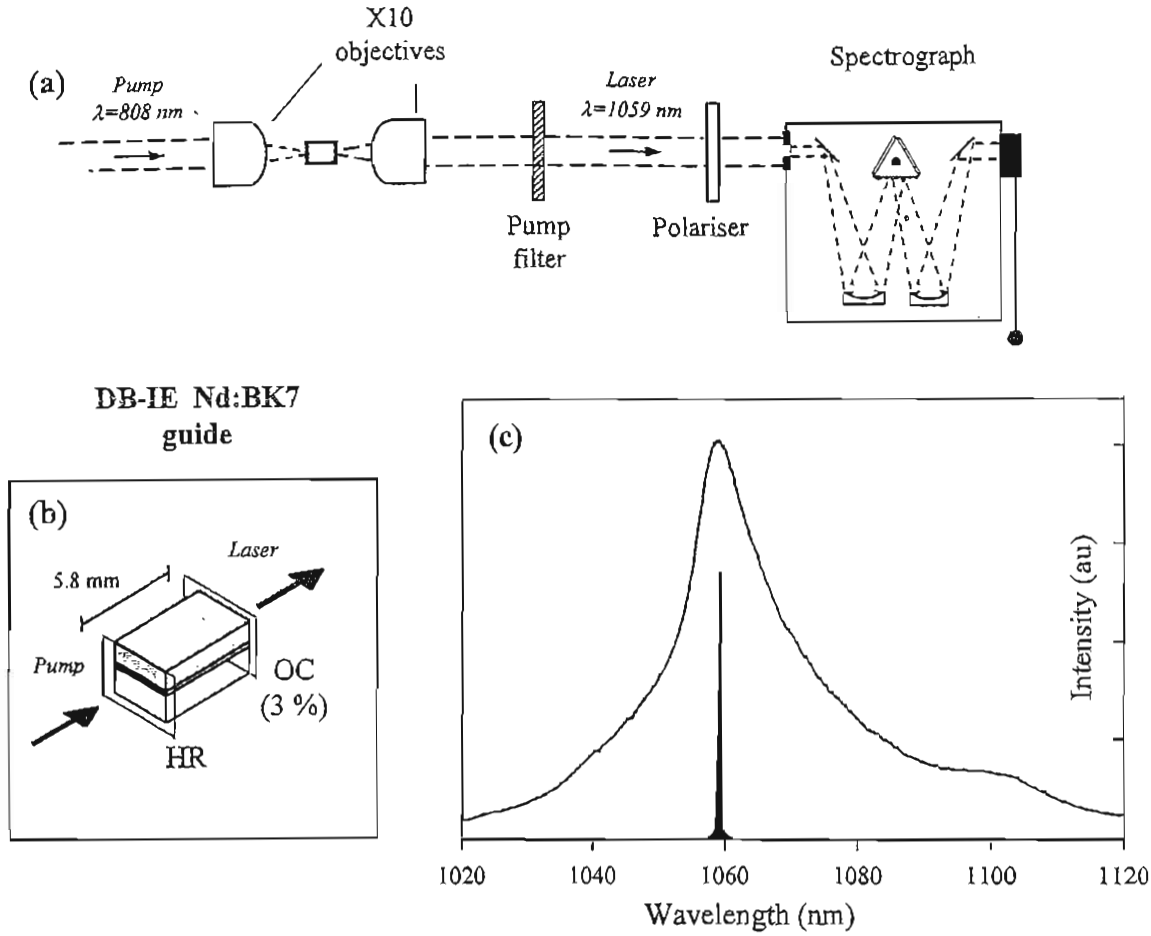

Figure 3.2.2 (a) Apparatus for emission spectroscopy (b) Arrangement for laser operation of DB-IE guide (c) Emission spectra for the $^4F_{3/2} - ^4I_{11/2}$ Nd transition (line : unpolarised flouresence spectrum, solid : TE polarised laser emission at 1059 nm)

The absorbed pump power required to reach threshold rose to 41 mW and a slope efficiency of 6 % with respect to absorbed pump power was achieved for this configuration, although no attempt was made to maximise the overlap of pump and laser modes in the non-guided axis. The laser output was focussed into the spectrum analyser via a polariser, which showed that the laser emission was TE polarised and at a wavelength of 1059 nm. It is well known that ion-exchange causes stress induced birefringence [8], and this is the most likely cause for the polarised output observed in these guides, however this will be subject to future investigation.

The optical modes for both the pump and laser were profiled by imaging the waveguide output onto a silicon camera using the x 10 objective, and these are shown in figure 3.2.3(a) and (b). The images indicate single mode pump propagation and laser operation, with guided spot sizes ($1/e^2$ intensity radius) $w_{px} = 2.9$ μm and $w_{lx} = 3.4$ μm, respectively. For the unguided axis the laser spot mode size at the output face was measured to be $w_{ly}(l_c) = 40$ μm while that of the pump was too large to be imaged completely by the output objective ($w_{py}(l_c) > 100$ μm).

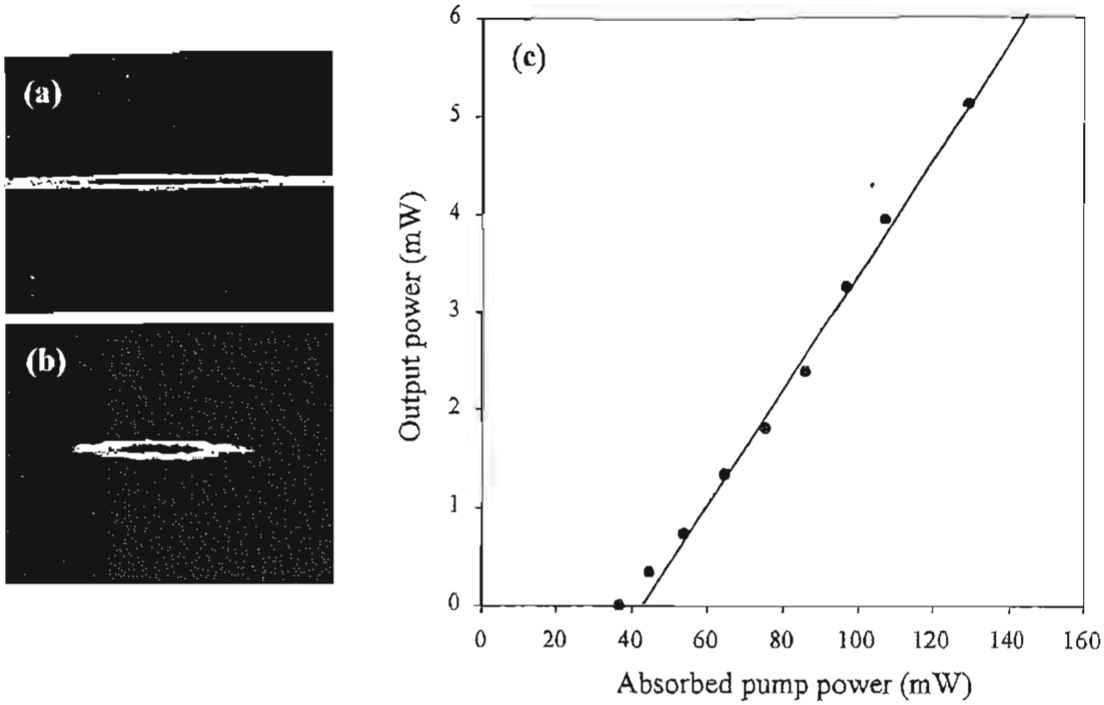

Figure 3.2.3 (a) Pump mode; guided spot size w_{px} = 2.9 μm (b) Laser mode; guided spot size w_{lx} = 3.4 μm (c) Laser output power as a function of absorbed pump power for 3% output coupling.

3.2.3 Estimation of propagation losses (Nd:BK7 planar waveguides)

A particularly useful, non-destructive and sensitive technique for determining the losses in active waveguides is the variation of threshold with output coupling. This method was first realised by Findlay and Clay for measuring the scattering losses in bulk lasers [9], however the same principle applies to guided wave devices and this technique is used throughout this work. From equation 2.3.16, we can see that if we assume that the pump and laser mode sizes do not vary with increasing pump power (corresponding to increasing output coupling T at threshold) then the threshold of a four level laser can simply be written as

$$P_{th} = C(L + T) \qquad [3.2.1]$$

Where C is a constant that encompasses all the material properties of the gain medium and also the spatial variation of the pump and laser modes. Although, equation 3.2.1 is for absorbed pump power we could equally re-define C to include the absorption and launch efficiencies (if we assume that these too remain constant with increasing pump power) so that 3.2.1 also holds for incident pump power. In any case, the assumption of the Findlay-Clay method is that the threshold increases linearly with roundtrip cavity loss. Consequently by making a plot of T = -ln$R$, (if R is reflectivity of the output coupler at the laser wavelength) against threshold and extrapolating to P_{th}=0 (-ln$R$ = L) a value for the intrinsic roundtrip loss can be determined. A plot of absorbed power threshold against –ln$R$ for the BK7 guide is shown in figure 3.2.4.

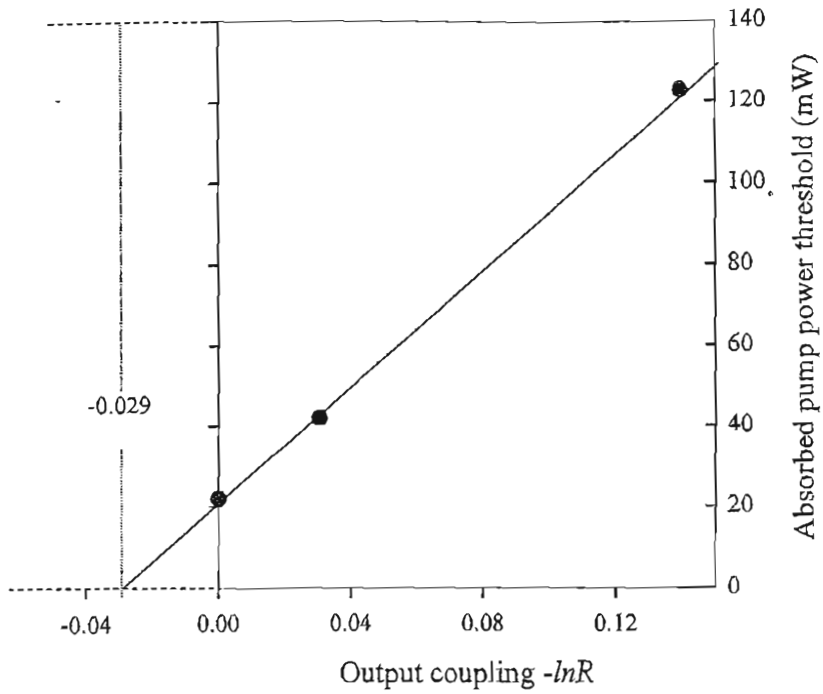

Figure 3.2.4 Findlay-Clay plot for estimation of intrinsic propagation loss of Nd:BK7 guide.

The graph x-axis intercept gives an intrinsic roundtrip loss L = -0.029 which corresponds to a single pass loss exponent per unit length of $\alpha_L = -L/2l_c = 0.02$ cm^{-1}. This value can be converted to dB/cm using equation 3.2.2 (if the guide length l_c is measured in cm).

$$\text{Loss} = 10\log\{\exp(-\alpha_L l_c)\}/\, l_c \qquad \text{(dB/cm)} \qquad [3.2.2]$$

which gives a propagation loss of 0.1 dB/cm for our planar waveguide laser. Unfortunately, the availability of suitable mirrors limited the Findlay-Clay plot to just three points on the graph and so to confirm this estimate the slope efficiency was considered [10]. The slope efficiency is a useful characteristic to estimate the optical losses, as it does not rely on knowledge of cross-sections, lifetimes or other parameters that are intrinsic to the guide material. The expression for slope efficiency (equations 2.3.17-18)

$$\eta_{SE} = \frac{T}{(T+L)}\frac{\nu_l}{\nu_p}\eta_p \; w_{lx}w_{ly}\frac{\sqrt{2w_{px}^2 + w_{lx}^2}\sqrt{2w_{py}^2 + w_{ly}^2}}{(w_{px}^2 + w_{lx}^2)(w_{py}^2 + w_{ly}^2)} \qquad [3.2.3]$$

is in fact only dependent on one intrinsic parameter, the pump quantum efficiency (η_p) and this can be set to 100 % to obtain an upper limit on the propagation loss. For the guided axis the measured spot sizes of w_{px} = 2.9 μm and w_{lx} = 3.4 μm can be used, while for the unguided axis it is assumed that the laser mode spot-size is approximately constant, (the confocal parameter for the measured spot-size at

the guide end-face is considerably longer than the length of the guide), so that w_{ly} = 40 μm. The effective spot size [11,12] for the unguided pump axis was calculated from the spot size at the input face of the guide of 3.2 μm. If the pump is focussed to a waist w_{0py} at the input face of the guide (z=0), the unguided spot size will obey the Gaussian beam propagation formula

$$w_{py}^2(z) = w_{0py}^2 + \left[\frac{\lambda_p z}{\pi n w_{0py}}\right]^2 \qquad [3.2.4]$$

The spot size squared, averaged over the length of the guide ($\overline{w_{py}^2}$), can then be determined by integrating equation 3.2.4

$$\overline{w_{py}^2} = \frac{1}{l_c}\int_0^{l_c} w_{py}^2(z).\partial z = w_{0py}^2 + \left[\frac{\lambda_p l_c}{\sqrt{3}\pi n w_{0py}}\right]^2 \qquad [3.2.5]$$

This expression can now be used in equations 3.2.3 for the end-pumped planar guide. For the purpose of this estimate the small variation of refractive index due to RE doping and ion-exchange was ignored and the value of undoped BK7 [13], n=1.507 was used to give a value of $\overline{w_{py}^2}$ = (204 μm)^2 for the average unguided spot size. In this manner, an upper limit of < 0.4 dB/cm for the propagation loss was reached. The estimate of the propagation loss based on the Findlay-Clay plot, combined with this estimate based on the slope efficiency, suggests a low value for propagation loss, certainly lower than 0.4 dB/cm and perhaps as low as 0.1 dB/cm, values that are comparable to waveguides fabricated by alternative potassium ion exchange processes in BK7 glass [7].

3.3 DB-IE Channel waveguide lasers

3.3.1 UV-written channel waveguides

Direct writing using a UV beam in photosensitive glasses has emerged as a viable means of channel waveguide fabrication over the last decade [14-16]. In comparison to more traditional techniques of masked ion exchange or etching, UV writing does not require direct access to the surface of the guiding layer so that channel guides can be written through a cladding layer. These features, and the ability to generate virtually any guide-pattern by direct computer control, makes UV writing a very flexible and attractive means of developing integrated optic components in buried DB-IE planar waveguides. To allow UV writing, a newly developed germanium borosilicate glass SGBN [17,18] was used for the superstrate, the composition of this glass being similar to that of BK7 with additional germanium for photosensitivity. For this initial demonstration the RE-ion content of the SGBN glass could not be optimised due to problems with annealing the glass and a doping level of only 0.2 wt % of Nd was available.

The channel guides were fabricated by Corin Gawith and Alexander Fu at the University of Southampton using the procedure shown schematically below [19]. The planar guide was fabricated using a substrate of the same potassium rich BK7 glass (see section 3.2.1) and a 0.2 wt % Nd doped SGBN cladding layer, which upon direct bonding created a planar guiding region at the DB interface.

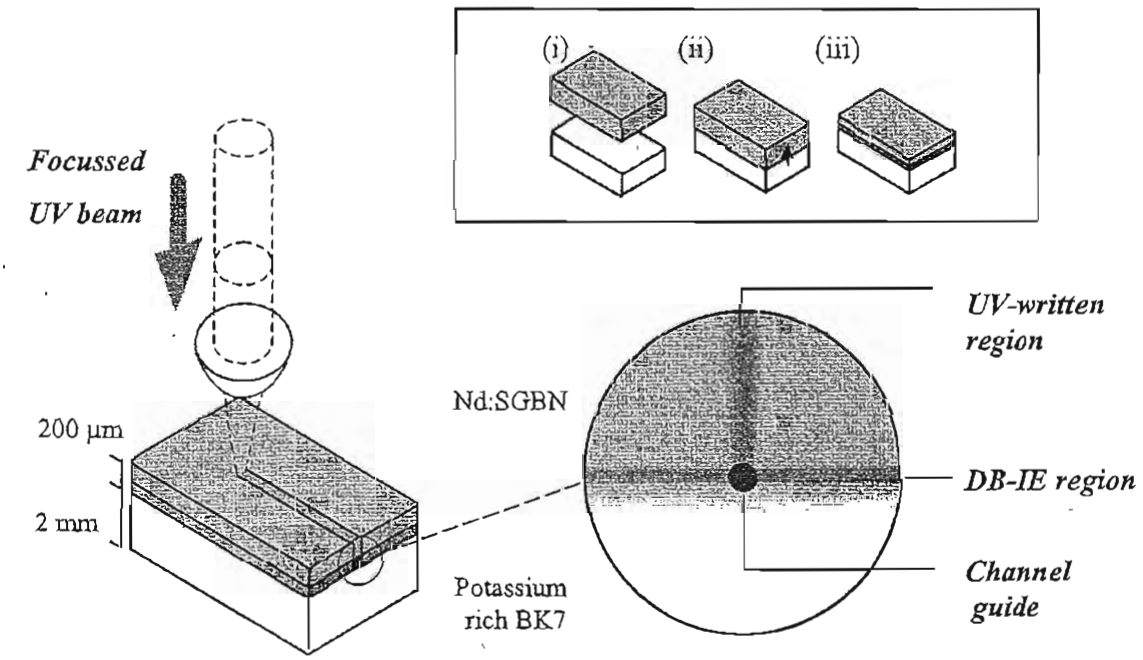

Figure 3.2.1- Fabrication of UV written channel waveguide lasers.

Inset; DB-IE process (i) Nd:SGBN superstrate and potassium rich BK7 substrate (ii) DB and inter-substrate IE (ii) top layer cut and polished to 200 µm

For these initial experiments the cladding layer was cut and polished to a thickness of 200 μm. UV writing of the channel guides was carried out using a 3.1 mm diameter, 200 mW frequency doubled argon ion laser beam (λ = 244 nm) focussed using a 35 mm lens through the cladding layer to a waist at the DB interface. Further details of the channel fabrication and SGBN glass composition can be found in Gawith (2002) [19].

3.3.2 Channel waveguide characterisation

Characterisation of the spectroscopy, laser performance and propagation loss was carried out using a sample cut and polished to a length of 7.5 mm; a longer sample than the original Nd:BK7 planar guide to compensate for the lower doping level present in the Nd:SGBN. The testing was carried out using the same procedure as that for the original DB-IE planar guide, with an 808 nm Ti-sapphire pump laser end-focussed to a spot size of 3 μm. However the pump coupling was not fully optimised to match the channel waveguide mode for this initial characterisation, resulting in a low launch efficiency of only η_L=0.13. The low Nd doping level in this guide also resulted in low pump absorption. The absorption efficiency η_A was measured to decrease from 0.37 for an incident pump power of 50 mW to 0.14 for the maximum available incident pump power of 550 mW, pump saturation limiting η_A at high pump powers for these far from optimised structures. The low value of the available absorbed pump power limited the signal at the laser wavelength. A typical fluorescence spectrum from the Nd:SGBN channel guides is shown below in figure 3.3.2 and although the low intensity part of the signal was below the threshold of detection, the spectrum is consistent with that obtained from the original Nd:BK7 planar guide, as was the measured 1/e fluorescence lifetime of 470 μs.

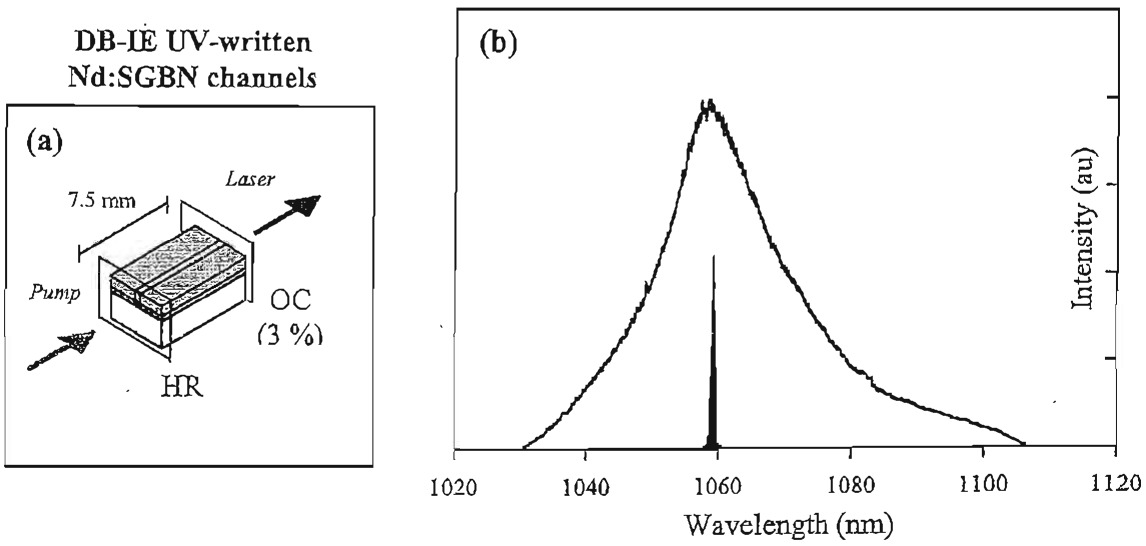

Figure 3.3.2 (a) Arrangement for laser operation of UV written DB-IE channel waveguides
(b) Emission spectrum for the $^4F_{3/2} - ^4I_{11/2}$ Nd transition
(line : unpolarised flouresence spectrum, solid : TM polarised laser emission at 1059 nm)

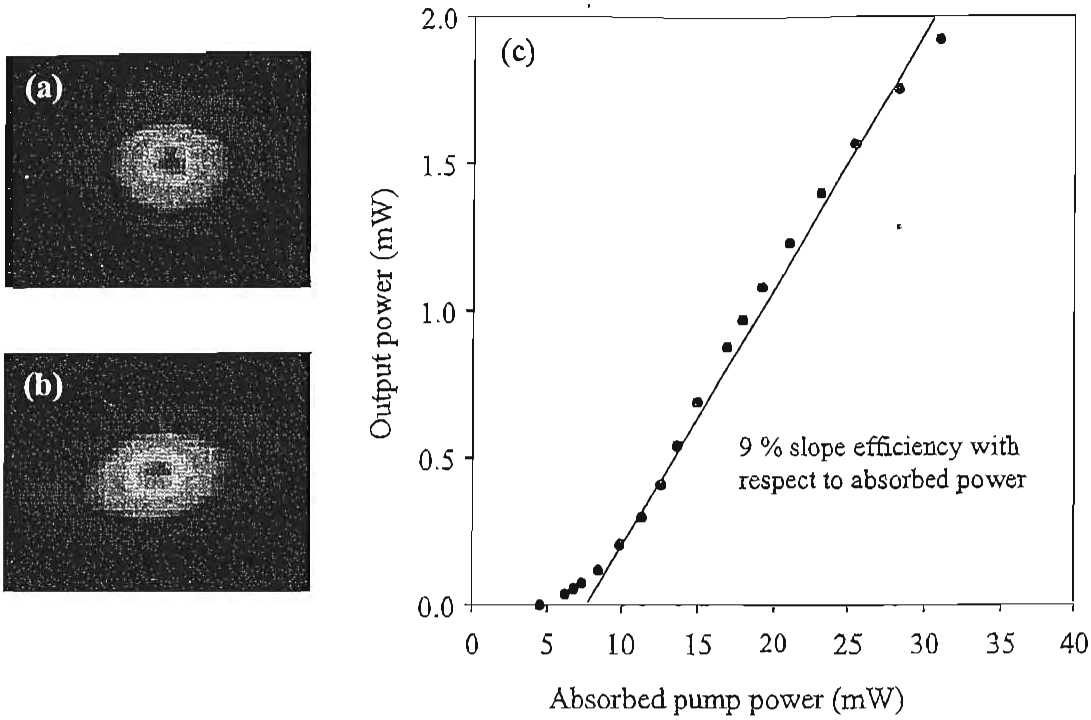

Figure 3.3.3 (a) Pump mode; guided spot sizes $w_{px} = 2.9$ μm by $w_{py} = 4$ μm.
(b) Laser mode; guided spot sizes $w_{lx} = 3.4$ μm by $w_{ly} = 5.5$ μm.
(c) Laser output power as a function of absorbed pump power for 3% output coupling.

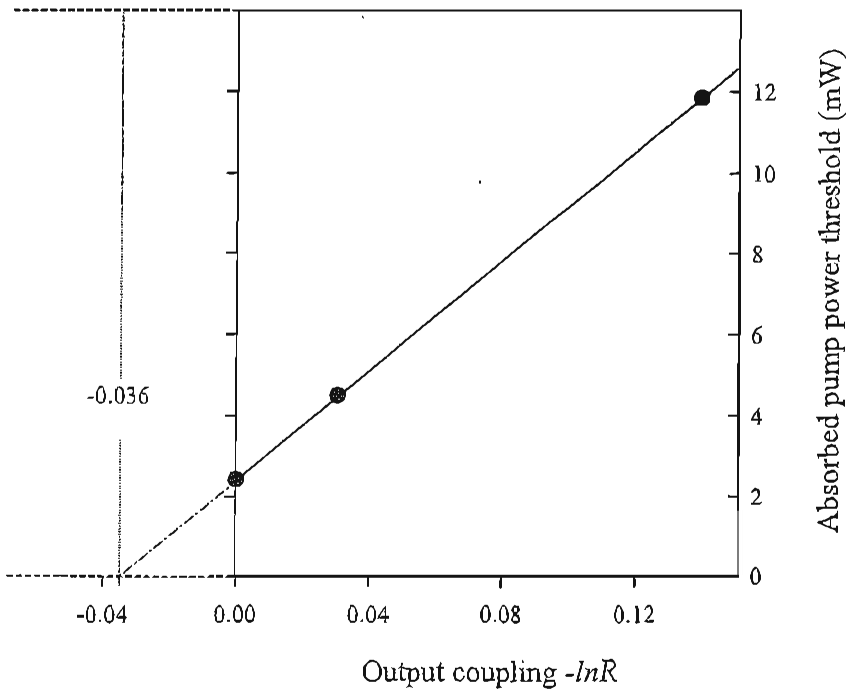

Figure 3.3.4 Findlay-Clay plot for estimation of intrinsic propagation loss of Nd:SGBN guide. The graph x-axis intercept gives an intrinsic roundtrip loss L = -0.036 which corresponds to a single pass loss per unit length in the 7.5 mm long device of $\alpha_L = 0.02$ cm^{-1} or 0.1 dB/cm.

Laser operation was achieved using the same mirror set as used for the planar guide. For two HR mirrors an absorbed pump power threshold of 2.7 mW was achieved, a significant improvement over the 21 mW absorbed power threshold observed in the Nd:BK7 planar guide. With a 3% output coupler the threshold rose to 4.5 mW and a slope efficiency of 9% with respect to absorbed pump power was obtained, again an improvement over the original planar guide due to a better overlap of the pump and laser modes in the channel guides. The maximum output power for this configuration was only 2 mW due to the low value of absorbed pump power available (32 mW). The laser was TM polarised for the UV written Nd:SGBN channel guides, as opposed to the TE emission observed in the Nd:BK7 planar guides. UV-written and ion-exchanged structures both display stress induced birefringence [20,8], and the dominant mechanisms that control the polarisation of the laser emission warrants future investigation. The optical modes for both the pump and laser were profiled by imaging the waveguide output onto a silicon camera using a x 16 objective, and these are shown in figures 3.3.3 (a) and (b).

The images indicate single mode pump propagation and laser operation, with guided spot sizes w_{px} = 2.9 μm and w_{py} = 4 μm for the pump and w_{lx} = 3.4 μm and w_{ly} = 5.5 μm for the laser. The near symmetric mode profiles indicate that these structures offer good possibilities of low-loss optical fibre coupling and the development of integrated optic devices based on this technology. The optical losses were estimated using the technique previously described in section 3.2.3. The Findlay-Clay plot for the channel guides is shown in figure 3.3.4, and corresponds to an optical loss of 0.1 dB/cm indicating that the introduction of lateral confinement by UV writing does not increase the overall propagation loss. The measured spot sizes and slope efficiency of 9 % with respect to absorbed power gives an absolute upper limit of < 0.3 dB/cm for the propagation loss, which is comparable to the best direct UV written channel waveguides in germanosilica layers (< 0.2 dB/cm) [16].

3.4 Summary

The DB-IE process provides a useful route to realising a buried platform for the fabrication of active integrated optic circuits in borosilicate glasses. The initial characterisation of the planar structures shows that direct-bonded ion-exchange is capable of producing guides with optical losses of <0.4 dB/cm comparable to those produced by conventional ion-exchange techniques. Photosensitivity can be introduced into these structures by using a germanium doped active superstrate which allows buried channel waveguides to be directly written into these structures using a UV laser. The characterisation of Nd:SGBN structures shows that these channel structures have optical losses of <0.3 dB/cm and absorbed power thresholds < 10 mW and provide a near symmetric laser output which should be compatible with low-loss coupling to optical fibres. The initial problems with annealing the glass which limited the RE active ion content for this initial demonstration is now being addressed and 5 wt% erbium doped SGBN has now been produced [21]. Direct bonding of these samples should allow the development of erbium-doped lasers operating at 1540 nm [22], suitable for applications in the field of telecommunications, as this is the wavelength of minimum attenuation for single mode silica fibres.

Glass substrates can be produced in large sizes and direct bonding would allow the production of large-scale platforms that could be cut to a number of smaller devices. UV writing allows automated fabrication of three-dimensional devices on these platforms without the need for photolithography, offering a low-cost and versatile route to the large-scale production of a wide variety of active integrated optical components.

3.5 References

[1] R.V. Ramaswamy & R. Srivastava, *"Ion-exchanged glass waveguides: a review"*, Journal of Lightwave Technology, Vol. 6, No. 6, p. 984-1002 (1988).

[2] T.G. Giallorenzi, E.J. West, R. Kirk, R. Ginther, & R.A. Andrews, *"Optical waveguides formed by thermal migration of ions in glass"*, Applied Optics, Vol. 12, No. 6, p. 1240-1245 (1973).

[3] P.G. Noutsios & G.L. Yip, *"Characterisation and modelling of planar surface and buried glass waveguides made by field-assisted K^+ ion exchange"*, Applied Optics, Vol. 31, No. 25, p. 5283-5291, (1992).

[4] N.V. Nikonorov & G.T. Petrovskii, *"Ion-exchange glasses in integrated optics; the current state of research and prospects (a review)"*, Glass Physics and Chemistry, Vol. 25, No. 1, p. 16-55, (1999).

[5] S. Pélissier, F. Pigeon, B. Biasse, M. Zussy, G. Pandraud, & A. Mure-Ravaud, *"New technique to produce buried channel waveguides in glass"*, Optical Engineering, Vol. 37, No. 4, p. 1111-1114 (1998).

[6] C.B.E. Gawith, T. Bhutta, D.P. Shepherd, P. Hua, J. Wang, G.W. Ross, & P.G.R. Smith, *"Buried laser waveguides in neodymium-doped BK-7 by K^+-Na^+ ion-exchange across a direct-bonded interface"*, Applied Physics Letters, Vol. 75, No. 24, p. 3757-3759, (1999).

[7] E.K. Mwarania, J. Wang, J. Lane, & J.S. Wilkinson, "*Neodymium-doped ion-exchanged waveguide lasers in BK-7 glass*", Journal of Lightwave Technology, Vol. 11, No. 10, p.1550-1558, (1993).

[8] A. Brandenburg, "*Stress in ion-exchanged glass waveguides*", Journal of Lightwave Technology, Vol. LT-4, No. 10, p.1580-1593, (1986).

[9] D. Findlay & R.A. Clay, "*The measurement of internal losses in 4-level lasers*", Physics Letters, Vol. 20, No. 3, p.277-278, (1966).

[10] W. Clarkson & D. Hanna, "*Effects of transverse-mode profile on slope efficiency and relaxation oscillations in a longitudinally pumped laser* ", J. of Modern Optics, Vol. 36, No. 4, p.483-489, (1989).

[11] K. Kubodera & K. Otsuka, "*Single transverse-mode $LiNdP_4O_{12}$ slab waveguide laser*", J. of Applied Physics, Vol. 50, No. 2, p. 653-659, (1979).

[12] M. Digonnet & C. Gaeta, "*Theoretical analysis of optical fiber laser amplifiers and oscillators*", Applied Optics, Vol. 24, No. 3, p. 333-342, (1985).

[13] Schott Optical Glass Catalogue, (1996).

[14] M. Svalgaard, C.V. Poulsen, A. Bjarklev, & O. Poulsen, "*Direct UV writing of buried singlemode channel waveguides in Ge-doped silica films*", Electronics Letters, Vol. 30, No. 17, p. 1401-1403, (1994).

[15] M. Svalgaard & K. Kristensen, "*Directly UV-written silica-on-silicon planar waveguides with low loss*", Electronic Letters, Vol. 33, No. 10, p.861-863, (1997).

[16] D. Zauner, K. Kulstad, J. Rathje, & M. Svalgaard, "*Directly UV-written silica-on-silicon planar waveguides with low insertion loss*", Electronics Letters, Vol. 34, No. 16, p. 1582-1584, (1998).

[17] G. Perrone, A. Moro, C. Contardi, & D. Milanese, "*Ion exchanged waveguide in new and active and photosensitive glass*", Electronics Letters, Vol. 36, No. 22, p.1845-1846, (2000).

[18] D. Milanese, A. Fu, C. Contardi, E.R.M. Taylor, & M. Ferraris, "*Photosensitivity and directly UV written waveguides in an ion-exchangeable bulk oxide glass*", J. of Optical Materials, Vol. 18, p.295-300, (2001).

[19] C.B.E. Gawith, A. Fu, T. Bhutta, P. Hua, D.P. Shepherd, E.R. Taylor, P.G.R. Smith, D. Milanese & M. Ferraris, *"Direct-UV-written buried channel waveguide lasers in direct-bonded intersubstrate ion-exchanged neodymium-doped germano-borosilicate glass",* Applied Physics Letters, Vol. 81, No. 19, p. 3522-3524, (2002).

[20] T.A. Strasser, T. Erdogan, A.E. White, V. Mizrahi, & P.J. Lemaire, "*Ultraviolet laser fabrication of strong, nearly polarization-independent Bragg reflectors in germanium-doped silica waveguides on silica substrates*", Applied Physics Letters, Vol. 65, No. 26, p.3308-3310, (1994).

[21] C.B.E. Gawith- *private communication.*

[22] T. Feuchter, E.K. Mwarania, J. Wang, L. Reekie, & J.S. Wilkinson, "*Erbium-doped ion-exchanged waveguide lasers in BK-7 glass*", IEEE Photonics Technology Letters, Vol. 4, No. 6, p.542-544, (1992).

Chapter 4

LANTHANUM FLUORIDE CRYSTAL WAVEGUIDE LASERS

4.1 Introduction

This chapter describes the optical characterisation of novel fluoride waveguide lasers. The first laser action from a dielectric waveguide fabricated by molecular beam epitaxy is demonstrated. The spectroscopy and laser operation of Nd:LaF_3 thin films is characterised, and the design and fabrication of channel waveguide lasers is investigated in a step towards developing integrated optical components on these thin films. Two techniques of producing slab-loaded channel lasers are demonstrated; etching using an argon ion beam and a novel technique using a photo-definable polymer. The waveguide structures reported here constitute the lowest phonon energy dielectric to show laser emission to date, offering the potential of developing compact integrated mid-infrared waveguide sources based on this technology.

4.2 Lanthanum fluoride waveguide lasers

4.2.1 Mid-IR waveguide sources

Fluoride waveguide lasers offer the potential to develop compact integrated laser sources that operate in the mid-IR. In recent years growing environmental concerns and increasingly stringent safety regulations have provided a strong incentive to develop low-cost, portable, room temperature laser gas sensors that operate in the mid-IR wavelength range (2 -20 μm). The mid-IR encompasses strong fundamental molecular absorptions bands of many atmospheric pollutants and toxic gases, including many hydrocarbons and greenhouse gases. Laser based gas sensors offer an exceptional combination of selectivity, real-time monitoring and sensitivity (detection down to parts-per-billion are readily achievable), however, their use has been limited because of the prohibitively high cost. The development of cheap, mass-producible sources for trace gas sensors would have a strong impact on quality control in many industries, especially for monitoring of toxic gases from industrial smokestacks and landfill sites and on-line monitoring of vehicle emissions and other environmental pollutants.

Solid-state guided-wave devices offer a promising route to the production of these types of mid-IR sources due to their inherent compactness, ruggedness and reliability. Mid-IR semiconductor diode technology is well established, and small bandgap Pb-salt based mid-IR diode lasers are commercially available. Although these diodes have been demonstrated to be suitable for trace-gas monitoring applications [1], they only operate below room temperature and the required cooling apparatus increases both the cost and size of these systems. These diodes are also typically less robust, less reliable and more difficult to fabricate than their near-IR counterparts (GaAs and InP). A more promising semiconductor based system, and one that is a very active area of research, is the quantum cascade laser [2,3]. These have the advantage that they are based on more mature GaAs and InP technology, and achieve mid-IR emission by a multi-step cascade process. Their cascaded nature means that these devices have efficiencies typically orders of magnitudes greater than those of diode lasers, and these lasers are now reaching cw operation at room temperature [3].

Progress is also being made in RE-doped dielectric waveguide devices. The optical confinement of both planar and fibre geometries means that optically-pumped dielectric waveguides can offer low thresholds and high efficiencies. They also have the potential for cw operation at room temperature, with the additional benefits of energy storage for q-switched applications. The limiting factor in achieving mid-IR emission from RE-doped dielectric materials is the non-radiative decay of the excited states of RE ions via multi-phonon emission. Consequently there has been considerable interest in the development of waveguide devices with low phonon energy materials such as fluorides. Most notable is the success of fluorozirconate (ZBLAN) fibre waveguides [4-7]. These have been demonstrated at wavelengths up to 3.9μm, [4], and an output power of nearly 700 mW has been

reported from a diode-pumped device at 2.7 μm, [5]. Demonstrations of laser action in fluoride planar geometries have so far been quite limited, with only reports of near-IR operation of Nd:YLF grown by liquid-phase-epitaxy [8], Nd-doped fluoroaluminate glass by spin coating [9], and this work on Nd:LaF_3 thin films fabricated by MBE [10].

4.2.2 MBE LaF_3 thin-films

MBE is a well-developed and versatile thin-film growth technique, which in principle is a straightforward deposition process in which thermally generated molecular beams are crystallized on a suitability-orientated substrate. The main attributes of MBE are a low growth temperature, which limits diffusion and maintains hyper abrupt interfaces, and low growth rate, which allows very accurate mono-atomic layer control. Although MBE is most widely used for the production of semi-conductor devices, several groups around the world have studied the growth of fluorides [10-13]. Rare-earth-doped ZnF_2, PbF_2, CaF_2, and LaF_3 have all been grown with various substrate materials, including GaAs and Si, however, excluding the work here, no laser action has been reported.

MBE offers an attractive method for the fabrication of fluoride waveguide lasers. Epitaxial thin films with the correct stoichiometry can be produced at low growth rates, allowing accurate control over both layer thickness and composition [14], and at low temperatures, which has been shown to be favourable for the incorporation of RE ions into the fluoride host [15]. Separate growth cells can be used for the host and RE dopant, which allows the doping level to be easily varied and optimised. There is also the potential for more sophisticated waveguide engineering as the thin film composition can be varied by changing the molecular beam fluxes to provide the desired refractive index or doping profile; the latter, for example, could be used for spatial mode control [16].

LaF_3 has a number of properties that make it attractive for active waveguide structures. In contrast to divalent flourides, the LaF_3 crystal lattice can accommodate triply ionised RE ions (such as Nd^{3+} and Er^{3+}) substitutionally into the La crystal site, without suffering from charge compensating defects or RE cluster formation. LaF_3 doped with Nd was in fact one of the first non-oxide based materials to show cw laser emission at room temperature [17]. In common with other flouride materials LaF_3 has low phonon energies, with a maximum phonon energy of between 350-400 cm^{-1} [18] which compares favourably with that of ZBLAN (520 cm^{-1}), offering the potential of developing mid-IR sources.

To prepare high quality waveguiding structures using MBE growth methods, it is necessary to meet a number of material requirements simultaneously. The doped active layer must have a refractive index larger than that of the adjacent material to confine the optical mode, there must be lattice match between the substrate and grown layer to facilitate epitaxial growth and the difference in thermal expansion co-efficients must as small as possible to reduce strain induced crystal defects. The

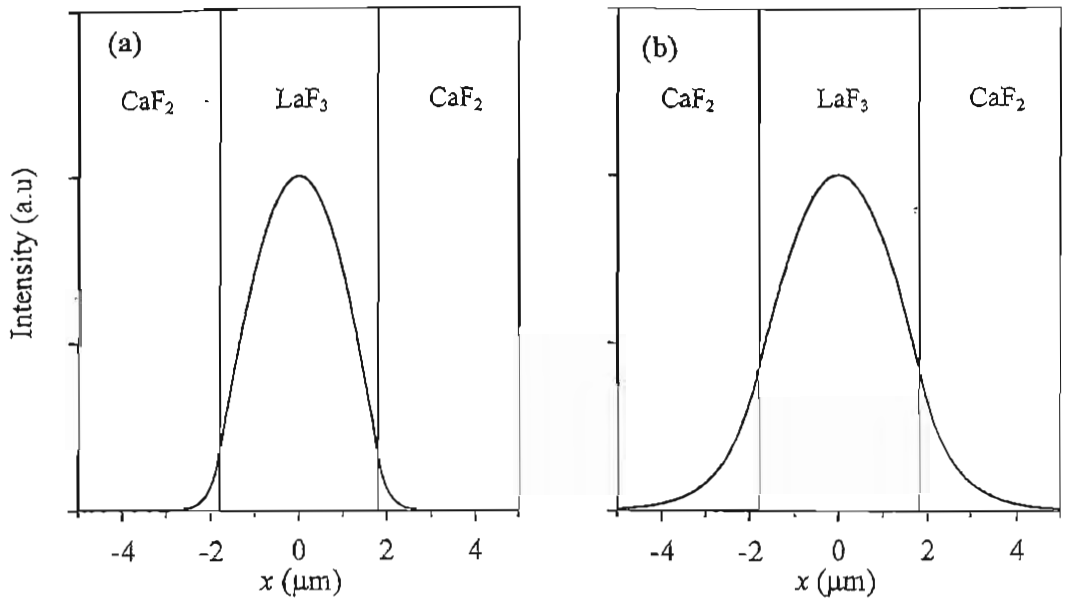

Figure 4.2.1 Predicted fundamental mode of LaF_3/CaF_2 MBE thin films at a wavelength of **(a)** 1 μm **(b)** 3 μm

growth of LaF_3 on CaF_2 substrates meets these requirements well [10]. Both (111) orientated CaF_2 and the tysonite structure of LaF_3 display a hexagonal surface arrangement of ions with lattice constants of 3.864 Å and 4.148 Å respectively, and they have closely matched thermal expansion co-efficients (α=19 x10^{-6} K^{-1} and 17 x 10^{-6} K^{-1}, respectively). Furthermore, there is a large difference in refractive index between the CaF_2 substrate and the LaF_3 thin film [19,20], which results in high NA (~0.7) structures that allow strong optical confinement in small core waveguides at both near-IR wavelengths and into the mid-IR. As an example figure 4.2.1 shows the calculated mode profiles for these structures (for a typical active region depth of 3.6 μm) at a wavelength of 1 and 3 μm. For the first demonstration of laser action from RE-doped waveguides fabricated by MBE, and as an initial step towards developing mid-IR waveguides, Nd-doped LaF_3 thin films operating at near-IR wavelengths are investigated and characterised.

4.3 Nd:LaF_3 thin film laser

4.3.1 MBE Nd:LaF_3 thin-film fabrication

The thin films used in the reported work were fabricated by our collaborators at the Laboratoire d'Analyze et d'Architecture des Systèmes (LAAS) in Toulouse, France. The MBE chamber used to fabricate our thin films is equipped with eight Knudsen effusion cells, however only three of these were used to produce the Nd-doped LaF_3 on CaF_2 structures. The first cell was loaded with a CaF_2 crystal for the growth of the cladding layer, and the other cells were loaded with LaF_3 crystal pieces and NdF_3 compacted powder, for the production of the Nd:LaF_3 active layer. Each of the three cells were calibrated separately, by growing separate films of the constituent compounds to determine the dependence of growth rate on cell temperature. The temperature of the cells could then be varied to give accurate control over the layer thickness and composition of the final structure. In particular, the use of two separate cells for the host and dopant, allowed the doping level to easily be changed by varying the NdF_3 beam flux, to optimise the Nd to LaF_3 content of the active layer. High - resolution spectroscopy of thin films with varying composition was used to determine the optimum doping level, which was found to be 1 at% for the Nd-doped films [21].

Before carrying out the growth of the thin film, the CaF_2 substrates were degreased using hot trichloroethylene and acetone, and then rinsed with de-ionised water before being mounted onto a molybdenum block (using indium soldering) and placed in the chamber. The substrate was then prepared for the growth of the active layer by preheating it (to a temperature above 600°C) under vacuum to ensure the surface was oxygen-free. The rare-earth-doped LaF_3 layer was then grown under ultra-high-vacuum on this prepared substrate using the LaF_3 and NdF_3 cells at temperatures of 1165°C and 993°C, respectively. Under these conditions a thin-film growth rate of 0.6 μm per hour was obtained.

4.3.2 MBE Nd:LaF_3 thin film characterisation

The MBE grown thin film was characterised in terms of spectroscopy, propagation loss and laser performance using a 3.6μm-thick Nd:LaF_3 guide with a 0.5μm CaF_2 cladding layer, cut and polished to a length of 7.5 mm. The maximum phonon energy of the Nd:LaF_3/CaF_2 MBE thin films was investigated by Raman spectroscopy using a Renishaw Raman microscope system and a 20 mW Helium-Neon laser (λ = 633 nm). The resulting spectrum is shown in figure 4.3.1 overleaf, along with that obtained from a bulk LaF_3 crystal. As can be seen, the two spectra are similar, and indicate a maximum phonon energy of 380cm^{-1} for the thin film, which is consistent with previously reported values for LaF_3 [18].

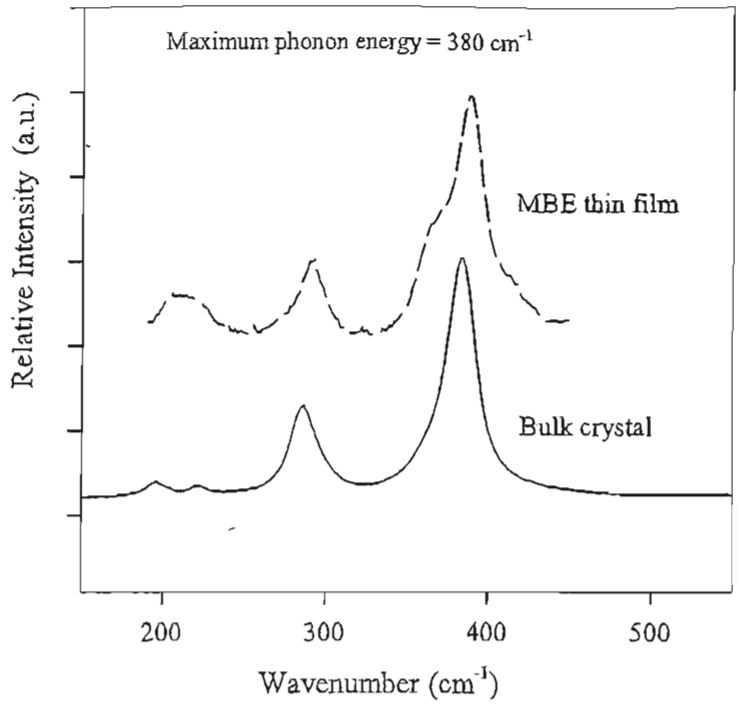

Figure 4.3.1 Raman spectra of bulk and MBE grown thin film LaF_3.
(the thin film spectra is offset for ease of comparison)

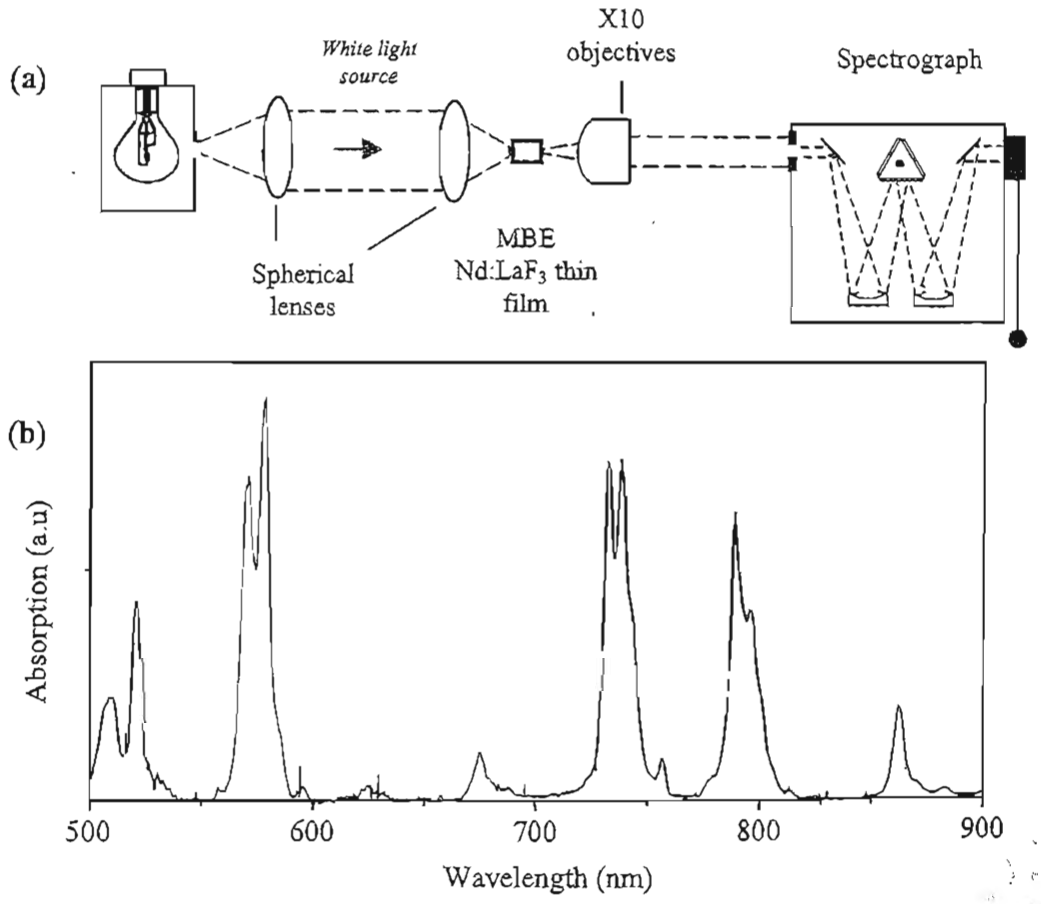

Figure 4.3.2 (a) Apparatus for white light absorption spectroscopy.
(b) Unpolarised absorption spectra (corrected for the response of the system).

Unpolarised absorption spectroscopy was carried out using a tungsten lamp white light source. The light was coupled into the waveguide using a large numerical aperture lens and the output was imaged with a microscope objective, into a Princeton Applied Research digital triple grating spectrograph with a silicon CCD detector array as shown in figure 4.3.2(a). The resulting absorption spectrum was corrected for the system response, which was measured with the waveguide removed from the apparatus, and is shown in figure 4.3.2(b). The spectrum is in good agreement with that of the bulk crystal [22].

Emission spectroscopy was carried out using the apparatus shown in figure 4.3.3(a) at room temperature with the Ti-sapphire laser tuned to 792 nm to excite the $^4F_{5/2}$ level of the Nd ion. The resulting luminescence was detected using an optical spectrum analyser, via a polariser and pump filter. The energy level diagram [23] and spectra for the $^4F_{3/2} - {}^4I_{11/2}$ transition around 1064 nm is shown below in figure 4.3.3, and is in good agreement with that of bulk Nd:LaF_3 [24]. A resonator was formed by attaching two plane dielectric mirrors to the polished end faces of the waveguide with fluorinated liquid for adherence. The MBE thin film gave TM polarised laser emission (corresponding to the π polarisation of the crystal) at 1.064 μm as would be expected from the fluorescence spectra (figure

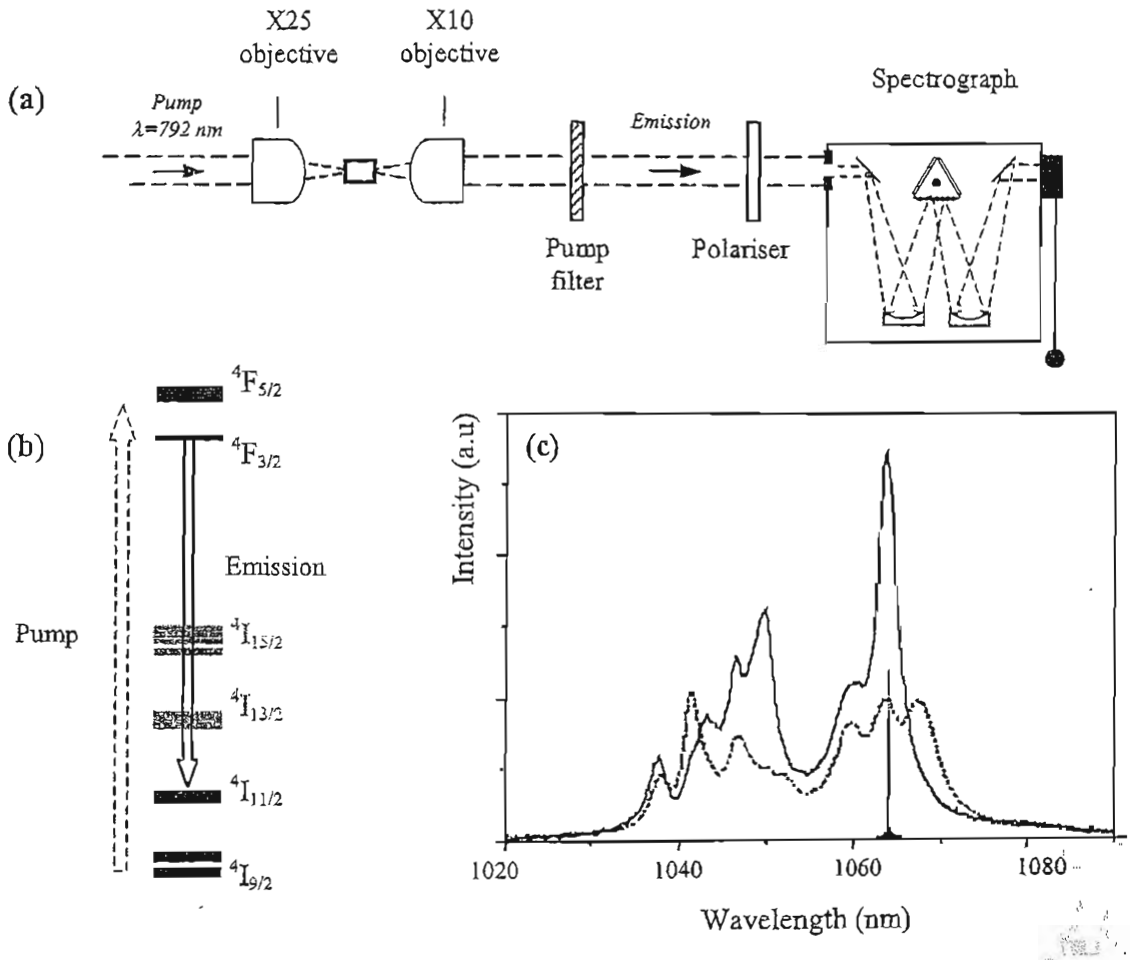

Figure 4.3.3 (a) Apparatus for emission spectroscopy.
(b) Energy level diagram for Nd:LaF_3, [23] showing pump and fluorescence transitions.
(c) Polarized emission spectra for the $^4F_{3/2} - {}^4I_{11/2}$ transition (line : π polarisation, dots : σ polarisation). Also shown is the π polarised laser emission at 1.064 μm (solid black).

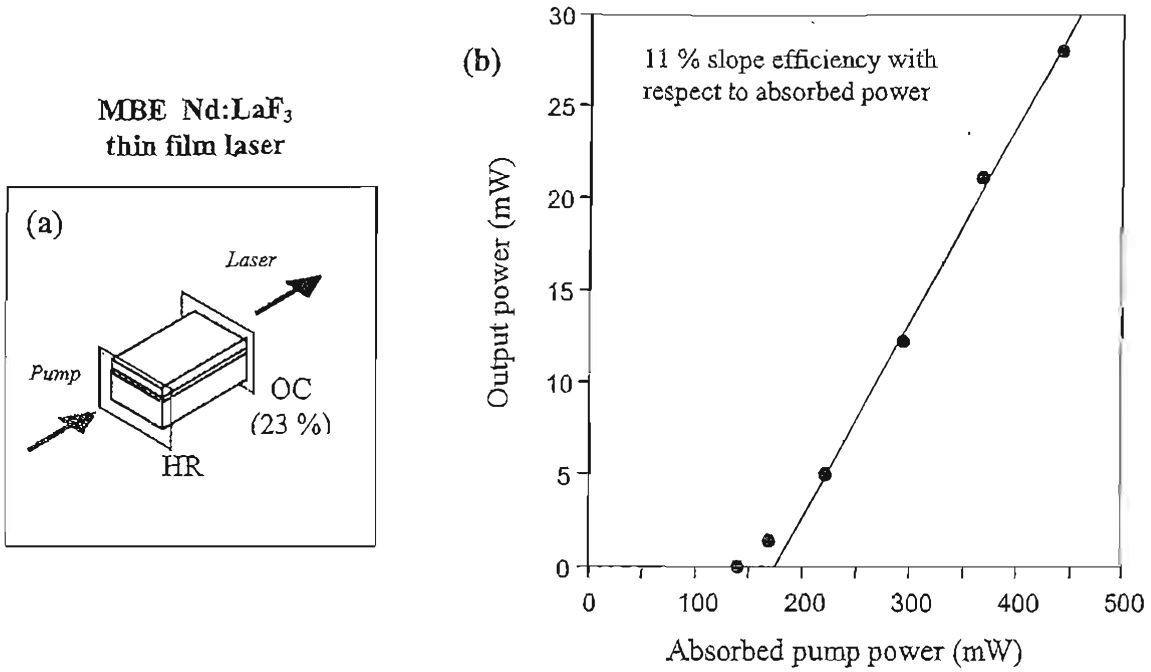

Figure 4.3.4 (a) Laser resonator (b) Output power as a function of absorbed pump power

4.3.3(c)). Using two highly reflecting mirrors a minimum absorbed pump-power threshold of 85 mW was achieved. By changing the output mirror to one with a transmission of 23%, the threshold rose to 140 mW and with this output coupling a maximum laser output power of 28 mW (for the available 440 mW of pump power) and a slope efficiency of 11 % was achieved, as shown in figure 4.3.4.

The optical loss of the thin film was estimated by the Findlay-Clay method as described in section 3.2.3 of chapter 3. The variation of laser threshold with different output couplers is shown in figure 4.3.5, and indicates that our planar thin film have quite a high propagation loss of 1.2 dB/cm. Nevertheless, the first laser action from a thin film fabricated by MBE had been demonstrated.

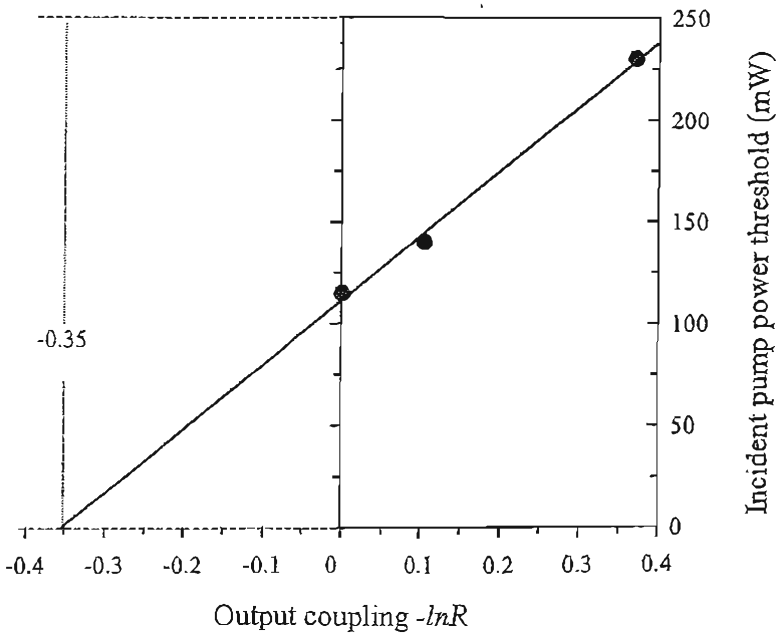

Figure 4.3.5 Findlay-Clay plot for MBE Nd:LaF_3 thin film

4.4 Nd:LaF_3 channel waveguide lasers

4.4.1 Slab-loaded channel waveguides

Channel waveguides have a number of advantages over their thin film counterparts that make them attractive sources for low power applications. The additional lateral confinement of both the pump and laser modes means that lower threshold devices are possible while, if additional propagation losses can be kept low, good slope efficiencies can be maintained. The channel geometry also provides a more circular spatial output, making them more compatible for low-loss coupling to fibre optic components. In addition, both passive and active channels can be integrated with other components on a single planar substrate to produce integrated optoelectronic circuits.

The work reported here describes the design, fabrication and laser operation of slab-loaded channel waveguides. Slab-loaded channels can be fabricated by using micro-structuring techniques to fabricate a strip layer, of lower refractive index, over the light guiding core. These provide lateral confinement of the pump and laser modes because the effective refractive index experienced by the guided light is higher in the regions underneath the strip layer than in the adjacent planar areas which have an air cladding (figure 4.4.1(a)). Compared to other channel structures, these structures have the advantage that no modification of the active layer is required, making them suitable for the first demonstration of channel waveguides on MBE LaF_3 thin films.

Two techniques of fabricating slab-loaded channel lasers on Nd:LaF_3 thin films are investigated and discussed in the following sections. The first is via etching using an argon ion-beam and the second is a novel method for producing slab-loaded channel lasers using an organic photo-definable polymer, benzocyclobutene (BCB). These structures were designed using a commercial modelling package (BBV Selene), using the refractive index values in table 4.4.1 (b) to calculate the predicted mode profiles by the effective index method.

(a)

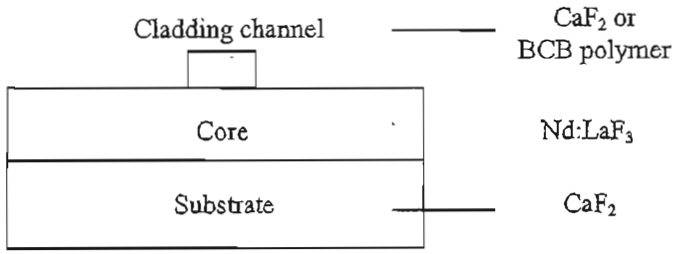

(b)

Wavelength(μm)	CaF_2 [20]	LaF_3 (n_e) [19]	BCB [25]
0.79	1.43065	1.59189	1.5512
1.06	1.42856	1.58922	1.5448

Figure 4.4.1 (a) Schematic slab-loaded channel waveguide and materials combinations used.
(b) Refractive indices of component materials.

4.4.2 Ion-beam etched channel design and fabrication

Ion-beam etching (or physical sputtering) is a versatile and accurate micro-structuring technique [26] and has been used to fabricate low-loss channel waveguide lasers on dielectric thin films [27]. The main attraction of ion-beam etching is that a high degree of control can be achieved. The ion energy, ion current density, etch angle and background pressure can all be varied independently to obtain optimum results.

To produce slab-loaded structures, a thin film with a cladding layer is required. Photolithography can then be used to prepare a positive-relief photoresist mask of the channels on this film so that when it is ion-beam etched the exposed areas of the cladding are removed to structure the thin film. For our Nd:LaF_3/CaF_2 MBE thin films, with a 3.6 μm core and 0.3 μm cladding, this results in the type of structure shown in figure 4.4.2(a). The example shown is for a 8 μm wide channel, which confines the mode in the plane of the thin with a predicted (average, 1/e) mode spot size of 13.2 μm at the laser wavelength (1064 nm). However, this idealised type of structure requires very accurate control over the fabrication process to etch exactly the right depth of material and so is difficult to produce from a practical point of view. If the channel is under etched, then this can significantly reduce the optical confinement of the slab-loaded structure, for example if 0.1 μm of cladding remains on the surface of the 8 μm wide channel, the fundamental mode spot size almost doubles to 24.7 μm as illustrated in figure 4.4.2(b). If the structure is over etched by the same amount, removing 0.1 μm of the active layer, this should provide an adequate safety margin to ensure that all the cladding is removed in the areas adjacent to the channels. This type of design, that can be thought of as a slab-loaded/rib hybrid channel also results in stronger optical confinement than the ideal slab-loaded structure, as illustrated in figure 4.4.3(a) for the 8 μm wide channel with a fundamental mode spot size of 8.3 μm.

This hybrid design also provides stronger confinement than the equivalent rib channel structure shown in figure 4.4.3(b), where 0.1 μm deep ribs are etched on an unclad film, giving a fundamental spot size of 12.2 μm. Our design also minimises the invasive nature of conventional rib structures and preserves the advantages of a protective cladding layer of slab-loaded structures (which, as discussed later, proved to be a very useful design feature).

The hybrid slab-loaded/rib structures were fabricated using a photolithographic mask prepared using Microposit S1828 photo-resist spun on to the clad thin film to produce a 3 μm thick resist layer. The resist-covered film was baked for 10 minutes at 90°C, before being exposed to a UV lamp through a patterned chrome mask and developed to remove the unexposed regions of photo-resist. The masked film was then baked for a further 30 minutes at 120°C, to remove any residual solvents and mounted in the ion-beam chamber on a rotating holder, at an angle of 40° [27]. The structures were etched using an argon-ion beam in an ambient air atmosphere at a pressure of

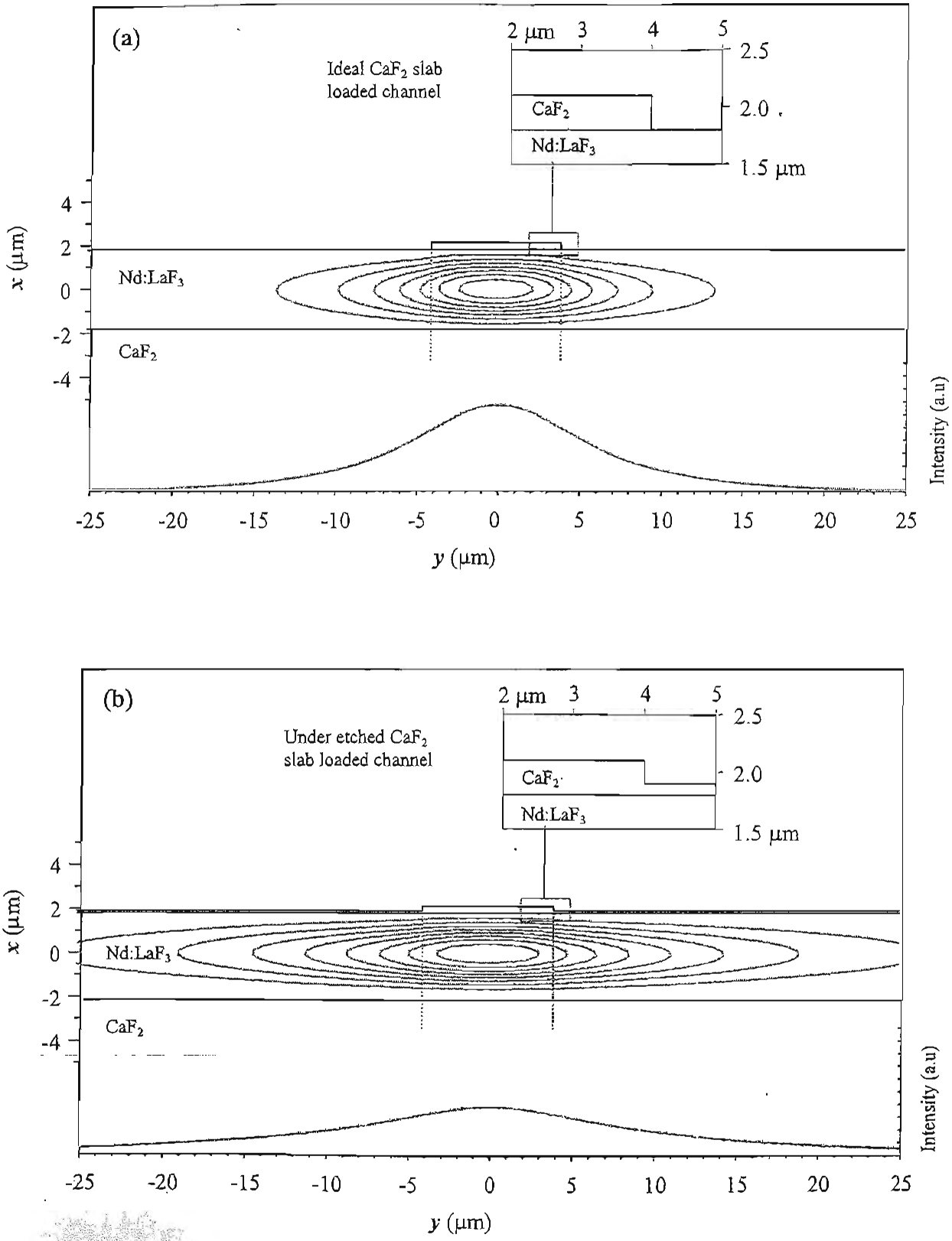

Figure 4.4.2 Channel structure and predicted fundamental mode profiles for 8 μm wide
(a) Ideal slab-loaded structure **(b)** 0.1 μm under-etched slab-loaded structure
(Inset: enlarged channel structure. Bottom: averaged *y* mode profile at λ=1064 nm)

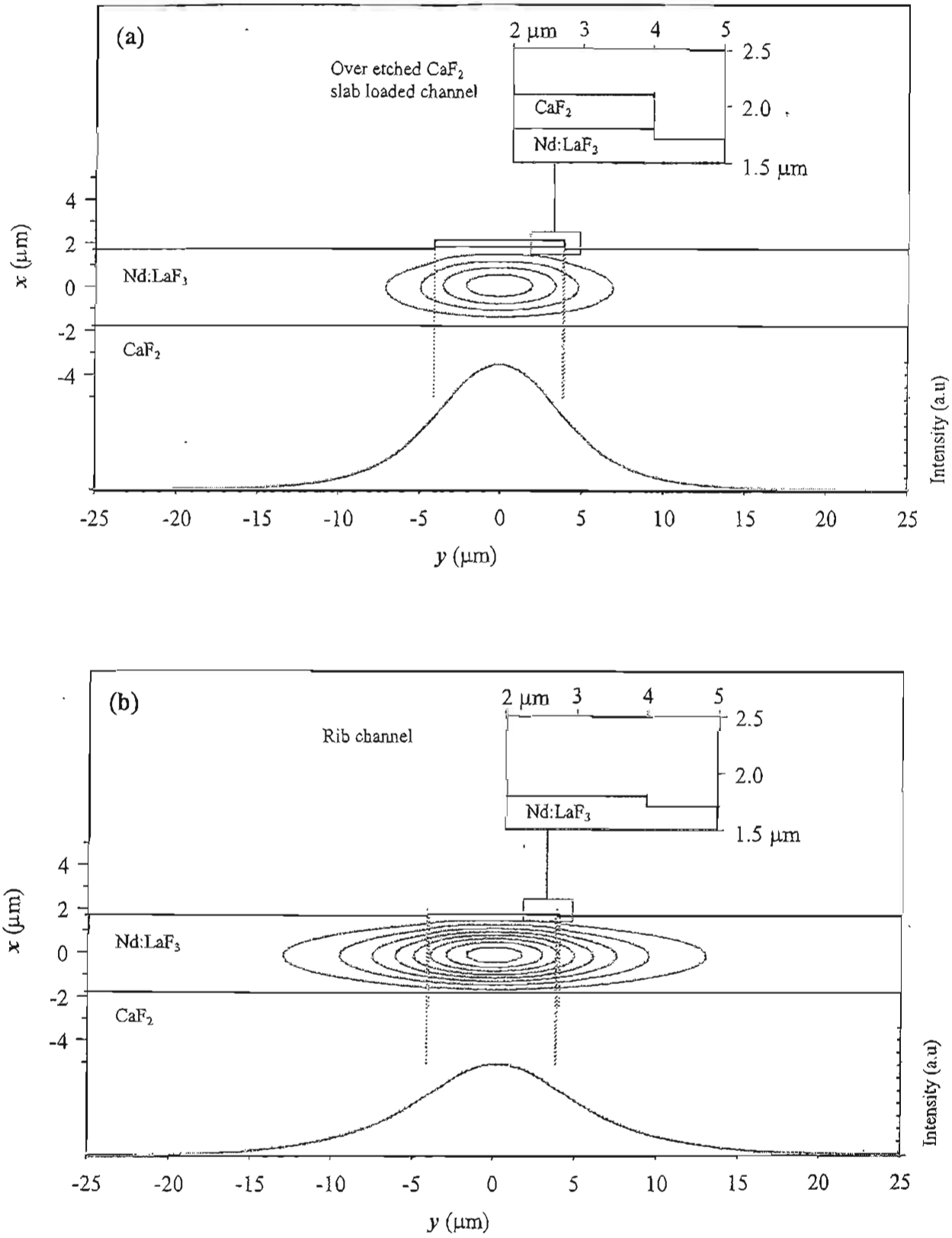

Figure 4.4.3 Channel structure and predicted fundamental mode profiles for 8 µm wide (a) 0.1 µm over etched slab-loaded/rib structure (b) 0.1 µm deep rib structure (Inset: enlarged channel structure. Bottom: averaged *y* mode profile at λ=1064 nm)

1.3×10^{-6} mbar with the argon-ion energy set to 500 eV and the ion current density to 0.45mA/cm^2. The thin film was etched for a total 14 minutes to remove 0.4 μm of the unprotected regions of the thin film to produce the hybrid channel design.

A number of structures were successfully produced, with widths of 8, 11, 13, 17 and 20 μm, however some post-fabrication problems were encountered. It was not possible to remove all the photoresist remnants from the top of some of the structures using either acetone or nitric acid (more abrasive methods could not be used due to the fragility of the structures). However, it is unlikely that these photoresist remnants significantly effect the operation of the device, as the scattering loss is not likely to be very high due to the negligible pump and laser mode intensities expected at the cladding-air interface.

4.4.3 BCB-overlay channel design and fabrication

As an alternative approach to ion-beam etching, channel waveguides were fabricated using BCB polymer overlays. The low-cost of polymer materials, combined with their versatility (in terms of waveguide geometry, material properties and architecture [28]) makes them very attractive for the fabrication of integrated optical components. Specifically, benzocyclobutene (BCB) is an organic polymer with excellent planarisation, low moisture uptake, good adhesion and thermal stability [29]. Although BCB was originally developed as a thin-film dielectric coating for use in electronic multi-chip-modules [29], its low optical loss (0.8 dB/cm at 1.3 μm) and refractive index of 1.5489 [30] (at 0.8 μm), makes it suitable for combining with LaF_3 planar films to make slab-loaded channel waveguide structures. BCB has previously been used to produce passive waveguide components [30], however (to the best of the author's knowledge) the reported work represents the first active channel device that incorporates this polymer.

BCB is available from DOW Chemical in a photosensitive form, which can be processed by using standard photolithographic techniques alone without the need for any etching. This greatly reduces both the time and cost of fabrication (compared to methods such as ion-beam etching) making it an attractive means for fabricating slab-loaded structures, from both a commercial and practical point of view.

Our collaborators at LAAS, fabricated the BCB channels on an unclad thin film, which originally consisted of a 3.6 μm deep Nd:LaF_3 layer on a CaF_2 substrate. The BCB can easily and quickly be applied to the thin film by spin coating, and then processed using the standard photolithographic techniques. To achieve a 3.5 μm thick layer, the BCB was spun on to the film at 4000 rpm for 30s, after an acceleration time of 30s, and was then pre-baked at 80°C for 95s in air to remove any residual solvents. The waveguides were patterned by placing the prepared sample in contact with a patterned chrome mask and exposing it to a UV lamp. After exposure, the sample was developed by immersing

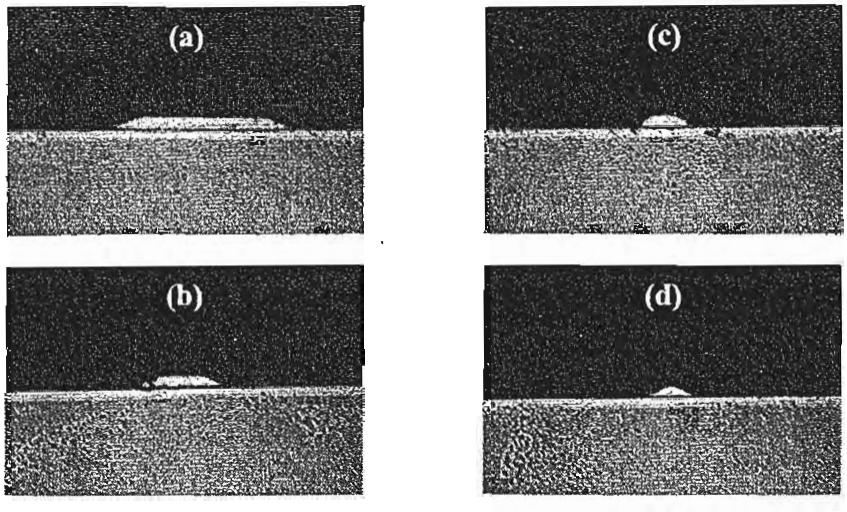

Figure 4.4.4 Completed BCB channel waveguide structures viewed through microscope with widths of (a) 50 μm (b) 20 μm (c) 10 μm (d) 5 μm

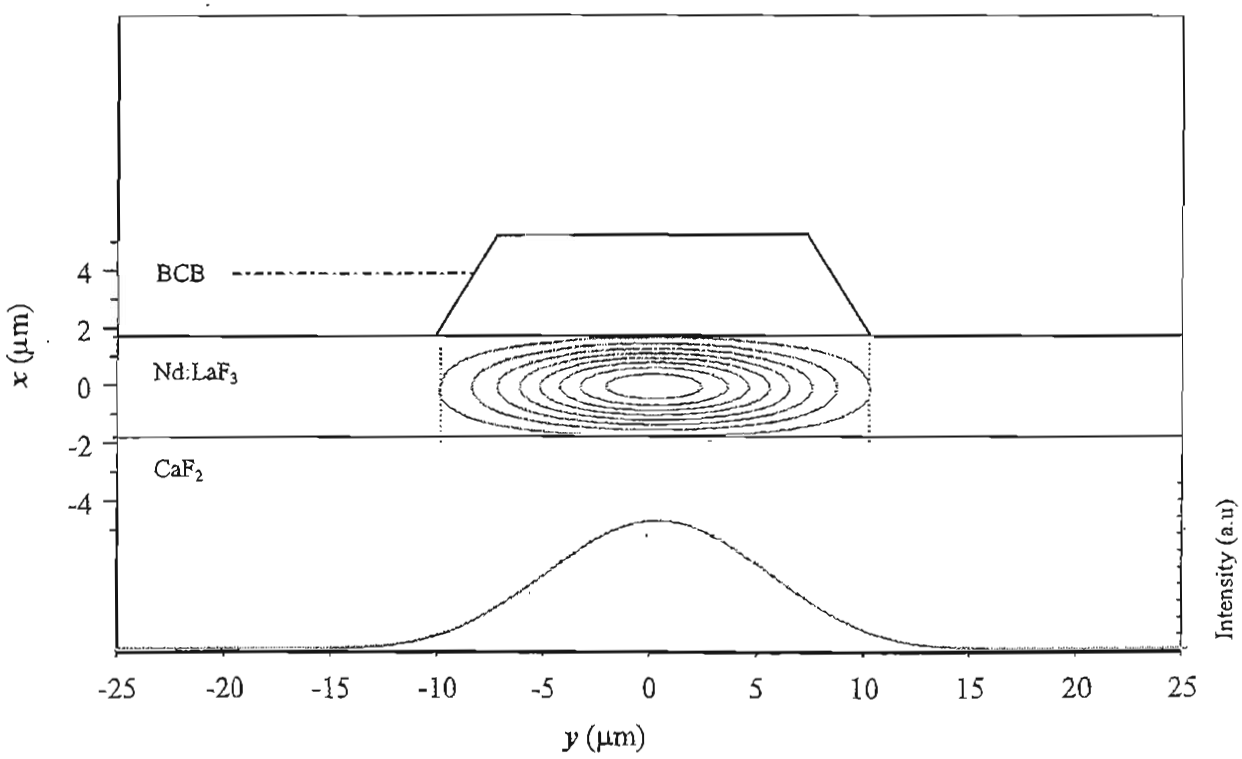

Figure 4.4.5 Channel structure and predicted fundamental mode profiles for 20 μm wide BCB channel

it in solvent to remove the unexposed regions of the BCB, leaving the channel structures. To complete the processing, the BCB was polymerised by curing it at 250°C for one hour in a tube furnace under nitrogen flow. The sample displayed well-defined channels and showed a smooth surface between these structures. The adherence of the BCB to the Nd:LaF_3 was sufficient to allow a standard end-polishing, resulting in waveguides as viewed through a microscope in figure 4.4.4. Similarly to the ion-milled structures, these guides support many modes in the vertical dimension at 1.06μm, and range from single-moded to supporting up to 6 modes in the lateral dimension. However, in comparison to the ion-etched structures the BCB channels provide stronger lateral confinement of the

optical mode due to the greater physical size of the loading strip. Modelling of these guides shows that the strongest lateral confinement at 1.06μm is obtained for the 10μm and 5μm width strips, which both give a mode spot size of around 5 μm. In practice many of our results were taken using a 20μm width BCB strip, as described in the next section, which could support up to 3 lateral modes and had a predicted fundamental mode spot size of 9.7 μm, as illustrated in figure 4.4.5.

4.4.4 Channel characterisation

Both types of channels were mounted on translation stages, which were calibrated in the *y* direction to aid channel alignment and identification, and tested using a Ti-sapphire laser. As with the original thin film, initially, the Ti-sapphire laser output was coupled into the device using a single x 25 microscope objective to produce a circular pump focus at the waveguide input face.

The optical confinement of the ion-beam etched structures was investigated by tuning the Ti-sapphire laser to 800nm and imaging the channel output onto a CCD camera, using another microscope objective (this could not be carried out at the precise pump wavelength of 792 nm because the strong Nd^{3+} absorption leads to a low signal at the CCD camera). The experimentally observed mode profiles for the smallest (8 μm) and largest (20 μm) width channels are presented in figure 4.4.6. For the circular pump input spot matched to the waveguide fundamental mode in the plane of the thin film (*x*-direction) we would expect single mode propagation in this axis for both structures. In the *y*-direction, the 8 μm wide channel should only support a single mode at 800 nm, while the 20 μm channel can, in theory, support two modes and so the modal content of the experimental image for this structure is less certain. Nevertheless, the images certainly show that we have achieved the optical confinement we were aiming for.

As with the thin film, laser operation of the ion-milled channels was achieved by attaching thin dielectric mirrors to the end faces of the guide using fluorinated liquid and pumping at 792 nm. This gave TM polarised laser emission at 1.064μm with pump power thresholds, incident on the input mirror, as low as 26 mW.

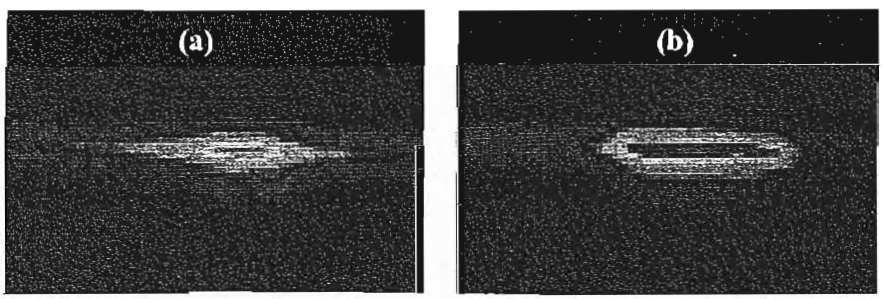

Figure 4.4.6 Pump transmission at 800 nm for ion beam milled channels
(a) 8 μm wide (b) 20 μm wide

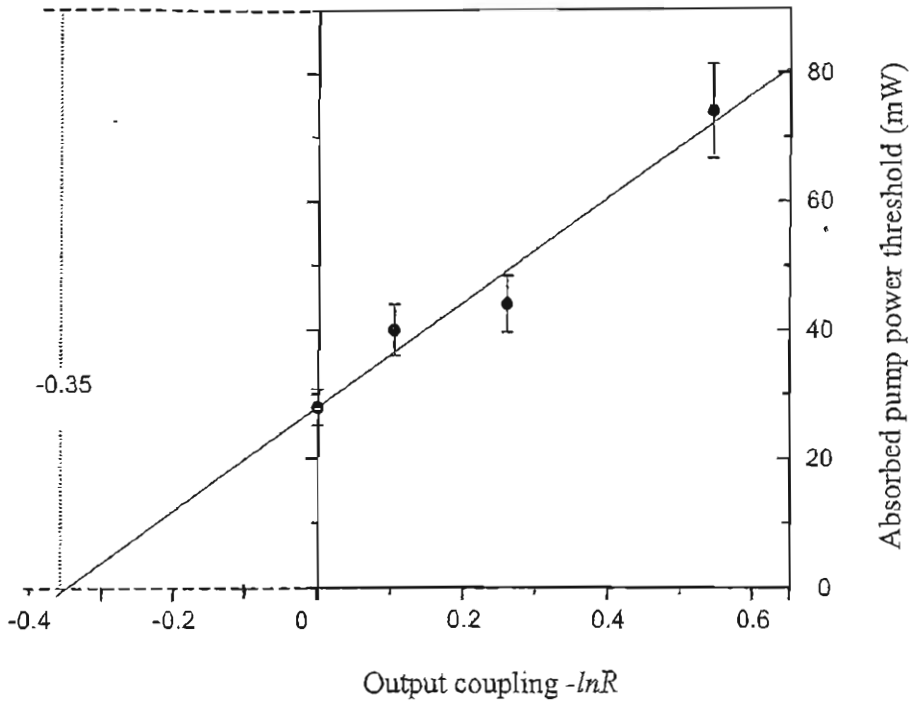

Figure 4.4.7 Findlay-Clay plot for 8 μm wide ion-beam etched Nd:LaF_3 thin film

A range of output couplers were used in an attempt to estimate the channel propagation loss by the Findlay-Clay method, however the small surface area of the channel end-faces made it difficult to ensure good mirror contact and there was variation of approximately 10% in the thresholds between measurements. The results of this analysis for the 8μm wide channel, shown in figure 4.4.7 (the error bars show the threshold variation) suggests a propagation loss of around 1 dB/cm, which is consistent with the value obtained for the planar thin film prior to ion beam milling (section 4.2.3). The continued re-attachment of mirrors quickly led to damage to the end-faces of the waveguide and this damage hindered and limited the full characterisation of these devices so that it was not possible to use beam shaping optics to improve the (~30 %) launch efficiency or to fully investigate the pump and laser optical modes. This damage, combined with the use of launching optics not matched to the asymmetric mode profile of the channels is the most likely cause of the low output power of just 5mW observed when using a 23% output coupler and 300mW of incident power. Nevertheless, despite these problems, a large reduction (x5) in the incident power required to reach threshold compared to the thin film waveguide had already been obtained and the results indicate that lateral confinement can be introduced without significantly increasing the propagation loss.

The BCB channel waveguides were also tested using the same procedure. Once again a large variation in the quality of the channel guides was observed and so it was decided to concentrate on a 20μm wide stripe channel, which gave relatively good performance. However in an attempt to improve the channel performance a cylindrical-lens telescope was used before the launch objective to shape the beam to an asymmetric beam focus better-matched to the expected mode profile of the waveguide (figure 4.4.5).

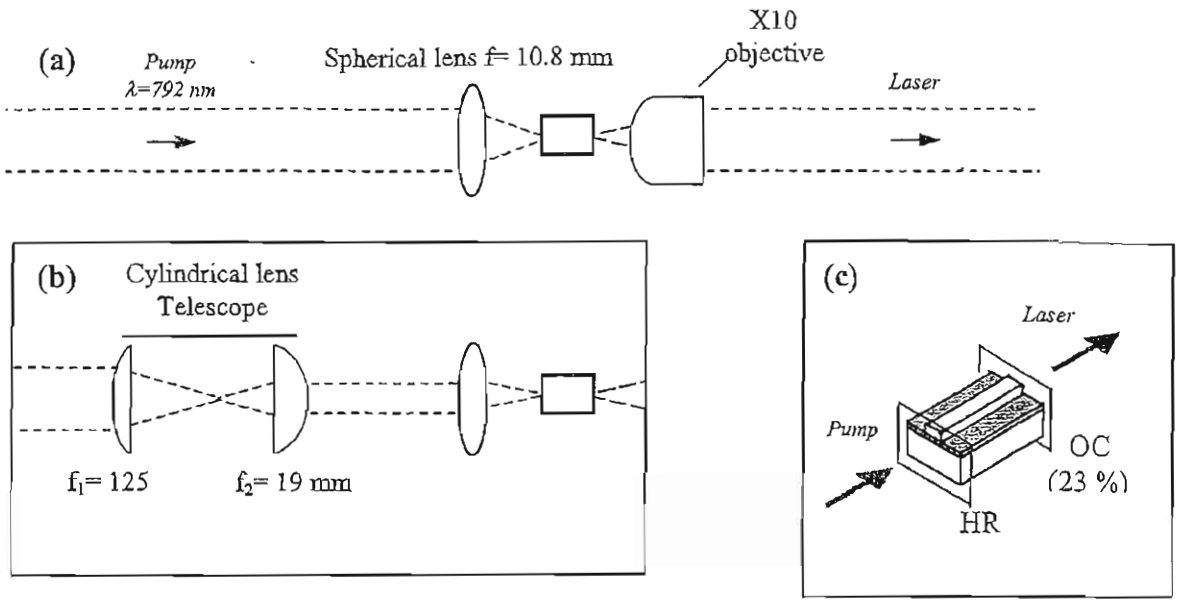

Figure 4.4.8 Experimental testing of BCB channels (top view)
(a) without telescope (b) with cylindrical lens telescope (c) laser resonator

For the 20μm channel the calculated ratio of the mode width to height is around 6.6 and using a telescope of similar magnification as illustrated in figure 4.4.8 it was possible to increase the measured launch efficiency from 30% (with no telescope) to as high as 73%. Using a final spherical focussing lens of focal length 10.8 mm and a 23% output coupler the laser results shown below in figure 4.4.9 were achieved.

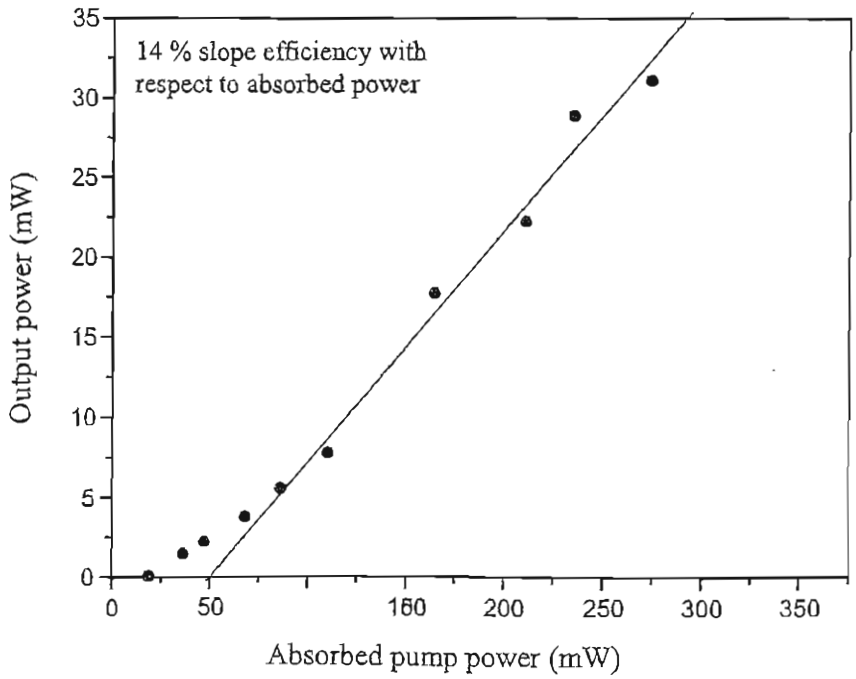

Figure 4.4.9 Output power as a function of absorbed power for 20 μm BCB channel.

The efficiency of 14% with respect to absorbed power is similar to 11% efficiency observed in the planar thin film using the same output coupling. The lowest observed incident power threshold of 17mW for a 23% output coupler is 2.6 times lower in comparison to the ion-etched channels, but this can be attributed to the improved launching optics used in the case of the BCB channels. Before end-face damage preceded too far we were also able to observe laser action at 1.3μm using two highly reflecting mirrors at this wavelength. However, this was using the non-optimised launching optics and so the observed incident power threshold of 250mW could certainly be improved upon.

It was not possible to carry out a Findlay-Clay analysis for these guides because the end-faces again became damaged due to the re-attachment of mirrors. However, the slope efficiency can be used to give an upper limit of the propagation loss. Using the procedure outlined in chapter 3, this gives an upper limit of <2 dB/cm for these structures. This again suggests that a negligible increase in propagation loss has been incurred due the application and structuring of the BCB cladding layer.

Although, the test procedure used to characterise our fragile LaF_3 crystal devices proved to be harmful to the prototype devices reported here and eventually lead to destruction of the channel structures after continued end-face polishing and mirror attachment, the limited results show that high quality slab-loaded channel waveguides can be fabricated on our MBE thin films. The mode profiles show that we have obtained the optical confinement we were aiming for, and the laser operation shows that low threshold devices can be produced.

4.5 Summary

The first dielectric waveguide lasers fabricated by molecular beam epitaxy have been demonstrated. The spectroscopic characterisation of the neodymium thin films shows the MBE process is well suited to producing high quality crystalline structures, with a phonon energy cut-off around 380 cm^{-1}, in good agrement to that found in the bulk crystal. The laser operation of these thin films show that the propagation loss is quite high (1 dB/cm) and future work should concentrate on lowering this loss level to improve efficiency and facilitate low threshold operation. Channel waveguides were fabricated on the thin films by two different methods; ion beam etching and the novel BCB overlay technique. Although an exhaustive characterisation of these devices was not possible due to the fragility of the structures, the results are consistent with a negligible increase in propagation loss compared to the background level of the MBE thin film and the increased optical confinement of the channel geometry leads to a significant reduction in laser threshold. The high index difference between CaF_2 and LaF_3 allows the small core size waveguide designs investigated here to be used for strong optical confinement out to mid-IR wavelengths. The prototype channel devices demonstrated, together with the exceptional control of the MBE fabrication method and possibilities for integration, makes MBE LaF_3 waveguides an interesting candidate for mid-IR laser sources, and this is discussed further in chapter 6.

4.6 References

[1] H.I. Schiff, G.I. Mackay & J. Bechara, *"The use of tunable diode laser absorption spectroscopy for atmospheric measurements"*, in Air Monitoring by Spectroscopic Techniques, M.W. Sigrist, (Ed), Wiley, New York, (1994).

[2] F. Capasso, C. Gmachl, D.L. Sivco & A.Y. Cho, *"Quantum Cascade Lasers"*, Physics World, Vol. 12 No. 6, p. 27-33, (1999).

[3] F. Capasso, R. Paiella, R. Martini, R. Colombelli, C. Gmachl, T. Myers, M. Taubman, R. Williams, C. Bethea, K. Unterrainer, H. Hwang, D. Sivco, A. Cho, A.M. Sergent & H. Liu, E. Whittaker, *"Quantum cascade lasers: Ultrahigh-Speed operation, optical wireless communication, narrow linewidth, and far-infrared emission"*, IEEE J. of Quantum Electronics, Vol. 38, No. 6, p. 511-532, (2002).

[4] J. Schneider, C. Carbonnier & U.B. Unrau, *"Characterisation of a Ho^{3+}-doped fluoride fibre laser with a 3.9μm emission wavelength"*, Applied Optics, Vol. 36, p. 85-95, (1997).

[5] B. Srinvasan, J. Tafoya, & R.K. Jain, *"High-power 'Watt-level' cw operation of diode-pumped 2.7μm lasers using efficient cross-relaxation and energy transfer mechanisms"*, Optics Express, Vol. 4, p. 493, (1999).

[6] S.D. Jackson *"8.8 W diode-cladding-pumped Tm3+,Ho3+-doped fluoride fibre laser"*, Electronics Letters, Vol. 37, No. 13, p. 821-822, (2001).

[7] M. Pollnau & S.D. Jackson, *"Erbium 3-μm fiber lasers"*, IEEE J. of Quantum Electronics, Vol. 7 No. 1, p. 30-40, (2001)

[8] P. Rogin & J. Hulliger, *"Epitaxial Nd:YLF linear waveguide laser"*, Optics Letters, Vol. 22, p. 1701, (1997)

[9] D.W.J. Harwood, E.R. Taylor, C.T.A. Brown, D.P. Shepherd & D.N. Payne, *"Novel fabrication technique for the realisation of planar glass waveguides"*, European Conference on Optical Communications, Madrid, paper WdA34, (1998).

[10] E. Daran, D.P. Shepherd, T. Bhutta, & C. Serrano, *"Laser operation of Nd:LaF_3 thin film grown by molecular beam epitaxy"*, Electron. Letters, Vol. 35, No. 5, p. 398, (1999).

[11] L.E. Bausa, C. Fontaine, E. Daran, and A. Munoz-Yague, *"Molecular beam epitaxy of Nd-doped CaF_2 and $CaSrF_2$ layers on Si and GaAs substrates"*, J. Applied. Physics, Vol.72, p. 499-503, (1992).

[12] R.A. McFarlane, M. Lui, & D. Yap, *"Rare earth doped fluoride waveguides fabricated using molecular beam epitaxy,"* IEEE J. Select. Topics Quantum Electron., Vol. 1, No. 1, p. 82-91, (1995).

[13] J.M. Ko & T. Fukuda, *"Molecular beam epitaxy of $Ca_{1-x}R_xF_{2+x}$ (R=Nd,Er) layers: study of RHEED pattern and lattice mismatch"*, J. of Crystal Growth, Vol. 200, p. 490, (1999).

[14] A.Y. Khilko, S.V. Gastev, R.N. Kyutt, M.V. Zamoryanskaya, & N.S. Sokolov, *"Structural and luminescence studies of CdF_2-CaF_2 superlattices on Si(111)"*, Applied Surface Science , Vol. 123-124, p. 595-598, (1998).

[15] E. Daran, R. Legros, A. Muñoz-Yagüe, C. Fontaine & L.E. Bausá, *"1.54μm wavelength emission of highly Er-doped CaF_2 layers grown by molecular beam epitaxy,"* J. of Applied. Physics, Vol. 76, p. 270-273, (1994).

[16] T. Bhutta, J.I. Mackenzie, D.P. Shepherd & R.J. Beach, *"Spatial dopant profiles for transverse-mode selection in multi-mode waveguides"*, J. of Optical Society of America B, Vol. 19, p.1539-1543, (2002)

[17] Y.K. Voron'ko, M.V. Dmitruk, A.A. Kaminskii, V.V. Osiko & V.N. Shpakov, *"Continuous stimulated emission of an LaF_3-Nd^{3+} laser at room temperature"*, Sv. Phys JETP, Vol. 26, No. 3, p. 400, (1968).

[18] W.M. Yen, W.C. Scott & A.L. Schawlow *"Phonon-induced Relaxation in exited states of Trivalent Praseodymium in LaF_3"* Physics Review, Vol. 136, No. 1A, p. A271, (1964).

[19] R. Laiho & M. Lakkisto, *"Investigation of the refractive indices of LaF_3, CeF_3, PrF_3 and NdF_3"*, Philisophical Magazine B, Vol. 48, p.203-207, (1983).

[20] E.D. Palik, *"Handbook of optical constants of solids II"*, Boston: Academic Press, p. 832, (1991)

[21] F. Lahoz, E. Daran, X. Zhang, A. Muñoz-Yagüe, R. Cases, & R. Alcala, *"Hetero- and homoepitaxial Nd^{3+} doped LaF_3 thin films grown by molecular beam epitaxy: a spectroscopic study"*, J. of Applied Physics, Vol. 86, p. 3699-3704, (1999).

[22] V. Ter-Mikirtychev & T. Tsuboi *"Up-converted luminescence by two- and three photon excitation in LaF_3:Nd^{3+} crystals"* Physical Review B, Vol. 52, No. 21, p. 15027-15030, (1995).

[23] W. Carnell, G. Goodman, K. Rajnak & R. Rana, *"A systematic analysis of the spectra of lathanides doped into single crystal LaF_3"* J. of Chem. Physics, Vol. 90, No. 7, p. 3443-3457, (1989)

[24] T.Y. Fan & R. Kokta, *"End-pumped Nd:LaF_3 and Nd:$LaMgAl_{11}O_{19}$ Lasers"*, IEEE J. of Quantum Electronics, Vol. 25, No. 8, p. 1845, (1989).

[25] S.W. Guo, G. Gustafsson, O.J. Hagel & H. Arwin, *"Determination of refractive index and thickness of thick transparent films by variable-angle spectroscopic ellipsometry: application to benzocyclobutene films"*, Applied Optics, Vol. 35, p. 1693-1699, (1996).

[26] P.R. Puckett, S.L. Michel & W.E. Hughes *"Ion beam etching"* in *"Thin Film Process II"*, J.L. Vossen & W. Kern (Eds), Boston Academic Press, p.749-782, (1991).

[27] R. Gerhardt, J. Kleine-Borger, L. Beilschmidt, M. Frommeyer, H. Dotsch, & B. Gather, *"Efficient channel-waveguide laser in Nd:GGG at 1.062μm wavelength,"* Applied Physics Letters, Vol. 75, p. 1210-1212, (1999).

[28] L. Eldada & L.W. Shacklette, *"Advances in polymer integrated optics"*, IEEE J. Select. Topics Quantum Electron, Vol. 6, p. 54-68, (2000).

[29] R. Foster, *"Photoimagable BCB technology lowers costs for MCMs"*, Solid State Technology, Vol. 38, p. 125-130, (1995).

[30] C.F.Kane & R.R.Krchnavek, *"Benzocyclobutene optical waveguides"*, Photonics Technology Letters, Vol. 7, p. 535-537, (1995).

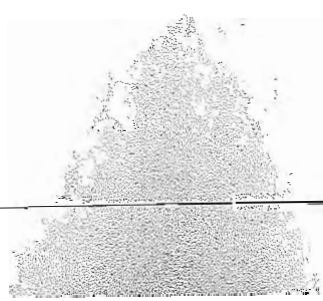

Chapter 5

WAVEGUIDES FOR HIGH AVERAGE POWER LASERS

5.1 Introduction

This chapter reports the development of high-power planar waveguide lasers. Proximity coupling - the direct coupling of diode-bar pump radiation into the waveguide without any intervening optics is investigated. Suitable waveguide structures are considered and 90 % pump coupling efficiencies are demonstrated for RE-doped YAG on sapphire waveguides fabricated by direct-bonding. Double-clad planar waveguides are utilised for spatial-mode control in the guided axis of the waveguide. The theory of transverse-mode selection by confined doping is developed and applied to design a double-clad planar waveguide. The first double-clad planar waveguide is demonstrated using a direct-bonded RE-doped YAG/YAG/sapphire device. This is then combined with proximity coupling to produce a very compact and simple diode-pumped laser system with diffraction-limited performance in the guided axis.

5.2 Pump delivery

5.2.1 Diode-bar pumped lasers

Efficient pump delivery is a critical factor for scaling solid-state lasers to high powers. A typical high power diode pump source is illustrated below in figure 5.2.1. The diode-bar laser consists of a linear array of a number of individual emitters each with typical dimensions of 1 μm by 200 μm, and there are usually about 20 such emitters equally spaced at about 200 μm apart, giving an overall emission aperture of 1 μm by 10 mm. This extremely asymmetric aperture is responsible for an output beam that has highly asymmetric spatial and divergence properties. The divergence in the plane of the array is smaller, however the segmented nature of the aperture results in an output with a very low beam quality, with an M^2 of several thousand. In the vertical plane orthogonal to the emitter array, the beam is near diffraction limited, however the small vertical dimension of the emitter means that this is highly divergent. The effective coupling of this highly divergent, asymmetric, non-diffraction limited pump beam into the laser medium is a major issue for diode-bar pumped lasers. Various techniques have been used in bulk laser systems including multi-prism arrays [1], reflective chambers [2], fibre coupling [3], lens ducts [4] and other beam shaping optics [5], while in fibre lasers, v-groove designs [6] and beam shaping have been combined with cladding-pumped geometries [7]. The planar waveguide has the distinct advantage that it is geometrically well suited to the output of diode-bars, reducing the need for beam shaping and offering the potential to develop systems with efficient and compact pump delivery.

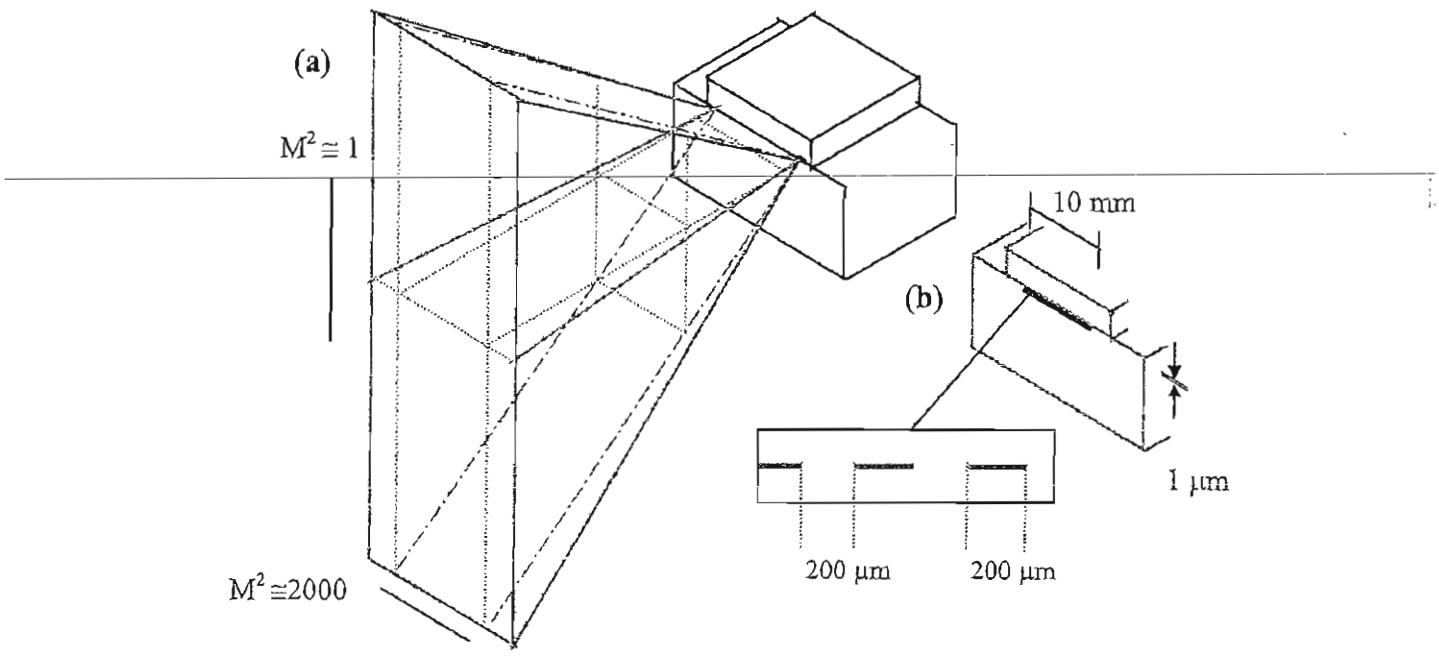

Figure 5.2.1- High power diode-bar pump sources
(a) Typical output beam characteristics (b) Typical emitter-array dimensions

The planar geometry permits three basic pumping configurations; face, end or side pumping, as illustrated in figure 5.2.2. Transversely pumping the waveguide through the largest face of the slab has the attraction of being area-scalable, and recent work has demonstrated that pump powers of 450W can be used by stacking 10 diode-bars across the top face of an Nd:YAG guide [10]. Although face pumping avoids the requirement of launching the pump light into the guide, and consequently does not require precision alignment or micro-optics for the diode-pump, face-pumped waveguides suffer from low single-pass pump absorption, limited by the depth of the active core. To overcome this problem a relatively thick (200 μm) core combined with a rectangular reflectance chamber to allow multiple passes of the pump have been used [8-10]. Although face-pumped configurations have shown the highest output powers to date (>100W) [10], they lose some of the advantages that a guided wave geometry has to offer, such as the high gain that can be achieved by confining the pump.

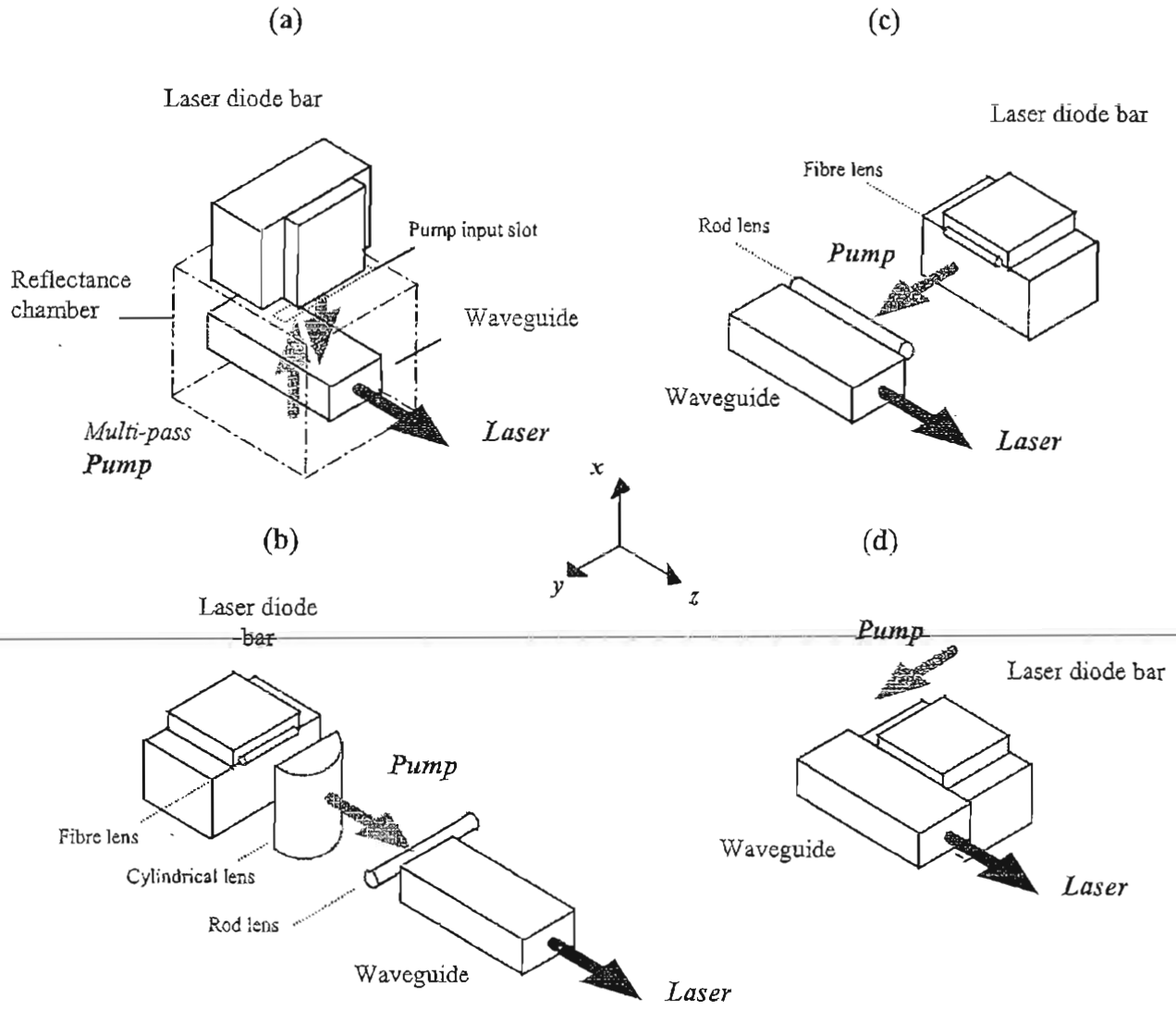

Figure 5.2.2- Examples of high power planar waveguide pumping configurations
(a) Face pumping using a reflectance chamber (b) End pumping using a three-lens system
(c) Side pumping using two lens system (d) Proposed proximity side pumping

In-plane pumping, either longitudinally through the end of the guide [11-13], or transversely through the side of the guide [13-15] allows much smaller waveguide cores and simpler pump delivery schemes. If the waveguide is used to confine the diode light in the fast divergence axis, the pump from a fibre-lens collimated diode can be launched into the guide using a single high NA lens. This has been combined with a cylindrical lens in end-pumped configurations to focus the diode beam in the slow axis. End pumping allows a good match of the pumped volume to the waveguide laser mode in the free propagation axis leading to efficient operation. However, it is limited to a single diode-pump source, whereas side-pumping allows power scaling by stacking diode-bars along both sides of the guide and increasing the guide length. Although the overlap of pump and laser modes may be relatively poor, side-pumping also has the advantage that focussing in the slow divergence axis is not necessary as the guide can easily be made long enough to contain the diode pump beam in this axis. Here the aim is to also eliminate the fast divergence axis coupling optics and directly side-pump the guide via proximity coupling as illustrated in figure 5.2.2 (d).

5.2.2 Proximity coupling

Proximity coupling can be achieved if a waveguide is positioned close to the diode emitters, and if the guide has a sufficient NA and core depth (D) to capture the pump beam, as depicted in figure 5.2.3 for a three-layer symmetric guide. Assuming that the pump has a top-hat distribution in the slow (z) axis and is diffraction limited in the fast (x) axis, for a pump beam propagating in the y direction with the beam waist at the diode emitters (y=0) the pump intensity is given by

$$I_p(x,y,z) = I_0(y)\exp\left(\frac{-2x^2}{[w_{px}(y)]^2}\right) \qquad [5.2.1]$$

Where $I_0(y)$ is the peak intensity and $w_{px}(y)$ is the $1/e^2$ radius spot size in the x-direction at a distance y from the diode-bar. For a waveguide at a distance $y = g$ from the diode bar and if the guide is made long enough to contain the pump beam in the slow axis the power launched into the guide is

$$P(A) = I_0(g)\, l_p \int_{-A}^{A} \exp\left(\frac{-2x^2}{[w_{px}(g)]^2}\right) \partial x \qquad [5.2.2]$$

Where $w_{px}(g)$ and $I_0(g)$ are spot size and peak intensity at the guide input face respectively and l_p is the width of the pump beam in the slow axis. The limit of integration (A) is determined by either the numerical or physical aperture of the waveguide. If the launched power is limited by the physical aperture of the waveguide then $A=x_b$ (the bottom half of figure 5.2.3) and x_b is simply given by the half depth of the waveguide.

$$x_b = \frac{D}{2} \qquad [5.2.3]$$

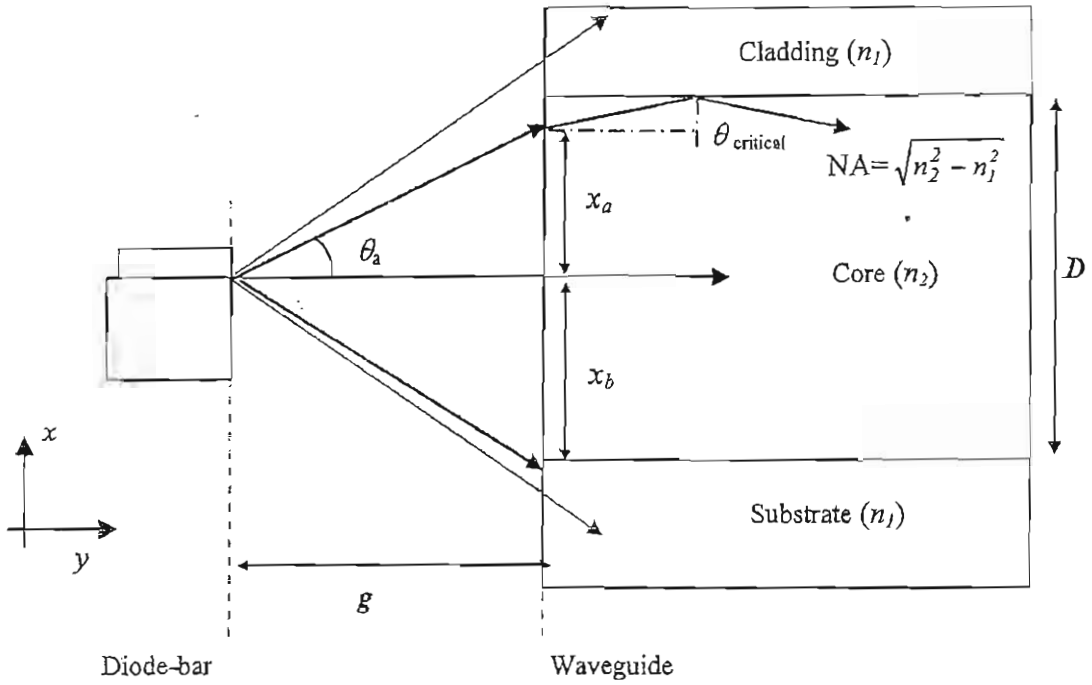

Figure 5.2.3- Schematic of proximity coupling to a three layer symmetric waveguide
TOP: NA limited case **BOTTOM:** Physical aperture limited case.

The second possibility is that the launched power is limited by the numerical aperture or acceptance angle θ_a=$\sin^{-1}$(NA) of the waveguide. In this case $A = x_a = g\tan\theta_a$ (the top half of figure 5.2.3) and x_a can be expressed in terms of the NA by using the trigonometric relationships $\tan\theta_a = \sin\theta_a / \cos\theta_a$ and $\cos^2\theta_a = 1-\sin^2\theta_a$ to give

$$x_a = \frac{g\mathrm{NA}}{\sqrt{1-\mathrm{NA}^2}} \qquad [5.2.4]$$

The limit of integration in equation 5.2.2 is given by which ever is smallest out of x_b and x_a. For $x_b > x_a$ (i.e. $A = x_a$) the power is limited by the numerical aperture of the waveguide, although parts of the beam with $x > x_a$ are incident on the waveguide, they travel at angles greater than those that can be confined by the NA of the waveguide. For $x_b < x_a$ (i.e. $A = x_b$) the power is limited by the physical size of the waveguide, in this case the waveguide has sufficient NA to guide all of the diode beam that is incident on core, but obviously any part of the beam that has $x > x_b$ cannot be launched into the guide. The theoretical launch efficiency η_L is given by the fraction $P(A)/P(\infty)$ where $P(\infty)$ is the total power in the beam, and at $y = g$ is given by

$$P(\infty) = I_0(g) l_p \int_{-\infty}^{\infty} \exp\left(\frac{-2x^2}{[w_{px}(g)]^2}\right) \partial x = I_0(g) l_p \sqrt{\frac{\pi [w_{px}(g)]^2}{2}} \qquad [5.2.5]$$

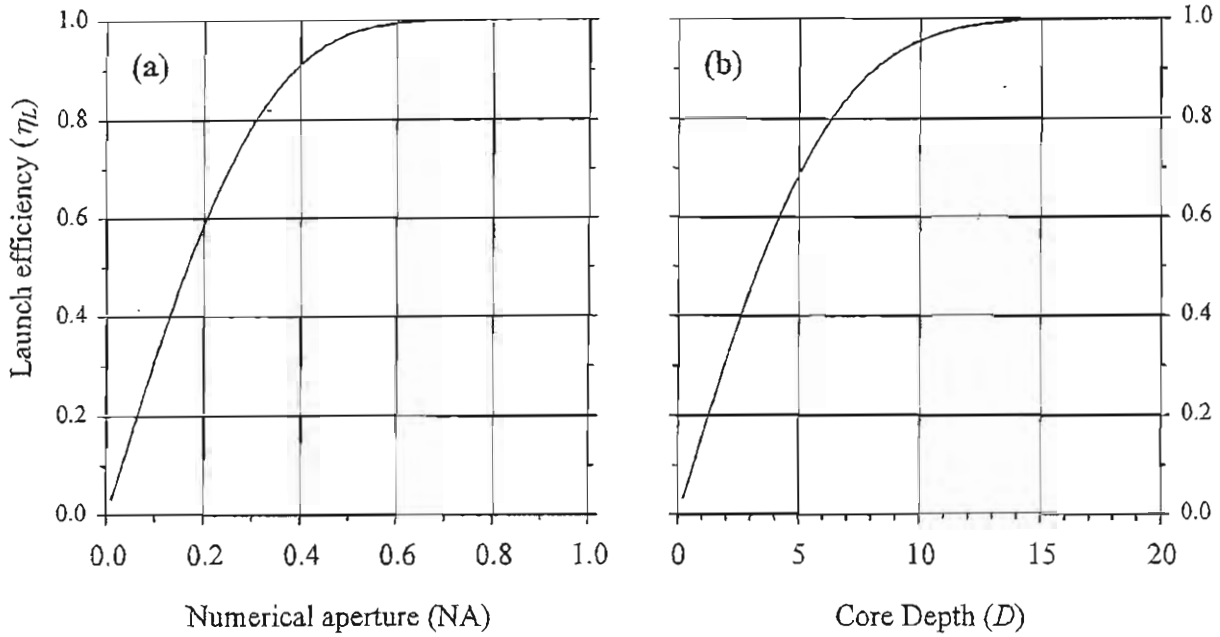

Figure 5.2.4- Predicted launch efficiency for proximity coupled waveguide
(a) Numerical aperture limited case ($x_b > x_a$) (b) Physical aperture limited case ($x_b < x_a$)

Taking the ratio of equations 5.2.2 and 5.2.5 gives the following expression for the launch efficiency via proximity coupling in terms of diode spot size $w_{px}(g)$ at the waveguide input plane, diode to guide separation g, guide NA and depth D.

$$\eta_L = \sqrt{\frac{2}{\pi\,[w_{px}(g)]^2}} \int_{-A}^{A} \exp\left(\frac{-2x^2}{[w_{px}(g)]^2}\right) \qquad A = g\mathrm{NA}\Big/\sqrt{1-\mathrm{NA}^2} \;\; or \;\; D/2$$

[5.2.6]

Figure 5.2.4(a) and 5.2.4(b) shows the pump delivery as a function of core depth D and NA for the physical and numerical aperture limited cases respectively. These were plotted by evaluating equation 5.2.6 for a diode to guide separation g = 10 μm, which represents a practical limit for proximity coupling as the emitters of commercially available diode-bars are commonly recessed by approximately this distance from the diode-bar front facet. The diode was assumed to operate at λ_p=808 nm and the FWHM divergence was taken to be 45° (a typical manufacturers specification for commercially available diode bars [16]), which corresponds to a spot size at the waveguide input plane of $w_{px}(g)$ = 4.98 μm for a diffraction-limited pump beam. As can be seen the model predicts that for efficient proximity coupling (η_L>90%) a waveguide with an NA of >0.39 and core depth D>8μm is required.

There are a few limitations of this model that should be noted. Diode-bar manufacture can often result in the displacement of the centres of individual emitters from each other. If the diode emitters do not form a perfect linear array this may reduce the launch efficiency, in which case these

graphs represent a lower limit for the required core depths and numerical apertures. The analysis also takes no account of parts of the beam travelling at angles beyond the NA of the guide, which would be partially reflected from the outer cladding-air and substrate-air (or heatsink) interfaces. This latter effect would increase the power delivery efficiency, although it is expected that this effect would be small, as on successive passes the power would be diminished due to reflection losses.

5.1.3 Waveguides for proximity coupling

The realisation of an efficient proximity coupled system requires waveguides with relatively high numerical apertures. Such high NAs cannot in general be achieved by incorporating ions into a material to increase the refractive index. RE doping in YAG only produces an index change of the order of 10^{-3} corresponding to an *NA* of less than 0.1 [17,18]. This index change can be increased slightly if other non-active dopants are also included, for example Ga has also been incorporated in LPE grown Nd:YAG on YAG guides [19] to increase the NA to nearer 0.2. However, to achieve efficient proximity coupled systems with launch efficiencies of >90 % an NA>0.39 is required, and it is necessary to use waveguides constructed of different materials. Two techniques that have recently attracted interest for the fabrication of high NA, high-power laser waveguides are direct bonding [27,28] and epitaxial growth by pulsed-laser assisted deposition (PLD) [21-25].

The attractions of using PLD are low cost, accurate control over layer thickness and exceptionally quick deposition times, making it an almost ideal fabrication technique. PLD does have one major drawback; the formation of particulates (macroscopic particles) in the grown layer, which has limited its use for laser waveguides [21]. The epitaxial growth of Nd:GGG on YAG lasers with NAs of 0.75 were first demonstrated by Gill (1995) [22], though the high number of particulates in the grown layer meant that these structures had losses of nearly 6 dB/cm [23]. Later work by Anderson (1997) [24,25] showed that the losses could be reduced to < 0.5 dB/cm if the number of particulates in the grown layer could be decreased, however no direct correlation between the number of particulates, waveguide structure and laser performance was reported. As an initial assessment, the laser performance of a number of unclad PLD Nd:GGG/YAG thin films of varying thickness and particulate densities were considered. These thin films were fabricated by Steven Barrington of the University of Southampton using a pulsed KrF excimer laser (λ=248 nm) to ablate and deposit a crystal Nd:GGG target on a (100) orientated YAG substrate and further details of the fabrication process can be found in Barrington (2001) [26]. The variation of laser threshold with particulate density was investigated using 2 mm long unclad samples of layer thickness 2, 4 and 8 μm and particulate densities ranging from 10^4 to 10^7 per cm^2. The guides were pumped at 808nm by a Ti-sapphire laser launched into the guides using a x 25 microscope objective for the 2 and 4 μm guides and a x 16 objective for the 8 μm thick guides.

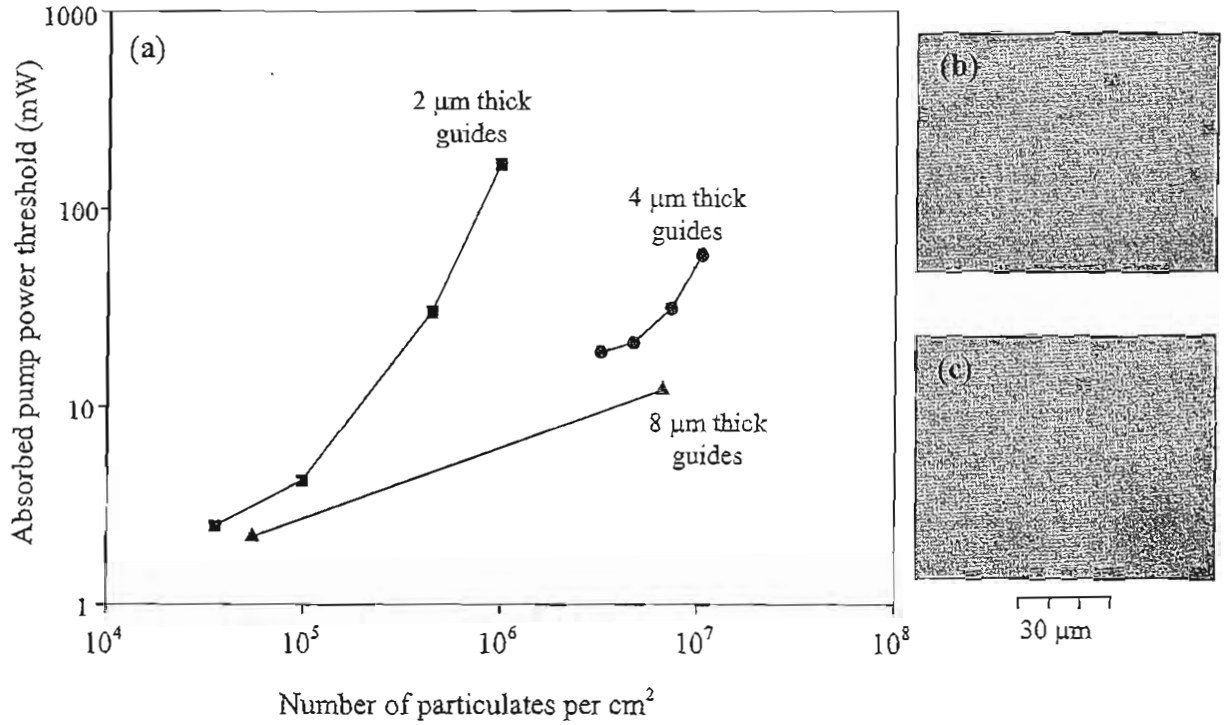

Figure 5.2.5 - (a) Effect of particulate density and core depth on absorbed power threshold for PLD Nd:GGG/YAG thin films for a laser cavity with two HR mirrors.
(b) Example of PLD thin film with low number of particulates.
(c) Example of PLD thin film with high number of particulates.

The laser cavity for all the guides was formed by using two highly reflecting mirrors at the laser wavelength (1060 nm) and figure 5.2.5 shows the absorbed pump power thresholds obtained for these films as a function of particulate density. It can be seen that high particulate density has a detrimental effect on the lasing threshold of these films and that the effect of the particulates has a more dramatic effect on the guides with smaller core sizes. An increase in particulate density from 3.5 x 10^4 to 9.7 x 10^5 cm^{-2} for the 2 μm thick films led to an increase in the absorbed pump power threshold from 2.5 to 167 mW. A 4 μm thick guide with a particulate density of 3.2 x 10^6 particulates cm^{-2}, however, lased easily at 19 mW, and even an increase of up to 1 x 10^7 particulates cm^{-2} (a very poor quality film) still lased at around 60 mW. The plot indicates that a 2 μm thick guide for particulate densities this high would be unable to lase for the available absorbed pump power of 220 mW. The 8 μm guide showed low threshold operation regardless of particulate densities, lasing at 2.2 and 12.2 mW with particulate densities of 5.5 x 10^4 and 6.6 x 10^6 cm^{-2} respectively, a change in particulate density of two orders of magnitude. Although a more systematic investigation is required to fully access the effect of particulates on loss, these initial results do show that the performance of

PLD guides can be improved by using large core guides. The loss mechanism due to scattering in waveguides from particulates is believed to be largely due to surface scattering, as opposed to scattering from within the guide, and the increased effect of particulates on the small core structures can be attributed to this. The particulate size is of the order of guide thickness for the 2 μm guides, consequently there is a higher probability that the particulates will protrude from the guide surface leading to higher scattering loss. In the larger guides the particulates are more likely to be enclosed within the guide and therefore will not contribute as significantly to the loss. These initial results suggest that low particulates in Nd:GGG structures can be tolerated if thick core sizes (8 μm or greater) are used, which is not a problem for PLD fabrication as deposition rates of 1 μm min^{-1} are readily achievable. Surface scattering loss could further be reduced if YAG cladding layers are deposited on these thin films to form a symmetric waveguide structure; again this is feasible as PLD allows simple target switching and YAG and GGG have closely matched lattice constants. A thick core size is also directly compatible with proximity coupling, and if a core size of 15 μm were used, combined with the NA of 0.75 for these GGG/YAG structures very efficient proximity coupling of nearly 100 % is predicted (figure 5.2.4).

An alternative fabrication process for high NA guides is direct bonding (DB). The major advantage of DB is that it does not require a lattice match between the substrate and core materials used, the only proviso being that the guide layers should display similar thermal expansion co-efficients. Although the need for precision-polishing of the components makes the process labour intensive and consequently more expensive than techniques such as PLD, the versatility of DB makes it very attractive for the development of high power waveguide lasers. Direct bonded YAG and GGG structures were first investigated by Brown (1997) [27], and guides with a range of NAs with optical losses of 0.4 to 0.7 dB/cm were demonstrated. More recent work shows that lower losses of 0.2 dB/cm can be achieved by bonding YAG to sapphire [28], and these structures are particularly attractive for the high-power operation of proximity coupled devices as both materials display good bonding behaviour, have excellent thermal conductivities, and the NA of 0.46 corresponds to a pump delivery efficiency of more than 95 %.

Of the two high NA guide fabrication techniques discussed here, the high quality and low-losses of DB YAG on sapphire structures offer the more attractive route to proximity-coupled lasers at present. DB YAG on sapphire structures are characterised in section 5.3.5 of this chapter and a double-clad structure with losses of 0.2 dB/cm is demonstrated. The results for the PLD guides however show that pulsed-laser assisted deposition offers a low-cost alternative. Techniques of controlling particulate formation in PLD structures is an active area of research [21], and the development of these techniques combined with large core guides holds considerable promise for the development of low-loss PLD Nd:GGG/YAG structures that are suitable for proximity coupling.

5.2.4 Demonstration of proximity coupling

For the initial demonstration of proximity coupling a 10W, 808 nm diode-bar from JenOptik was used to pump an unclad 8 μm deep 18 x 2 mm DB Nd:YAG on sapphire waveguide. The 8 μm guide core size represents a strong test for the capabilities of proximity coupling in the fast axis, while the 18 mm guide length is considerably longer than the diode-bar emission aperture of 10mm so that the pump beam was contained in the slow divergence axis. The experimental arrangement used to test proximity coupling is shown schematically in figure 5.2.6 and also in figure 5.2.7(b) overleaf.

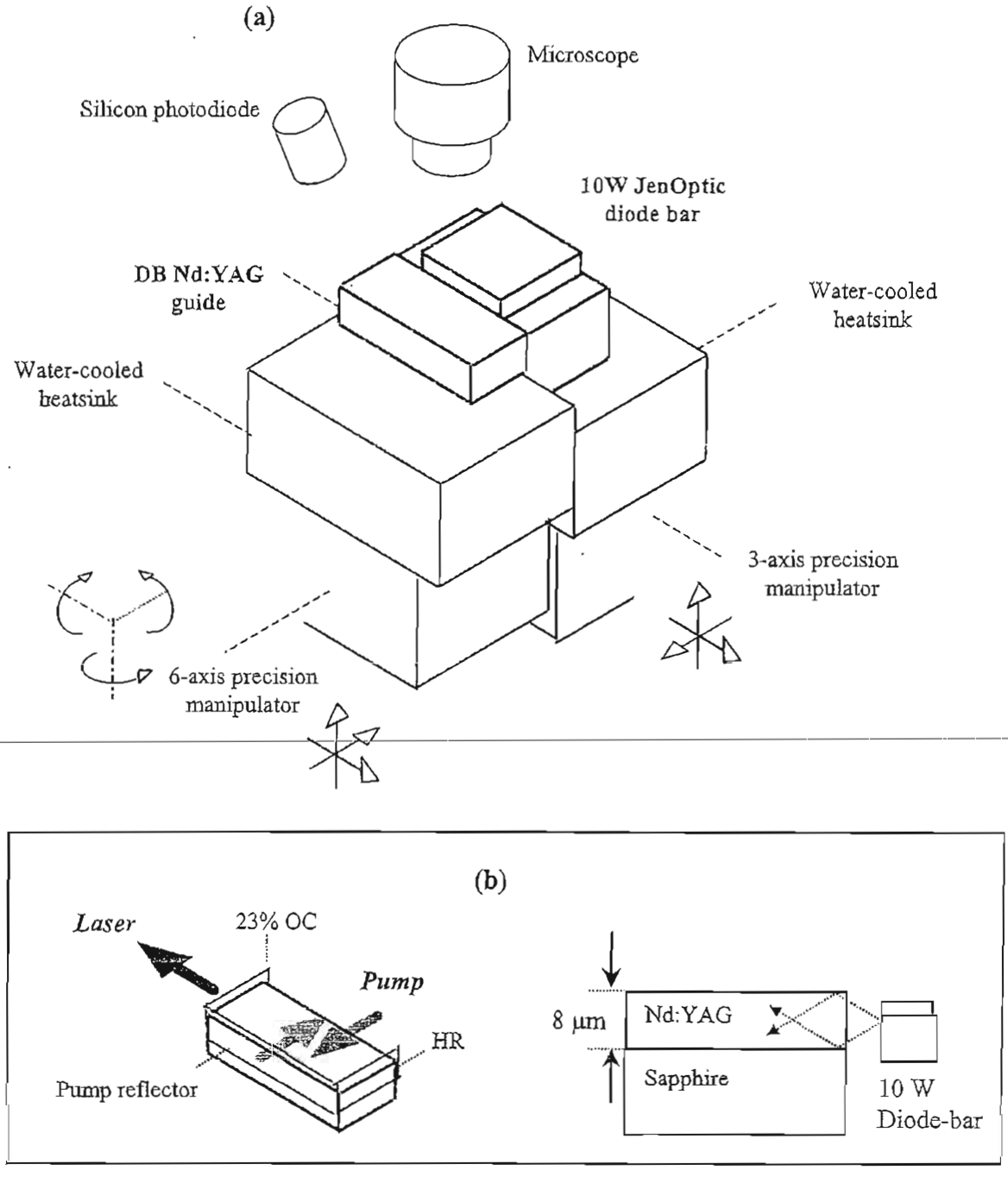

Figure 5.2.6 (a) Experimental arrangement for first demonstration of proximity coupling
(b) Side pumped laser resonator

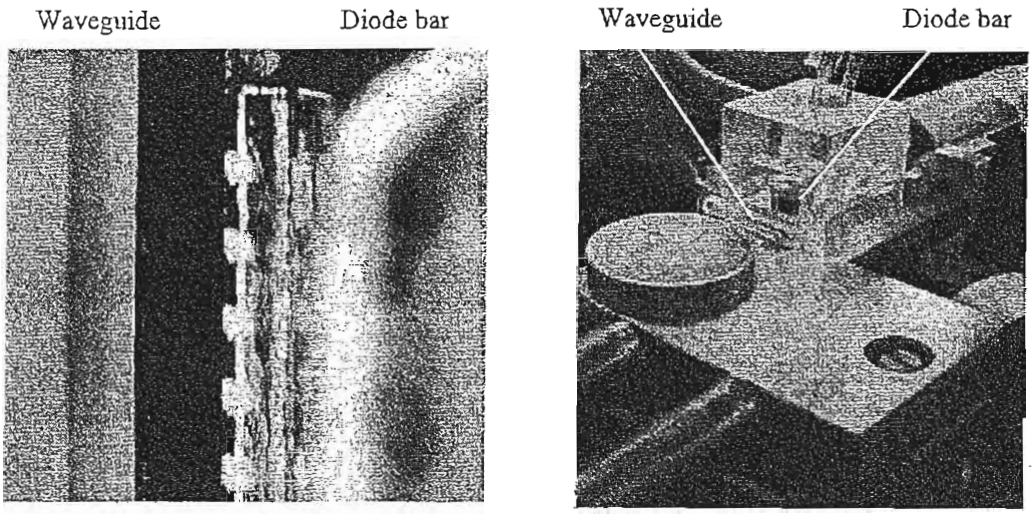

Figure 5.2.7 (a) Microscope view (b) Experimental set-up (pound coin shown for scale)

Both the waveguide and diode bar were mounted on water-cooled heat sinks, which in turn were on precision manipulator stages. The diode bar was housed in a Perspex box with a inlet at the top so that nitrogen could be blown across the diode front facet, to ensure that dust or moisture did not contaminate it. The waveguide fluorescence intensity was monitored using a silicon detector and the diode to guide separation viewed via a microscope overhead. The image from this was displayed using a camera attached to the microscope and is shown in figure 5.2.7.

Proximity coupling was achieved by bringing the diode and waveguide into close vicinity (a few tens of microns) while observing their separation on the microscope. The diode and guide were then orientated to each other by rotating them using the precision controls on the manipulator stages so that the separation was equal along the length of the set up, ensuring that the pump input face of the guide was parallel to the front facet of the diode bar. Angular alignment in the other planes was carried out by observing the pump diffraction pattern after the guide using an infrared viewer and the height was adjusted to produce maximum fluorescence intensity from the doped core. After this preliminary alignment, the waveguide was gently moved towards the diode while maintaining an optimum launch by making fine adjustments to the height. Observation of the fluorescence intensity showed that the launched pump power increased as the diode approached the guide, and that the fluorescence signal became steady once contact between the diode and guide was made.

It should be noted however that this did not represent 'butt' coupling of the pump as the diode emitters were recessed by about 9 μm from the front facet of the JenOptik diode-bar (determined by examining the diode-bar under a microscope prior to proximity coupling). To assess launch efficiency the pump power before and after the guide was measured. By taking account of the Fresnel reflections a value of 45 % was calculated for the combined launch and absorption efficiency. The absorption

was estimated by diode pumping a bulk piece of Nd:YAG rod with the same doping level, which gave a value of 3 mm for the absorption length, and corresponds to absorption of about 50% for our 2 mm wide guide. Thus, we arrive at a figure of nearly 90 % for the proximity coupled launch efficiency, which is good agreement with the efficiency predicted by the analysis developed in section 5.2.2, and is clearly a very efficient coupling between the diode-bar and waveguide.

After successfully proximity coupling the diode-bar, a laser cavity was formed by attaching a high reflector mirror to one end-face and a 23 % transmission output coupler (at 1064 nm) to the other end face of the waveguide. A high reflector at the pump wavelength (808 nm) was also used to double-pass the pump to increase the absorbed pump power. This gave 0.5W of unpolarised laser output for a diode-bar pump power of 6W. This output was however highly multimode, as would be expected due to the large gain width in the unguided direction and as the NA of 0.46 and guide depth of 8 μm results in a structure that can support up to seven modes at the laser wavelength in the guided direction. Nevertheless, the feasibility, compactness and efficiency of proximity coupling had been demonstrated. Such a coupling scheme could be extended to various in-plane-pumped planar devices, allowing the development of very compact systems.

5.3 Double-clad structures

5.3.1 Double-clad structures for spatial-mode control

Double-clad structures provide an attractive means of achieving diffraction-limited performance from multi-mode waveguides. These structures have a central active ion doped layer surrounded on both sides by undoped layers, which in turn are surrounded by a lower refractive index outer cladding layer. The outer structure is used to capture the pump radiation and the inner structure controls the laser beam quality. The way in which the central structure achieves this depends on the relative size of the doped region. For a small doping fraction the laser mode is selected by the optical confinement of the RE doped region as this has a higher refractive index than the undoped region. This type of structure will be termed a waveguide mode selection (WMS) device and is illustrated in figure 5.3.1(a). Two-dimensional WMS structures have been used quite widely in fibre lasers and typically have doped to undoped (core to inner-cladding) ratios of less than 0.1. In these cladding pumped fibres [29], the change of refractive index associated with the RE-doped core is sufficient to form a separate waveguide within the large NA, multi-mode guide made by the outer layers. The large NA waveguide of the outer layers captures the diode pump, which is gradually absorbed by the RE doped region, as it is guided along the fibre. Once the device reaches threshold the low NA guide made by the inner layers confines the laser radiation and, as this is designed to be single mode at the laser wavelength, diffraction-limited output is achieved. There is a very small overlap of the pump modes with the doped region in WMS devices, so that the effective pump absorption length for these structures is greatly increased compared to a fully doped three-layer structure. WMS designs are well suited to fibre geometries, as devices that are several metres long with very low propagation losses can readily be fabricated. Double-clad WMS fibre designs have proved very successful and diffraction-limited outputs in excess of 100W have been achieved [30].

However, a WMS design is not suitable for a planar geometry because fabrication techniques limit waveguide dimensions to a few centimetres. The approach here is to increase the size of the doped region so as to increase the overlap of the pump and doped region as illustrated in figure 5.3.1(b). This reduces the effective absorption length, which results in a compact design compatible with a planar geometry. For these double-clad structures the low NA of the RE-doped region no longer confines the laser mode (the RE-doped region can no longer support isolated modes, as these have an appreciable intensity at the outer-cladding interface). The high NA guide of the outer layers dominates so that the waveguide essentially behaves as a multi-mode three-layer structure. Two-dimensional structures of this type have been used in large mode area fibre lasers, primarily because the larger gain region reduces non-linear effects and increases the energy storage capabilities for q-switch applications [31]. One might expect multimode laser output from such a device, but, as shown

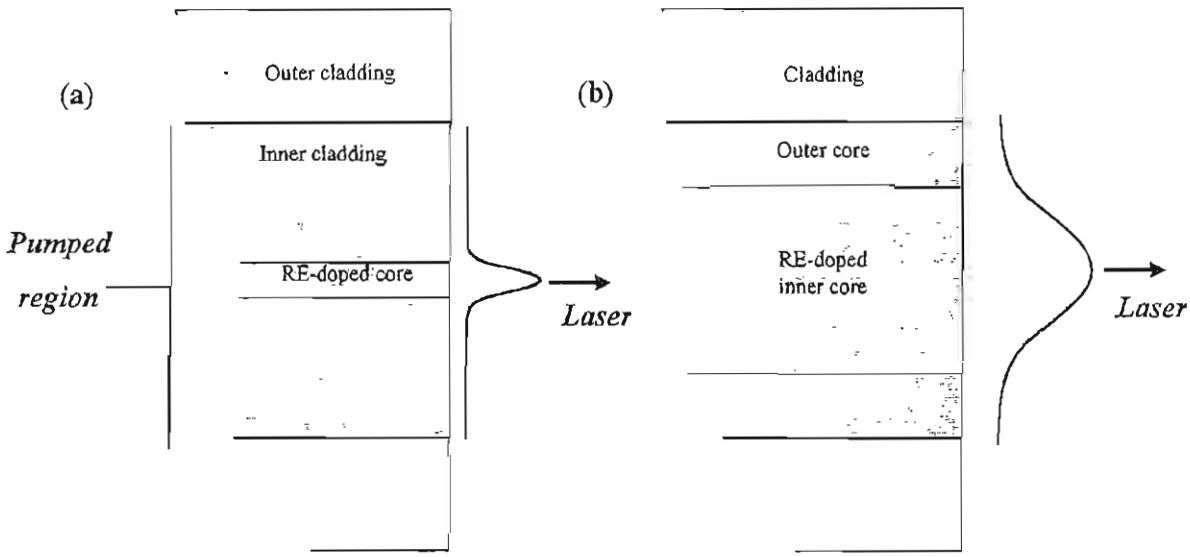

Figure 5.3.1 Waveguide structures and fundamental modes for double-clad structures
(a) Waveguide mode selection (WMS) (b) Gain mode selection (GMS)

in the following section, careful selection of the ratio of doped to undoped regions can be used for mode discrimination. The mode selection mechanism can be understood by considering the overlap of the mode with the gain profile. Qualitatively, the restricted doping means that the fundamental mode will see the most gain and so reach threshold first. Diffraction-limited output can be maintained at higher powers because the gain is efficiently extracted by the laser mode leaving no unsaturated gain for higher-order-mode oscillation. These types of structures will be termed gain mode selection (GMS) devices as the laser mode is one of the overall five-layer structure and mode discrimination is achieved by the restricted doping. Confined doping has been demonstrated to improve beam quality in both fibre geometries [31, 32] and bulk systems [33], however, no theoretical investigation of how a restricted gain region can lead to mode discrimination had previously been reported (to the best of the author's knowledge). This is presented in the following section [34], and is then applied to design a five-layer planar waveguide.

In WMS devices, such as cladding-pumped fibres, the outer layers are conventionally termed the outer cladding, the inner undoped layers the inner cladding and the RE-doped region the core. Although, physically GMS devices are very similar, it would be misleading to use the same terminology as the RE-doped core does not form a separate waveguide structure. The proposed labelling of this structure is shown in figure 5.3.1(b); the whole central three-layer structure (doped and undoped regions) will be referred to as the core (or inner and outer core) and the outer layers as the cladding.

5.3.2 Theory of gain mode selection

The way in which a confined doping profile can lead to preferential selection of the fundamental mode for laser action can be modelled by considering how the gain saturates with increasing laser power. Using the rate equation analysis and terminology described in chapter 2 (and originally formulated by Fan [35] and Risk [36]), the population inversion density for a quasi-three level system is described by equation 2.3.9.

$$\frac{\partial \Delta N(x,y,z)}{\partial t} = f\eta_p R r_p(x,y,z) - \frac{\Delta N(x,y,z) + N_1^0}{\tau} - fc_n \sigma \Delta N(x,y,z)\Phi\phi_l(x,y,z) = 0 \qquad [2.3.9]$$

However, for proximity coupled double-clad waveguide structures we can simplify the analysis by assuming a uniform pump distribution due to the highly multi-mode nature of the waveguide and diode pump source, and the double-pass side-pumped geometry. Assuming no ground state depletion means the absorbed pump energy will have the same spatial distribution as the dopant ions. For clarity, we can replace $r_p(x, y, z)$, the normalised absorbed pump power distribution, by $\delta_o(x, y, z)$ the dopant distribution, such that $r_p(x, y, z) = \delta_o(x, y, z)$. Where the dopant distribution is also normalised such that

$$\iiint_{cavity} \delta_o(x,y,z)\partial x\partial y\partial z = 1 \qquad [5.3.1]$$

The assumption of no ground-state depletion also means that the un-pumped lower laser level population density $N_1^0(x,y,z)$, will maintain the same spatial dependence as the dopant ions. It is convenient to separate the spatial dependence, and express it in terms of the total number of ions N_T, such that $N_1^0(x,y,z) = f_1 N_T \delta_o(x,y,z)$. Consequently, the relationship for the population inversion density can be expressed as

$$\frac{\partial \Delta N(x,y,z)}{\partial t} = f\eta_p R\delta_o(x,y,z) - \frac{\Delta N(x,y,z) + f_1 N_T \delta_o(x,y,z)}{\tau} - fc_n \sigma \Delta N(x,y,z)\Phi\phi_l(x,y,z) = 0 \qquad [5.3.2]$$

From equation 5.3.2 we can see that at or below threshold ($\Phi = 0$) the inversion has the same spatial distribution as the dopant ions.

$$\Delta N(x,y,z) = [f\eta_p R\tau - f_1 N_T]\delta_o(x,y,z) \qquad \textit{below threshold} \qquad [5.3.3]$$

As shown in chapter 2, at threshold and above the inversion averaged over the laser-mode profile becomes clamped such that

$$\iiint_{cavity} \Delta N(x,y,z)\phi_l(x,y,z)\partial x\partial y\partial z = \frac{L+T}{2\sigma l_c} \qquad [5.3.4]$$

In other words the gain experienced by the laser mode is equal to the loss. However, this does not mean that the spatial distribution of the inversion remains the same. In fact from equation 5.3.2, the inversion above threshold is given by

$$\Delta N(x,y,z) = \frac{[f\eta_p R\tau - f_1 N_T]\delta_o(x,y,z)}{1 + c_n\sigma\tau f\Phi\phi_l(x,y,z)} \qquad [5.3.5]$$

Combining equations 5.3.4 to 5.3.5, and defining a new parameter $S = c_n\sigma\tau f\Phi$, the population inversion distribution can be expressed in terms of the losses and laser power only

$$\Delta N(x,y,z) = \frac{\delta_o(x,y,z)[L+T]}{2\sigma l_c\left[1+S\,\phi_l(x,y,z)\right]\iiint_{cavity}\left[\frac{\delta_o(x,y,z)\phi_l(x,y,z)}{1+S\,\phi_l(x,y,z)}\partial x\partial y\partial z\right]} \qquad [5.3.6]$$

The S parameter is proportional to the intracavity power and gives a measure of the degree of saturation (from equation 2.3.12 this parameter can also be written as $S = 2l_cP_l / I_{sat}$). The gain exponent, G_m, for a particular mode, m, with spatial distribution ϕ_m, is given by

$$G_m = 2\sigma l_c\iiint \Delta N(x,y,z)\phi_m(x,y,z)\partial x\partial y\partial z \qquad [5.3.7]$$

Equations 5.3.6 and 5.3.7 can now be combined to give the gain for any mode above threshold, where the gain is saturated by a laser mode ϕ_l

$$G_m = [L+T]\iiint_{cavity}\frac{\delta_o(x,y,z)\phi_m(x,y,z)}{2\sigma l_c\left[1+S\,\phi_l(x,y,z)\right]\iiint_{cavity}\left[\frac{\delta_o(x,y,z)\phi_l(x,y,z)}{1+S\,\phi_l(x,y,z)}\partial x\partial y\partial z\right]}\partial x\partial y\partial z \qquad [5.3.8]$$

Equation 5.3.8 can be evaluated to give the gain for each waveguide mode for a given dopant distribution, laser mode, and intra-cavity laser power. It should be noted that, as a direct result of the uniform pumping distribution in a highly multi-mode side-pumped waveguide, this selectivity is independent of $N_1^0(x,y,z)$, and thus the same results will be obtained for 4-level or quasi-3-level lasers.

The general analysis developed here can be applied to a variety of resonator geometries and dopant distributions [34]. In practice however, the simplest devices to fabricate in a planar geometry, and also the ones that have been demonstrated experimentally in fibre [31, 32] and bulk lasers [33] use a step-function dopant distribution restricted to a central region of the crystal or waveguide. The simple one-dimensional case for a step-function doping is examined next for the guided axis of a planar guide. Although the following analysis is specific to a planar device, it does generally illustrate the way in which a confined doping profile can lead to preferential selection of the fundamental mode for CW laser action. The procedure of the next section could equally be applied to bulk lasers with composite rods, where the selectivity is between the modes of the resonator rather than the propagation modes of a waveguide. Similarly, it could also be applied to large mode area fibres. However, the mode selectivity will be somewhat compromised in the latter case, as bending of the fibre means that there is always some degree of coupling between the propagation modes.

5.3.3 Modelling of gain mode selection in planar waveguides

Modelling of planar waveguides is carried out for the structure illustrated in figure 5.3.2, where the doping in the guided axis is restricted to the central region of the core. If d is the width of the doped region, l is the length of the guide, and W is the width of the guide, then the normalised dopant distribution will be given by

$$\delta_o(x,y,z) = \frac{1}{dl_c W} \qquad [5.3.9]$$

To reduce the analysis to a one-dimensional case, we can assume that the laser modes in the unguided y-axis and propagation z-axis remain uniform. We now make the assumption that the waveguide modes are far from cut-off and so are fully confined to the core, so that, (from equation 2.2.9 of chapter 2), the normalised spatial distribution of photons for the even and odd modes, for a waveguide with a core depth D, is given by

$$\phi_m^{even}(x,y,z) = \frac{2}{WDl_c}\cos^2\left(\frac{(m+1)\pi x}{D}\right) \qquad m=0,2,4\ldots \qquad [5.2.10a]$$

$$\phi_m^{odd}(x,y,z) = \frac{2}{WDl_c}\sin^2\left(\frac{(m+1)\pi x}{D}\right) \qquad m=1,3,5\ldots \qquad [5.2.10b]$$

The dopant distribution and, as an example, the three lowest order modes are illustrated in figure 5.3.2b.

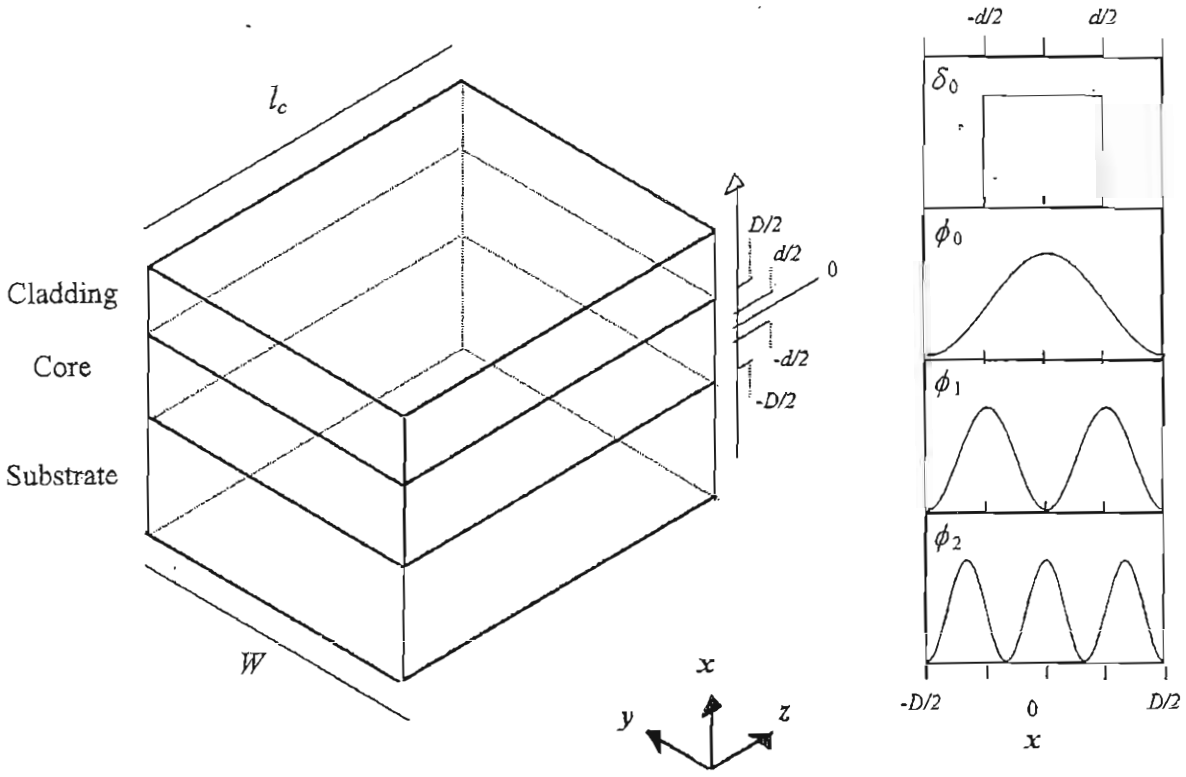

Figure 5.3.2 Modelling of GMS in planar waveguides
(a) Guide structure
(b) Doping distribution and three lowest-order propagation modes

We can use equation 5.3.7 and 5.3.3 to determine which mode sees the most gain below threshold and so will reach laser threshold first. For our simple centralised doping distribution ($D > d > 0$), and as we would expect intuitively from figure 5.3.1(b), the fundamental mode ($m=0$) sees the most gain. As the pump rate is increased the gain for the fundamental mode will increase until it becomes equal to the loss and so reach threshold and become the laser mode ($\varnothing_l = \varnothing_o$). We can now calculate the gain experienced by any of the other modes by applying equation 5.3.8 and using the fundamental waveguide mode as the laser mode at different values of S. Figure 5.3.3 shows the results of this calculation for the eight lowest-order modes, and how the gain varies with doping fraction for the case of no signal saturation (at laser threshold). As would be expected, for very small doped-fractions the gain for all the even modes becomes equal as all these modes have a central peak in their intensity profiles, whereas the gain for the odd modes tends to zero as these modes have zero intensity at the centre of the core. The gain for all the modes becomes equal for a fully doped core, showing that a normal multi-mode waveguide will indeed suffer from multi-mode laser output, however for intermediate doping fractions ($d/D < 1$) the fundamental mode has the advantage.

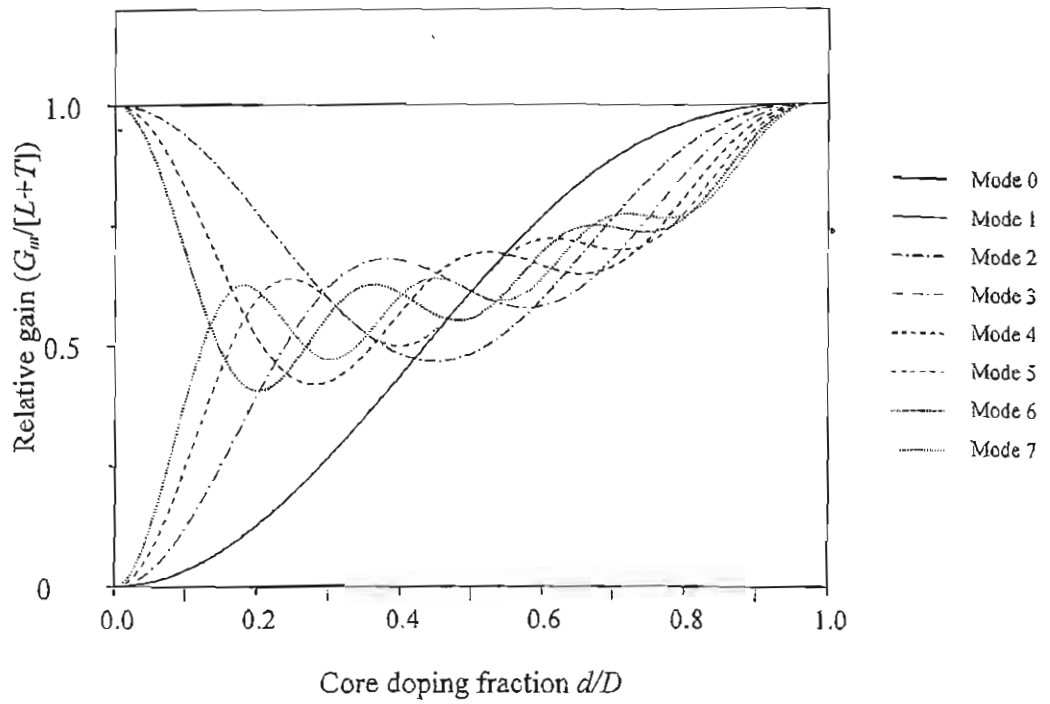

Figure 5.3.3 Relative gain for the eight lowest order modes against doping fraction at threshold ($I_0/I_{sat}=0$)

Once lasing occurs, the fundamental mode will start to saturate the population inversion. Although the gain experienced by the laser mode remains fixed the spatial profile of the population inversion will change, which may provide sufficient gain for higher-order modes to oscillate. The way in which the population inversion changes with increasing laser power is illustrated below in figure 5.3.4 for three different doped fractions (for this one-dimensional case this is in terms of I_0, the peak intracavity fundamental mode laser intensity).

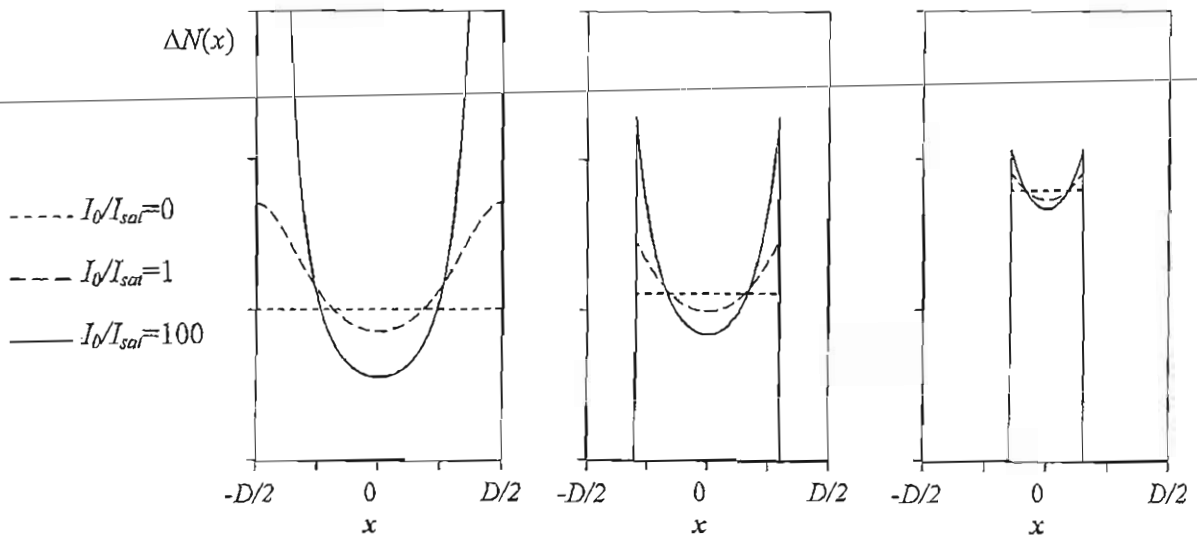

Figure 5.3.4 Population inversion profile at different laser powers for
(a) Fully doped core, (b) 60% doped core and (c) 30% doped core.

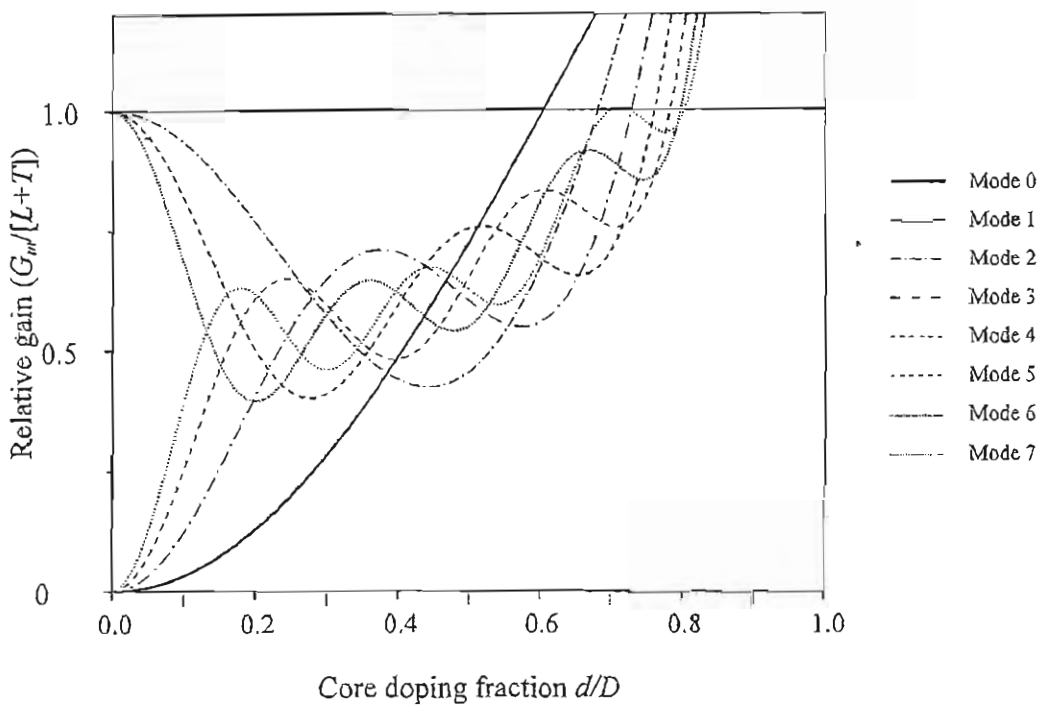

Figure 5.3.5 Relative gain for the eight lowest order modes at high laser power (I_0/I_{sat}=100)

As can be seen from figure 5.3.4, the change in shape of the inversion profile is much less for smaller doping fractions. The modelling also shows that there is very little change in the inversion profile after the laser intensity reaches several times the saturation intensity. Figure 5.3.5 shows the relative gain for the eight lowest-order waveguide modes calculated using equation 5.3.8 under highly saturated conditions (I_0/I_{sat}=100). It can be seen that, as expected, heavy saturation can lead to the gain for the high-order modes becoming larger than that for the fundamental mode. It appears that it is always the lowest-order odd mode (m=1) that is the first higher-order mode to oscillate. However, we can also see that there is still a window for doping fractions below 0.6 in which none of the higher order modes receive sufficient gain to reach threshold (assuming that they suffer the same loss) and single fundamental mode operation is maintained. Figure 5.2.5 shows a plot of the doping fraction at which the gain for the m=1 mode becomes equal to the m=0 mode as a function of the lasing intensity. We can see that required doping fraction is virtually constant once the intensity is greater than a few times the saturation intensity.

It should be noted that once a higher-order mode starts to oscillate equation 5.3.8 is no longer valid as this new mode will now contribute to the saturation of the gain as well. However this need not concern us, as we are only interested in the regime where a single transverse mode is oscillating and at which point this breaks down. There are some practical limitations of this model. Firstly, the active-ion doping normally brings with it a small change in refractive index. Therefore, at a certain doping width, it will create its own waveguide, rather than merely modifying the properties of the multi-mode guide (as is the case for WMS devices). The influence of this refractive index change will

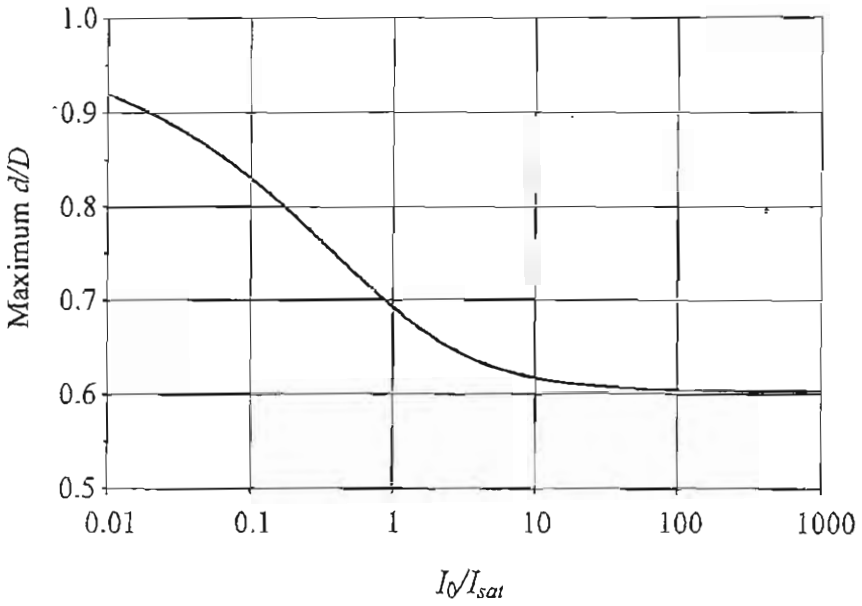

Figure 5.3.6 Doping fraction at which the gain for the $m=1$ mode becomes equal to the $m=0$ laser mode

depend on the specific structure, and is discussed in the following section for the Yb:YAG device used in the subsequent experiments. Secondly, for high-power operation the thermal loading of the doped region will also have an effect upon its refractive index, which must also be taken into consideration. In reality, the regions that are heavily saturated by the laser signal would have corresponding increased pump absorption due to the increased population in the ground level. This would then act against the effects described previously and aid fundamental-mode selection. Thus it appears that this model may be a worst-case limit, which can be seen as a useful design feature. We have also assumed that the losses for each mode are the same, which may not necessarily be the case. However, once again higher order modes in general tend to see higher loss, so any effect is likely to aid fundamental-mode selection rather than hinder it. Although the results presented have been for the one-dimensional case, the principle will still be valid for our device as the mode structure in the y-axis is independent of that in the x-axis for a planar geometry.

A final point to be noted is that this analysis has assumed uniform pumping. This is valid for a side pumped geometry (as used here), however for longitudinal pumping this analysis may break down, especially for quasi-three level case where poorly pumped end-sections of the guide may give preferential re-absorption loss for the fundamental mode.

5.3.4 Double-Clad Yb:YAG waveguide design

For the first demonstration of a GMS planar waveguide, a direct-bonded Ytterbium doped YAG waveguide is used. The advantages of using Yb:YAG derive from simple electronic energy level structure of the dopant ion. As discussed in the introductory chapter, Yb^{3+} has only two active

manifolds; the $^2F_{5/2}$ pump manifold, which contains the upper laser level and the $^2F_{7/2}$ ground manifold containing lower laser level. As the lower laser level is thermally populated, the laser transition is quasi-three level leading to an increased threshold when compared to systems such as Nd:YAG. However for high power operation, the very small energy mismatch between the pump (941 nm) and laser (1029 nm) photons results in a very efficient system with a low thermal load [37]. The absence of intermediate or higher lying energy levels also means that exited state absorption and concentration dependent ion-ion energy transfer effects that lead to well known concentration quenching in Nd systems [38] are not present. This allows very high doping levels to be used; in fact Patel and co-workers have recently demonstrated a 100 at % Yb:YAG (YbAG) device [18], which could be a useful feature for our double-clad designs where we want to maintain compact waveguide components. Reducing the doped region of the core for increased mode selectivity results in an increase in the effective pump absorption length, thus for a side-pumped system we would require a wider device. However in a Yb:YAG device, reducing the size of the active region can be compensated for by increasing the doping level.

The 5mm by 10 mm double-clad Yb:YAG device was manufactured by Onyx Optics by the direct-bonding fabrication technique. The central core structure consisted of a 8 μm-deep, 10 at. % Yb:YAG active layer bonded to 5 μm of undoped YAG on either side. This in turn was surrounded by an approximately 1 mm-thick sapphire cladding to form the structure shown in figure 5.3.7(a). The large core structure (18 μm) and the high YAG/sapphire NA (0.46) should allow efficient proximity coupling, whereas the inner structure provides a core doping fraction d/D=0.44 suitable for gain mode selection.

The propagation modes of this structure are considered in figure 5.3.7. The mode profiles (TE in this case) were calculated for a wavelength of 1029 nm using refractive index values of 1.8166, 1.8154 and 1.755 for Yb:YAG [18], undoped YAG [39] and sapphire [27] respectively. Figure 5.3.7 (b) shows the predicted propagation modes for the core structure assuming an infinite undoped YAG layer thickness. This guide can support two modes, however both modes have a significant intensity at the point where, in reality, they would reach the outer sapphire cladding interface. Consequently, unlike a WMS system the propagation modes for the five-layer guide are not associated with the inner RE doped core. Figure 5.3.7 (c) shows the modes of the structure formed by the outer layers, assuming an infinite sapphire cladding thickness and that there is no change in refractive index due to RE doping. This structure supports a total of 18 TE modes, and the propagation modes of this structure correspond closely to the modelling presented in the previous section as all the modes, (other than the highest order TE_{17} mode), are strongly confined to the core. In reality the effect of the refractive index change due to RE doping must also be taken into account and this is illustrated in figure 5.3.7 (d) for the fundamental mode. This profile is calculated using the five-layer waveguide

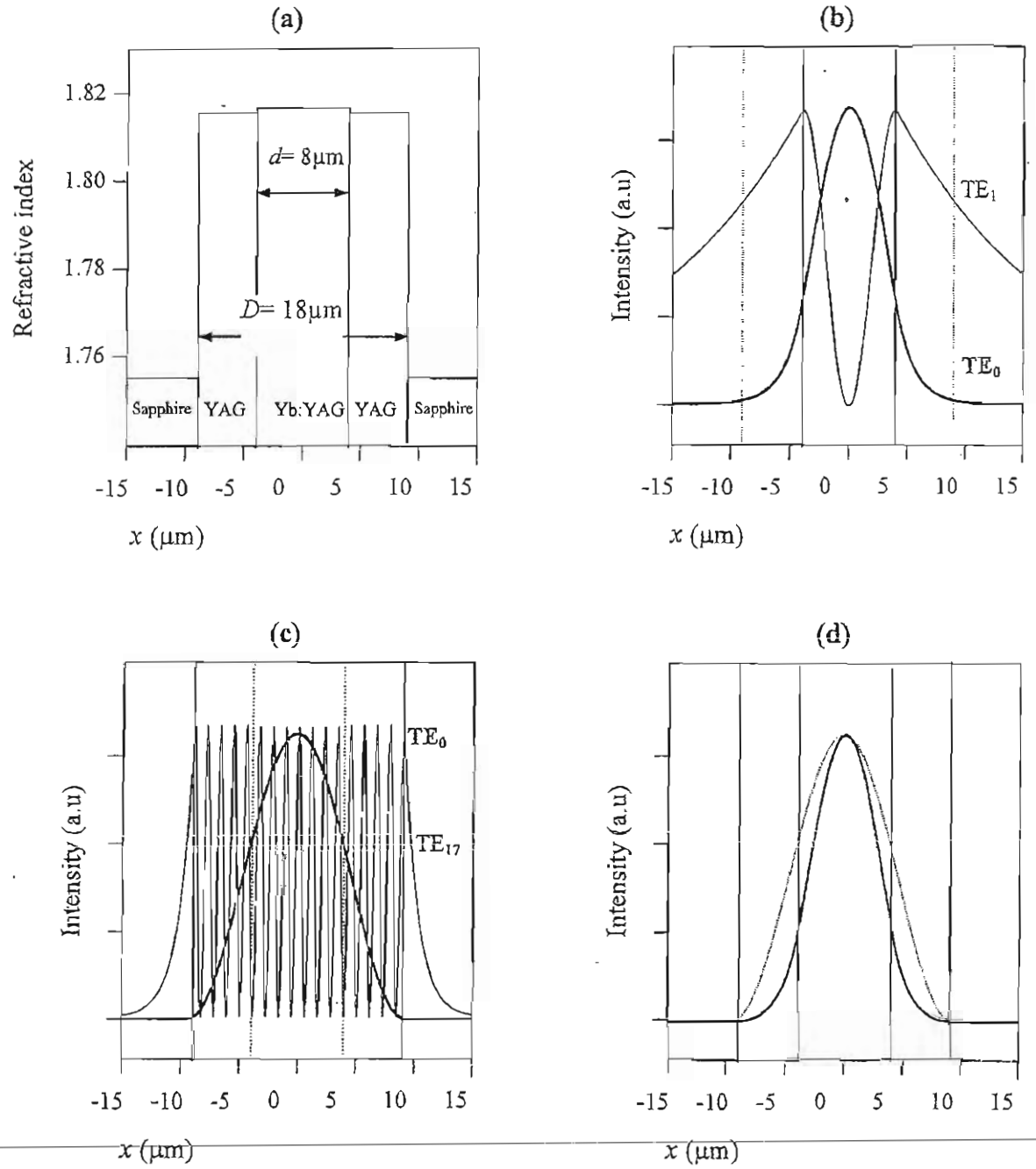

Figure 5.3.7 Yb:YAG GMS waveguide
(a) Structure and refractive index profile
(b) TE propagation modes for a three-layer waveguide of the core structure.
(c) Fundamental and highest order TE modes for a three layer waveguide of the outer layers.
(d) Fundamental mode of five layer waveguide (dotted line is the mode profile calculated assuming no change in refractive index due to RE doping)

theory presented in appendix A (an extension of the basic three-layer theory of chapter 2). As can be seen, the increase in refractive index due to RE doping has the effect of confining the mode more strongly, which may reduce how effectively the mode saturates the gain. However, the core-doping fraction of 0.44 is well in the limit indicated by the modelling and as demonstrated experimentally fundamental-mode-selection is retained.

5.3.5 Characterisation of double-clad Yb:YAG waveguide laser

Characterisation of the Yb:YAG double-clad structure was carried out by end-pumping the guide using a Ti-sapphire laser. The pump absorption length was estimated using the results of Lacovara [40], giving values of about 1.1 mm at a pump wavelength of 941 nm.and 968 nm and 1.9 mm at 915 nm. This length is expected to increase approximately by ratio of the doped to undoped areas of the pumped region for a double-clad planar structure. For Ti-sapphire pumping the weaker absorption at 915 nm was used because the pump had a higher output power at this wavelength, resulting in an effective absorption length of approximately 4.3 mm, which allows end-pumping the guide in the shorter 5mm direction.

Initially, using a x 6 microscope objective, care was taken to couple the pump to the guide such that propagation of the pump fundamental mode was observed by imaging the pump throughput onto a CCD camera. To estimate propagation loss, the 1029 nm laser threshold was measured as a function of output coupling (as described in chapter 3, section 3.2.3). The guide had sufficient gain to lase off just the bare end faces, which allowed the use of only Fresnel reflections (8.4 %) and highly reflecting mirrors (HR) for the Findlay-Clay plot shown in figure 5.3.8. To account for the re-absorption loss a slightly modified version of the equation presented in chapter 3 is used to estimate propagation loss.

$$P_{th} = C(2N_1^0\sigma l_c - lnR_1R_2 + 2\alpha_L l_c) \qquad [5.3.12]$$

Where R_1 and R_2 are the reflectivities of either the HR mirrors or bare-end faces. Extrapolating to P_{th} = 0, gives an intercept of $-(2N_1^0\sigma l_c + 2\alpha_L l_c)$ = -1.291, which, using values of σ=1.8 x 10^{-24} m^2 [40] N_1^0 = 6.9 x10^{25} m^{-3} (5 % of the total population) [41] and l_c= 5 x 10^{-3} m, gives a value of α_L= 0.05 cm^{-1} or equivalently 0.2 dB/cm for the intrinsic propagation loss of the guide. This loss is similar to that of previously reported two-layer DB YAG/sapphire structures [28] and demonstrates the suitability of direct bonding as a route to fabricating GMS multi-layer guides.

The focussing of the Ti-sapphire laser was then changed by using a 5 cm focal-length lens in place of the x 6 objective. When viewed on the CCD camera, it was clear that the pump was being coupled to the higher order modes of the five-layer structure, as would be the case for diode pumping. Under these conditions, measuring the pump power before and after the guide gave a combined launch and absorption efficiency of 0.77. Taking into account the estimated 4.3 mm absorption length, this corresponds to a near 100 % launch efficiency, as might be expected for such a large high NA waveguide pumped by a Ti-sapphire laser. The laser operation was tested by using a resonator formed by one HR mirror and one bare end-face of the guide. The results are shown in figure 5.3.9, and the slope efficiency of 76 % with respect to absorbed power is close to the quantum limit for 915 nm pumping (89 %), a further indication of a low-loss waveguide.

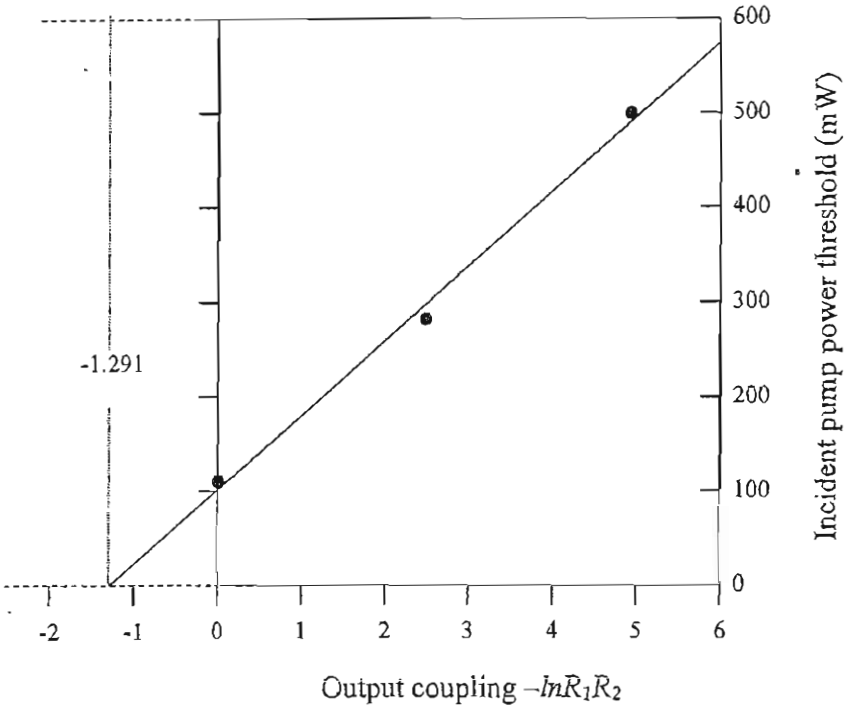

Figure 5.3.8 Findlay-Clay plot for estimation of propagation loss of DB Yb:YAG//YAG/sapphire guide.

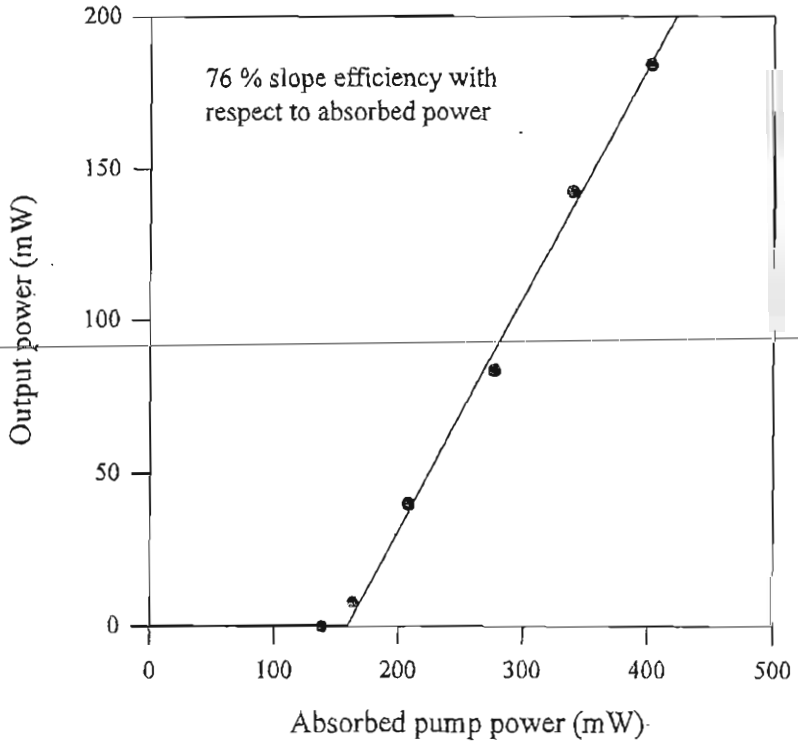

Figure 5.3.9 Laser output power as a function of absorbed pump power for Ti-sapphire pumped DB Yb:YAG//YAG/sapphire.

As an initial test of gain mode selection the laser output was imaged into a Coherent M^2 meter and despite the deliberately multimode pumping, near-diffraction-limited performance was confirmed by an M^2 measurement of 1.2 in the guided axis. The laser output was at 1029 nm, at the peak of the Yb emission spectrum and was found to be TE polarised. This linearly polarised output is in contrast to the unpolarised output observed with two-layer YAG-on-sapphire guides and perhaps is an indication of increased stresses in this five-layer structure leading to a difference in TE and TM mode propagation losses and/or mode sizes. At present it is not known if such effects are responsible for this behaviour, but in practice this is a very convenient method of obtaining polarised output, which may be useful for future applications to non-linear frequency conversion.

5.3.6 Proximity coupled Yb:YAG waveguide laser

The double-clad Yb:YAG waveguide was side-pumped in the 5mm direction by proximity coupling to a 20W, 941 nm- diode bar using the same procedure as that for the 8 μm two-layer Nd:YAG device as described in section 5.3.4. The alignment in this case however proved simpler due to the larger overall pumping area of the double-clad structure.

The proximity-coupling efficiency was assessed by measuring the diode-power with and without the waveguide component in place. Unfortunately, the very compact nature of the set-up made this difficult, and it was not possible to capture all the unabsorbed pump power after the guide, so we can only arrive at a upper limit for the combined launch and absorption efficiency (< 63 %). The laser resonator was formed along the 10 mm direction by attaching a high-reflector and a 7 % output coupler to the waveguide end faces. Laser operation at 1048 nm was achieved, corresponding to a transition to the highest stark level of the $^4F_{7/2}$ ground state manifold of the Yb ion. Although this line has a much lower emission cross section than the flouresence peak around 1029 nm, it also has less ground-state absorption and so can be quite easily be made to lase [20]. With a 7 % output coupling we achieved a maximum output power of 2.2 W, and a slope efficiency of 14.5 % with respect to incident power. This corresponds to a slope efficiency of > 23 % with respect to absorbed pump power. As previously observed under Ti-sapphire pumping the output was TE polarised.

The beam quality of the output was investigated by profiling the un-collimated far-field laser intensity. This was carried out using a silicon detector to vertically scan the laser beam at various distances from the waveguide as illustrated in figure 5.3.10(a). As an example the mode profile at a distance of 130 mm from the guide end-face is shown in figure 5.3.10(b) and, as can be seen, the results fit well to a Gaussian profile. The second moments radius [42,43] for the intensity profiles were calculated at various distances from the guide and the results are shown in figure 5.3.10(c).

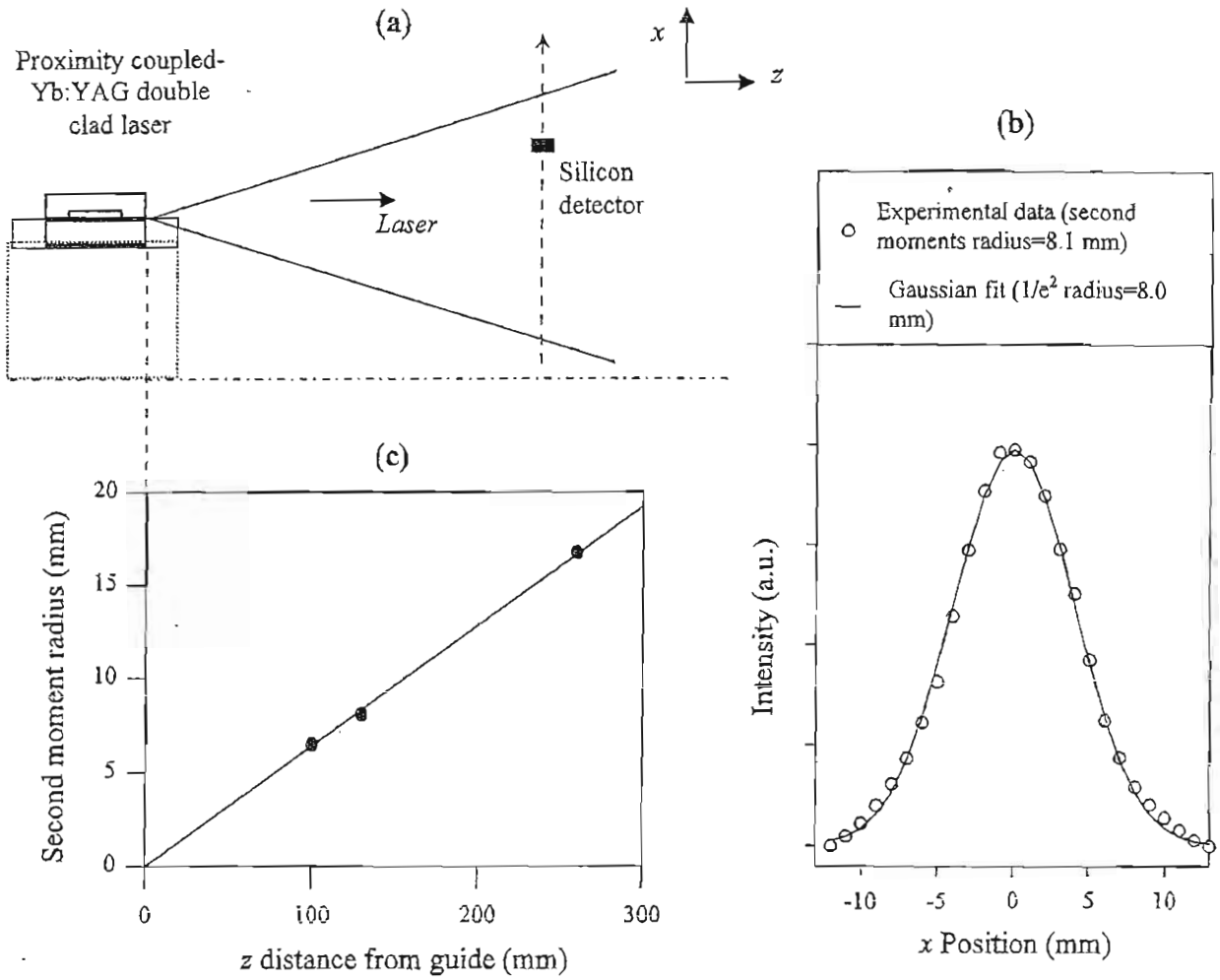

Figure 5.3.10 (a) M^2 measurement using scanning slit method
(b) Measured intensity profile in guided direction at z =130 mm
(c) The measured second moments radius at various distances from guide end face.

The predicted radius for the fundamental mode of the Yb:YAG double-clad guide is 5.26 μm, which would lead to an output divergence of 63.4 mrad, while the experimental results correspond to a beam divergence of 64.1 mrad. This divergence is equivalent to an $M^2 < 1.1$ for the guided direction. In the unguided direction, as with the original two-layer Nd:YAG guide, the output was highly multi-mode as no attempt was made to control the beam quality in this axis.

5.4 Summary

Proximity coupling combined with double-clad waveguide structures offer an attractive route to very compact high power lasers. The direct coupling of the pump energy, afforded by the optical confinement and geometry of the planar waveguide, leads to very efficient pump delivery with delivery efficiencies approaching 100 %. The first demonstration of proximity coupling has shown that this technique is effective for waveguides with cores as small as 8 μm and the simplicity of the technique results in inherently compact systems, with device footprints of < 1 cm^2. The simplicity and effectiveness of proximity coupling certainly makes it an attractive technique for pumping any planar waveguide with a sufficiently high NA and allows power scaling for side-pumped devices.

Spatial mode control can be achieved by using a confined doping profile for fundamental mode selection. The GMS theory developed can in principle be applied to many laser systems, here it was applied to design a double-clad planar waveguide that gave fundamental mode operation in the guided plane of the device for output powers of over 2 W. However the theory shows that diffraction-limited performance should be possible at much higher powers. Since the reported proof-of-principle work reported here was carried out considerable progress has been made in GMS proximity-coupled devices [13] and the power scaling, techniques for mode control in the unguided axis and other recent developments in high power laser systems based on proximity coupling and GMS double-clad waveguides are discussed in the following chapter.

5.5 References

[1] S. Yamaguchi, T. Kobayashi, Y. Saito & K. Chiba, *"Efficient Nd:YAG laser end pumped by a high power multistrip laser-diode bar with multiprism array coupling"*, Applied Optics, Vol. 35 No. 9, p. 1430-1435, (1996).

[2] J.J. Chang, E.P. Dragon, C.A. Ebbers, I.L. Bass, & C.W. Cochran, *"An efficient diode-pumped Nd:YAG laser with 451W of CW IR and 182W of pulsed green output"* , in OSA TOPS on Advanced Solid-State Lasers, W.R. Bosenberg & M.M. Fejer (Eds), Vol. 19, p. 300-304, (1998).

[3] M. Karszewski, U. Brauch, K. Contag, S. Ergard, A. Giesen, I. Johannsen, C. Stewart, & A. Voss, *"100W TEM_{00} operation of Yb:YAG thin disc laser with high efficiency"*, in OSA TOPS on Advanced Solid-State Lasers, W.R. Bosenberg & M.M. Fejer (Eds), Vol. 19, p. 296-299, (1998).

[4] R.J. Beach, *"Theory and optimization of lens ducts,"* Applied. Optics, Vol. 35, p. 2005-2015, (1996).

[5] W.A. Clarkson & D.C. Hanna, *"Two-mirror beam-shaping technique for high-power diode bars"*, Optics Letters, Vol. 21, p. 375-377, (1996).

[6] E. Snitzer, H. Po, F. Hakimi, R. Tumminelli & B.C. McCollum, *"Double-clad, offset core Nd fiber laser"*, in Proceedings of Conference on Optical Fiber Communication, paper PD5, (1988).

[7] M. Hofer, M.E. Fermann, & L. Goldberg, *"High-power side-pumped passively mode-locked Er-Yb fibre laser"*, IEEE Photonics Technology Letters, Vol. 10, p. 1247-1249, (1998).

[8] A. Faulstich, H.J. Baker & D.R. Hall, *"Face pumping of thin, solid-state slab lasers with laser diodes"*, Optics Letters, Vol. 21, No. 8, p. 594-596, (1996).

[9] H.J. Baker, A. Chesworth, D. Palaez & D.R. Hall, *"A planar waveguide Nd:YAG laser with a hybrid waveguide-unstable resonator"* Optics Communications, Vol. 121, p. 125-131, (2001).

[10] J. Lee, H.J. Baker, G. Friel, G. Hilton & D.R. Hall, *"High-average-power Nd:YAG planar waveguide laser that is face pumped by 10 laser diode bars"*, Optics Letters, Vol. 27 No. 7; p. 524-526, (2002).

[11] C.L. Bonner, C.T.A. Brown, D.P. Shepherd, W.A. Clarkson, A.C. Tropper & D.C. Hanna *"A diode-bar end-pumped, high power, Nd:$Y_3Al_5O_{12}$ planar waveguide laser"*, Optics Letters, Vol. 23, No. 12, p. 942-944, (1998).

[12] J.L. Blows, J.M. Dawes & J.A. Piper, *"A simple, thermally stabilised, diode end-pumped, planar Nd:YAG laser"*, Optics Communications, Vol. 162, p. 247-250, (1999).

[13] D.P.Shepherd, S.J.Hettrick, C.Li, J.I.Mackenzie, R.J.Beach, S.C.Mitchell & H.E.Meissner, *"High-power planar dielectric waveguide lasers"*, J. of Physics D: Applied Physics, Vol. 34, p. 2420-2432, (2001).

[14] D.C. Hanna, A.C. Large, D.P. Shepherd, A.C. Tropper, I. Chartier, B. Ferrand, & D. Pelenc, *"A side-pumped Nd:YAG epitaxial waveguide laser"*, Optics Communications, Vol. 91, p. 229–235, (1992).

[15] U. Griebner, R. Grunwald & H. Schonnagel, *"Thermally bonded Yb:YAG planar waveguide laser"* Optics Communications, Vol. 164, p. 185–190, (1992).

[16] Optopower Corp., Tuscon Arizona, USA, *Private communication and product information*, (1998).

[17] S.J. Field, D.C. Hanna, A.C. Large, D.P. Shepherd, A.C. Tropper, I. Chartier, B. Ferrand, & D. Pelenc *"Growth and low-threshold laser oscillation of an epitaxially grown Nd:YAG waveguide"*, Optics Letters, Vol. 17, No. 11, p. 810-812, (1992)

[18] F. Patel, E. Honea, J. Speth, S.A. Payne, R. Hutcheson & R. Equall *"Laser demonstration of $Yb_3Al_5O_{12}$ (YbAG) and material properties of highly doped Yb:YAG"*, IEEE J. of Quantum electronics, Vol. 37, No. 1, p. 135-144, (2001).

[19] D.C. Hanna, A.C. Large, D.P. Shepherd, A.C. Tropper, I. Chartier, B. Ferrand, & D. Pelenc, *"Low threshold quasi-three-level 946nm laser operation of an epitaxially grown Nd:YAG waveguide"*, Applied Physics Letters, Vol. 63, p. 7-9, (1993).

[20] D. Pelenc, B. Chambaz, I. Chartier, B. Ferrand, C. Wyon, D.P. Shepherd, D.C. Hanna, A.C. Large & A.C. Tropper, *"High slope efficiency and low threshold in a diode-pumped epitaxially grown Yb:YAG waveguide laser"*, Optics communications, Vol. 115, p. 491-497, (1995).

[21] S.J. Barrington, *"Planar waveguide devices fabricated by pulsed laser deposition"*, University of Southampton, Thesis, p 140-154, (2001).

[22] D.S. Gill, R.W. Eason, J. Mendiola, & P.J. Chandler, *"Growth of crystalline $Gd_3Ga_5O_{12}$ thin-film optical waveguides by pulsed laser deposition"*, Materials Letters, Vol. 25 p. 1-4 , (1995).

[23] D.S. Gill, A.A. Anderson, R.W. Eason, T.J. Warburton & D.P. Shepherd, *"Laser operation of an Nd: $Gd_3Ga_5O_{12}$ thin-film. optical waveguide fabricated by pulsed laser deposition"*, Applied Physics Letters, Vol. 69, p 10-12 (1996)

[24] A.A. Anderson, C.L. Bonner, D.P. Shepherd, R.W. Eason, C. Grivas, D.S. Gill & N. Vainos, *"Low loss (0.5 dB/cm) Nd:$Gd_3Ga_5O_{12}$ waveguide layers grown by pulsed laser deposition"*, Optics Communications, Vol. 144, p. 183-186, (1997).

[25] C.L. Bonner, A.A. Anderson, R.W. Eason, D.P. Shepherd, D.S. Gill, C. Grivas & N.A. Vainos, *"Performance of a low loss pulsed laser deposited Nd:$Gd_3Ga_5O_{12}$ waveguide laser at 1.06μm and 0.94μm"*, Optics Letters, Vol. 22, No. 13, p 988-990, (1997).

[26] S.J. Barrington, T. Bhutta, D.P. Shepherd & R.W. Eason, *"The effect of particulate density on performance of Nd:$Gd_3Ga_5O_{12}$ waveguide lasers grown by pulsed laser deposition"*, Optics Communications, Vol. 185, p. 145-152, (2000).

[27] C.T.A. Brown, C.L. Bonner, T.J. Warburton, D.P. Shepherd, A.C. Tropper, & D.C. Hanna, *"Thermally bonded planar waveguide lasers"*, Applied Physics Letters, Vol. 71, No. 9, p. 1139-1141, (1997).

[28] D.P. Shepherd, C.L. Bonner, C.T.A. Brown, W.A. Clarkson, A.C. Tropper, D.C. Hanna & H.E. Meissner, *"High-numerical-aperture, contact-bonded, planar waveguides for diode-bar-pumped lasers"*, Optics Communications, Vol. 160, p.47-50, (1999).

[29] D. Richardson, J. Minelly & D.C. Hanna, *" Fiber laser systems shine brightly"*, Laser Focus World, September 1997, p. 87-95, (1997).

[30] V. Dominic, S. MacCormack, R. Waarts, S. Sanders, S. Bicknese, R. Dohle, E. Wolak, P.S. Yeh & E. Zucker, *"110W fibre laser"*, Electronic Letters, Vol. 35, p. 1158-1160, (1999).

[31] H.L. Offerhaus, N.G. Broderick, D.J. Richardson, R. Sammut, J. Caplen, & L. Dong, *"High-energy single-transverse-mode Q-switched fiber laser based on a multi-mode large-mode-area erbium-doped fiber,"* Optics Letters, Vol. 23, p. 1683-1685, (1998).

[32] J.A. Alvarez-Chavez, H.L. Ferhaus, J. Nilsson, P.W. Turner, W.A. Clarkson, D.J. Richardson, *"High-energy, high-power, ytterbium-doped Q-switched fiber laser"*, Optics Letters, Vol. 25, p. 37-39, (2000).

[33] A. Lucianetti, R. Weber, W. Hodel, H.P. Weber, A. Papashvili, V.A. Konyushkin, & T.T. Basiev, *"Beam-quality improvement of a passively Q-switched Nd:YAG laser with a core-doped rod"*, Applied Optics, Vol. 38, p 1777-1783, (1999).

[34] T. Bhutta, J.I. Mackenzie, D.P. Shepherd & R.J. Beach, *"Spatial dopant profiles for transverse-mode selection in multi-mode waveguides"*, J. of Optical Society of America B, Vol.19, p.1539-1543, (2002).

[35] T. Fan & R. Byer, *"Modelling and CW operation of a quasi-three level 946 nm Nd:YAG laser"*, IEEE J. of Quantum Electronics, Vol. QE-23 , p. 605-612, (1987).

[36] W. Risk, *" Modelling of longitudinally pumped solid-state lasers exhibiting re-absorption loss"*, J. of Optical Society of America B, Vol. 5, No 7, p. 1412-1423, (1988).

[37] T.Y. Fan, *"Heat generation in Nd:YAG and Yb:YAG"*, IEEE J. of Quantum Electronics, Vol. 29 , No. 6, p. 1457-1459, (1993).

[38] V. Lupie, A. Lupei, S. Georgescu & C. Ionescu, *"Energy transfer between Nd ions in YAG"*, Optics Communications, Vol. 60, No. 1-2, p. 59-63, (1986).

[39] D.N. Nikogosyan, *"Properties of optical and laser-related materials"*, Wiley UK, p. 5, (1997).

[40] P. Lacovara, H.K. Choi, C.A. Wang, R.L. Aggarwal & T.Y. Fan, *"Room temperature diode-pumped Yb:YAG laser"*, Optics Letters, Vol. 16, No. 14, p. 1089-1091, (1991).

[41] T. Taira, W. Tulloch & R. Byer *"Modelling of quasi-three level lasers and operation of CW Yb:YAG lasers"*, Applied Optics, Vol. 36, No. 9, p. 1867-1874, (1997).

[42] M.W. Sasnett *"Propagation of multimode laser beams- The M^2 factor"*, Chapter 9 of *"The physics and technology of laser resonators"*, D.R. Hall & P.E Jackson (Eds), Institute of Physics Publishing, p. 132-142, (1992).

[43] A. Siegman, *"How to (maybe) measure laser beam quality"*, TUL1, Tutorial at OSA annual meeting, Long Beach, California, USA, 12-17 October, (1997).

Chapter 6

CONCLUSION

6.1 Introduction

The diverse nature of materials and fabrication techniques covered in this thesis, from low-phonon-energy to high-power devices, and from precision MBE deposition to waveguide construction by direct-bonding reflect the numerous possibilities for the development of novel RE-doped planar waveguide lasers. This chapter summarises the experimental work reported in the three different areas investigated; borosilicate glass waveguide lasers, MBE lanthanum fluoride waveguide lasers and planar waveguides for high power operation, and briefly discusses some future directions for this work.

6.2 Borosilicate glass waveguide lasers

Chapter 3 reported the optical characterisation of novel laser waveguide structures in borosilicate glasses. Planar structures fabricated by a new method of ion-exchange based on the direct-bonding of glass substrates of opposing chemical gradients were investigated. The novel direct-bonded ion-exchange (DB-IE) fabrication technique offers advantages over conventional thermal ion-exchange for the production of buried waveguide structures. In particular, there is no need to apply a secondary process such as a subsequent bonding step to attach a cladding layer, or a further heat, electric field or exchange process to bury the waveguide. Furthermore, the hostile environment of the molten salt bath is avoided as the ions required for the exchange process are provided by a previously unexplored solid-state source, i.e. the glass substrates that are bonded.

The characterisation of the Nd:BK7 glass structures shows that optical losses of these structures are < 0.4 dB/cm. Buried channel waveguides were fabricated by using a germanium doped active superstrate which allowed buried channel structures to be directly written using a UV laser. The characterisation of Nd:SGBN glass structures shows that these channel structures have optical losses of <0.3 dB/cm, and absorbed pump power thresholds < 10 mW were demonstrated. The UV-written channels provide a near symmetric laser output compatible with low-loss coupling to optical fibres.

The next stage in the development of this technology will concentrate on developing Er-doped samples for laser operation at 1540 nm, the minimum attenuation wavelength for silica fibres. At the time of writing Er:SGBN waveguides are being prepared and the characterisation of these structures should be reported in the near future. A further area that warrants future investigation is the fabrication of gratings and couplers in these structures, which have been demonstrated by UV writing in other germosilicate thin film-layers [1]. The incorporation of such structures on the buried DB-IE platform could lead to highly functional, compact, low-loss optical sources and amplifiers that would be useful for applications such as telecommunications.

In conclusion, buried ion-exchanged waveguides are important for applications in integrated optics because these minimise both surface scattering and fibre-optic coupling loss. Direct bonded ion-exchange offers a new single-step process to realising these devices. Glass substrates can be produced in large sizes and direct bonding would allow the production of large-scale platforms that could be cut to a number of smaller devices. UV writing allows automated fabrication of devices on these platforms without the need for photolithography, offering a low-cost and versatile route to the large-scale production of a wide variety of active integrated optical components.

6.3 MBE Lanthanum-fluoride waveguide lasers

Chapter 4 reported the optical characterisation of lanthanum fluoride waveguide lasers. Molecular beam epitaxy (MBE) is an attractive route to the fabrication of fluoride waveguide lasers as thin film layers can be deposited mono-atomically, which allows exceptional control over both RE-doping level and layer thickness. The first laser action from a dielectric thin film fabricated by MBE was demonstrated using Nd:LaF_3 thin films grown on CaF_2 substrates. The characterisation of these thin film structures shows that the MBE process is well suited to producing high quality crystalline structures, with a phonon energy cut-off around 380 cm^{-1}, in good agrement to that found in bulk LaF_3 crystals.

Future work should concentrate on lowering the propagation loss of the MBE thin films, which was estimated to be approximately 1 dB/cm for the devices reported here. Although this relatively high propagation loss did not inhibit laser action for the thin film structures investigated, it clearly limits the efficiency of these and future devices. The most likely cause of the high propagation loss is strain in the grown layer due to the lattice mismatch between the RE-doped LaF_3 thin film and CaF_2 substrate. The MBE process is well suited to the incorporation of additional ions into the growth process by simply using additional effusion cells, consequently an approach analogous to that used in liquid-phase epitaxy in which Lu ions are incorporated into a grown YAG layer to increase the lattice match to the substrate [2] may prove successful in reducing the propagation loss. Alternatively homo-epitaxial growth of RE-doped LaF_3 on undoped LaF_3 substrates [3] is expected to have lower strain induced losses, however this will significantly reduce the numerical aperture of these devices and it may be necessary to increase the core size of the waveguide to strongly confine the radiation, especially at mid-IR wavelengths.

Slab-loaded channel waveguides were designed on the MBE thin films, and fabricated by two different methods; ion-beam etching and the novel BCB polymer overlay technique. Although an exhaustive characterisation of these devices was not possible due to the fragility of the structures, the results are consistent with a negligible increase in propagation loss compared to the background level of the MBE thin film and the increased optical confinement of the channel geometry leads to a significant reduction in laser threshold. The novel technique employing a BCB polymer loading strip was demonstrated to be a particularly versatile technique that can be processed using photolithographic techniques alone, and this approach could be applied to a wide variety of crystals and glasses for the fabrication of near-IR channel waveguide lasers. Although the testing procedure used here proved to be destructive for the channel waveguides, the fragility of the structures may not be a critical limitation for a final MBE device because the mirror coating can be directly applied to the guide end-faces. The robustness of the structures could also be enhanced by depositing a low-refractive index layer to bury the structures completely, or alternatively different waveguide

fabrication techniques such as indiffusion could be considered. All these approaches to channel fabrication on MBE thin films warrant further investigation.

Initial characterisation of MBE Er-doped-LaF_3 thin films is underway with a view to developing mid-IR sources. Fluorescence at around 3 μm over the $^4S_{3/2}$-$^4F_{9/2}$ and $^4I_{11/2}$-$^4I_{3/2}$ Er^{3+} transitions has been reported [4] and achieving laser emission on these transitions is currently being attempted. The BCB channel waveguide design is probably not feasible for the development of mid-IR technology as the polymer is likely to suffer material absorption at these wavelengths, however, the mid-IR transparency of CaF_2 means that the ion-beam etched, hybrid slab-loaded/rib channel design should be suitable.

In conclusion, the first laser action from a dielectric waveguide fabricated by MBE has been demonstrated. The laser action from the MBE LaF_3 thin films constitutes the lowest phonon energy dielectric material to show waveguide laser emission to date, and, as an initial step to developing integrated optical sources slab-loaded channel waveguide structures have been demonstrated on these thin films. The low phonon energies of the host, combined with the exceptional control of the MBE process and the possibilities for integration make MBE RE-doped LaF_3 waveguide lasers interesting candidates for the development of compact mid-IR lasers sources.

6.4 Waveguides for high average power lasers

Chapter 5 reported the design and development of compact high-power planar waveguide lasers. Waveguide structures suitable for both high power operation and proximity coupling - the direct coupling of diode-bar pump radiation into the waveguide without any intervening optics, were investigated. High NA (>0.4) RE-doped GGG on YAG and RE-doped YAG on sapphire waveguides fabricated by pulsed-laser assisted deposition (PLD) and direct-bonding (DB), respectively, with core sizes of 8 μm or greater were shown to be suitable. The first demonstration of proximity coupling was achieved using an 8 μm thick core DB Nd:YAG/sapphire waveguide. Proximity coupling was demonstrated to be both a highly efficient and compact technique. The pump delivery efficiency was measured to be 90 % and the overall device footprint (diode and waveguide) was < 1 cm^2.

The versatility of the direct-bonding technique and the low-loss (0.2 dB/cm) of DB YAG/sapphire guides makes these structures very attractive for the development of compact high power sources. However, the initial investigation of the effect of particulates on device performance for Nd:GGG/YAG structures show that PLD may offer a quick, low-cost alternative route to the fabrication of these components. The results of this study indicate that the large core sizes required for proximity coupling can also reduce the scattering losses for PLD structures, and recent work by Barrington [5] shows that depositing a YAG cladding layer on the active GGG core can further reduce

the propagation losses due to particulates. The prospects for the production of low-loss, multi-layer proximity coupled PLD planar waveguides for high-power operation look good.

A double-clad planar waveguide design suitable for proximity coupling was considered. The desire to retain compact components and the limitations of planar waveguide fabrication meant that a multi-mode waveguide with a large RE-doped region is required. The theory of fundamental mode selection in such a device through confined doping and gain mode selection (GMS) was developed. Although this theory was specifically applied to design a GMS planar waveguide, the approach developed could equally be used for large-mode-area fibres and bulk resonators with composite rods, and so, prove generally useful for designing high power waveguide and bulk lasers. The GMS modelling showed that doping 60 % or less of a planar waveguide core robustly selects the fundamental mode for laser operation. The first double-clad planar waveguide laser was demonstrated using a 44 % core doping fraction DB Yb:YAG/YAG/sapphire waveguide, which gave diffraction-limited performance in the guided axis for an output power of greater than 2 W. Double-clad waveguides similar to the GMS DB design investigated here have now been demonstrated using Nd^{3+} and Tm^{3+} dopants [6,7], and these devices also give diffraction limited output in the guided axis at powers > 10 W.

Scaling of the output power of proximity coupled double-clad GMS devices can be achieved by stacking multiple pump sources along both sides of the guide. Initial experimental work on achieving this has already begun; the Yb:YAG device used here has now been scaled to an output power of 12 W by using two 20 W diode bars on either side of the guide [8]. Diffraction limited performance in the guided axis has also been demonstrated at an output power of 15 W from a Tm:YAG device operating at 2 μm [7]. The theory developed here, however, shows that GMS waveguide designs should be capable of diffraction-limited performance in the guided axis at much higher powers. Further power scaling can be achieved by using higher power pump sources (commercially available diode-bars now produce in excess of 50 W) and so pump powers can be easily be scaled to >100W by simply replacing the 20 W diode-bars used to date with these higher power pump sources. Further power scaling could also be achieved by increasing the length of the waveguides to allow the use of more diode-bar pump sources.

The issue of mode control in the unguided axis is important if truly diffraction-limited devices are to be developed. A key consideration for any design is the desire to keep a compact monolithic format and not use any external resonator components. Two techniques that are attractive for combining with proximity-coupled GMS waveguides are a tapered waveguide design or an unstable resonator [9]. A tapered waveguide in the 'unguided axis' of the GMS waveguide would consist of a wide multimode channel section to allow side pumping by diode-bars, connected, via a tapered waveguide section, to a single mode channel for diffraction limited output. Initial investigations of tapered structures in glass [10] and techniques for fabricating these structures in crystals are currently underway [11]. The width of the multimode section of such a design is, however,

restricted by the need to minimise the mode-coupling and hence the losses between this, and the single mode channel section. Consequently, a taper design may only prove effective for proximity coupled, side-pumped waveguides fabricated from strongly absorbing materials such as Nd:$YV0_4$ [9]. The high gain available in a planar waveguide could also allow a hybrid GMS waveguide/unstable resonator approach. The unstable resonator in the unguided axis of the GMS guide could be monolithically integrated by directly polishing, or attaching a curved end-section with a mirror coating to the waveguide. Initial investigations suggest that a M^2 of 2 in the unguided axis could be achieved using such a design [8]. It may also be possible to use a stable resonator if a 'zig-zag' lasing path that sweeps out a broad gain region can be produced, however incorporating this in a monolithic fashion may prove difficult from a fabrication point of view.

The monolithic incorporation of other components, for example, to allow passive Q-switching or intra-cavity frequency doubling is also another important area for future investigation. A passively Q-switched double-clad planar waveguide has recently been demonstrated using a Nd:YAG device with a short direct-bonded Cr^{4+}:YAG section [8], and $LiNbO_3$ waveguides have previously been fabricated by direct bonding [12], so the prospects for developing compact, highly functional sources based on double-clad planar waveguides look good.

In conclusion, the work reported here included the first demonstration of a proximity coupled laser and the design and demonstration of the first double-clad planar waveguide. A highly compact laser system with diffraction-limited performance in the guided axis of the waveguide was realised. Research is now concentrated on mode control in the unguided axis of these devices, the implementation of these techniques, and combining them with a proximity-coupled double-clad design offers a promising route to the development of very compact, diffraction limited, high-power planar waveguide lasers.

6.5 References

[1] M. Svalgaard, *"Optical waveguides and gratings made by UV-photogeneration"*, ECIO, p.333-338 (1999).

[2] D.C. Hanna, A.C. Large, D.P. Shepherd, A.C. Tropper, I. Chartier, B. Ferrand, & D. Pelenc, *"Low Threshold quasi-three-level 946nm laser operation of an epitaxially grown Nd:YAG waveguide"*, Applied Physics Letters, Vol. 63 p.7-9, (1993).

[3] F. Lahoz, E. Daran, X. Zhang, A. Muñoz-Yagüe, R. Cases, & R. Alcala, *"Hetero- and homoepitaxial Nd^{3+} doped LaF_3 thin films grown by molecular beam epitaxy: a spectroscopic study"*, J. of Applied Physics, Vol. 86, p. 3699-3704, (1999).

[4] A. Chardon, E. Daran, T. Bhutta, D.P. Shepherd & A. Munoz-Yague, *"Rare-earth-doped LaF_3 waveguide laser devices"*, MIOMD 2001 Montpellier 2-3 Apr 2001 Y-3, (2001).

[5] S.J.Barrington & R.W.Eason, *"Buried Nd:gadolinium garnet waveguide lasers grown by pulsed laser deposition"*, CLEO/Europe-EQEC Munich 18-22 Jun 2001, p.140, (2001).

[6] C.L. Bonner, T. Bhutta, D.P. Shepherd & A.C. Tropper, *"Double-clad structure and proximity coupling for diode-bar-pumped planar waveguide lasers"*, IEEE J. of Quantum Electronics, Vol. 36, No. 2, p. 236-242, (2000).

[7] J.I. Mackenzie, S.C. Mitchell, R.J. Beach, H.E. Meissner & D.P. Shepherd, *"A 15W diode-side-pumped Tm:YAG waveguide laser at 2μm"*, Electronic Letters, Vol. 37, p. 898-899, (2001)

[8] R.J. Beach, S.C. Mitchell, H.E. Meissner, O.R. Meissner, W.F. Krupke, J.M. McMahon, W.J. Bennett, D.P. Shepherd, *"CW and passively Q-switched cladding-pumped planar waveguide lasers"*, Optics Letters, Vol. 26, No. 12, p. 881-883, (2001).

[9] D.P. Shepherd, S.J. Hettrick, C. Li, J.I. Mackenzie, R.J. Beach, S.C. Mitchell & H.E. Meissner, *"High-power planar dielectric waveguide lasers"*, J. of Physics D: Applied Physics, Vol. 34, p. 2420-2432, (2001)

[10] S.J. Hettrick, J.I. Mackenzie, R.D. Harris, J.S. Wilkinson, A.C. Tropper & D.P. Shepherd, *"Ion-exchanged tapered waveguide laser in neodymium-doped BK7 glass"*, Optics Letters, Vol. 25, No. 19, p. 1433-1435, (2000).

[11] S.J. Hettrick, J.S. Wilkinson & D.P. Shepherd, *"Neodymium and gadolinium diffusion in yttrium vanadate"*, J. of Optical Society of America B, Vol. 19 p. 33-36, (2002).

[12] C.B.E. Gawith, D.P. Shepherd, J.A. Abernethy, D.C. Hanna, G.W. Ross & P.G.R. Smith, *"Second harmonic generation in a direct-bonded periodically-poled-$LiNbO_3$ buried waveguide"*, Optics Letters, Vol. 24, No. 7, p. 481-483, (1999).

Appendix A:

FIVE-LAYER PLANAR WAVEGUIDE MODES

To determine the optical modes of a five-layer planar waveguide we follow the procedure of section 2.2 of chapter 2, however in this case we consider a five-layer rather than three-layer structure as depicted below in figure A1. Once again the symmetry of the structure suggests the modes will either be odd or even with respect to x=0 and so we assume TE solutions of the following form.

$$E_y(x) = E_{yo} \begin{cases} A_1 e^{-\alpha_1 x} & x > D/2 \\ A_2 e^{-\alpha_2 x} + A'_2 e^{\alpha_2 x} & D/2 > x > d/2 \\ \begin{pmatrix} \cos(\kappa x) \\ \sin(\kappa x) \end{pmatrix} & \begin{matrix} even \\ odd \end{matrix} \quad d/2 < x > -d/2 \\ \pm (A_2 e^{\alpha_2 x} + A'_2 e^{-\alpha_2 x}) & -D/2 < x < -d/2 \\ \pm A_1 e^{\alpha_1 x} & x < -D/2 \end{cases} \qquad [A1]$$

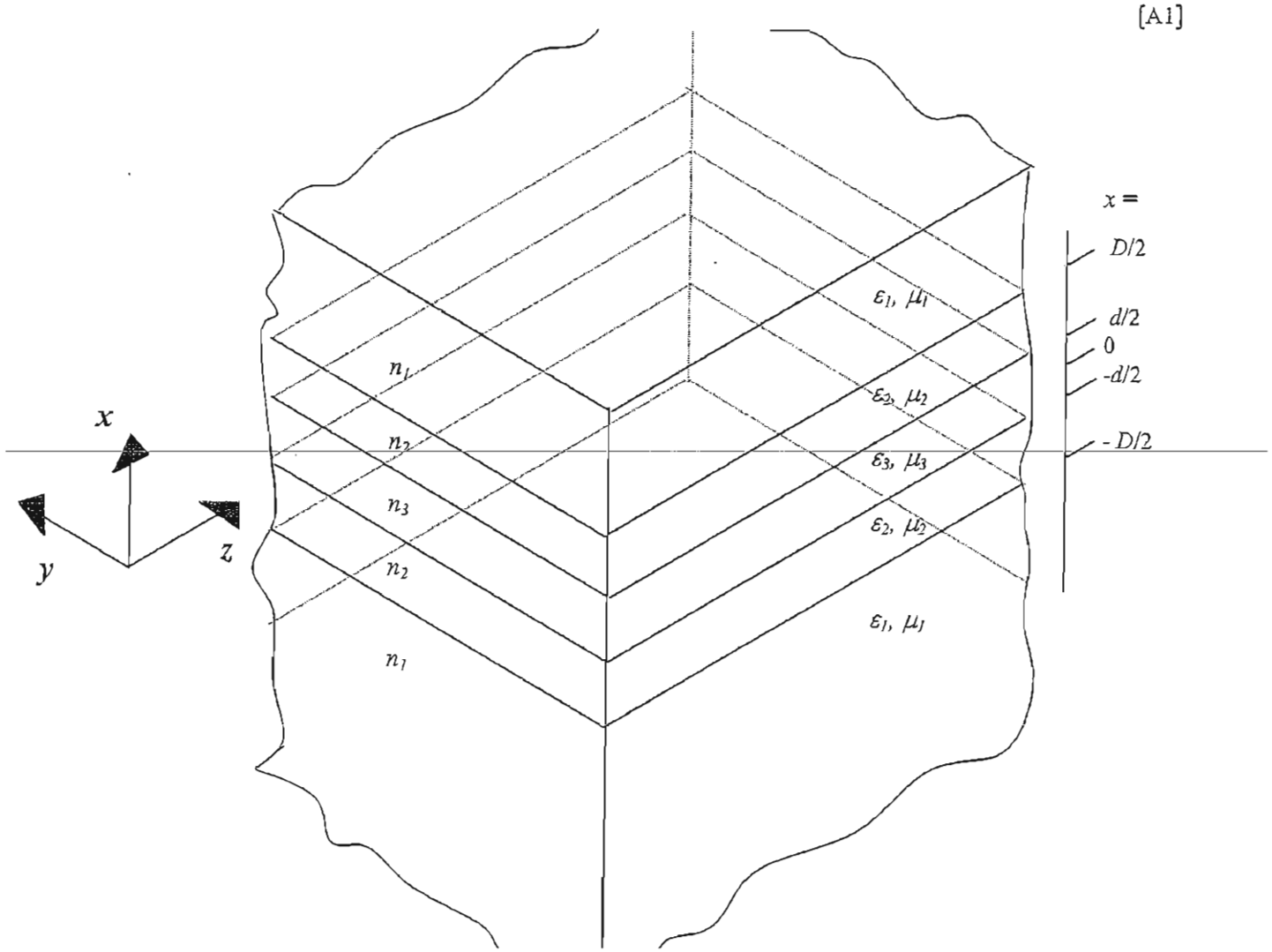

Figure A1 Five-layer planar waveguide structure

E_{yo} is the maximum electric field amplitude, A_1 , A_2 and A'_2 are the relative amplitude coefficients for the outer layers, κ is the transverse wavenumber in the central core region, α_1 is the decay constant for the outer cladding layer and α_2 can either be real or imaginary corresponding to a decaying or oscillatory solution for the region $D/2 > |x| > d/2$. For equation A1 to satisfy the wave equation (equation 2.2.9a of chapter 2) the mode constants have to obey the following relationships.

$$\alpha_1^2 = \beta^2 - \omega^2 \mu_1 \varepsilon_1 \qquad [A2a]$$

$$\alpha_2^2 = \beta^2 - \omega^2 \mu_2 \varepsilon_2 \qquad [A2b]$$

$$\kappa^2 = \omega^2 \mu_3 \varepsilon_3 - \beta^2 \qquad [A2c]$$

Applying the condition that E_y and H_z (equation 2.2.7a) must be continuous across the boundaries $x = D/2$ and $x = d/2$ (or equivalently $x = -D/2$ and $x = -d/2$) gives four simultaneous equations that can be combined to solve for A_1 , A_2 , and A'_2 . This reveals the following expressions for the amplitude co-efficients for the even modes

$$A_1 = \frac{2\left(\frac{\alpha_2}{\alpha_2 + \alpha_1}\right)\cos(\kappa d/2)e^{\alpha_2(d-D)/2}e^{\alpha_1(D/2)}}{1 + \left(\frac{\alpha_2 - \alpha_1}{\alpha_2 + \alpha_1}\right)e^{\alpha_2(d-D)}} \qquad [A3a]$$

$$A_2 = \frac{\cos(\kappa d/2)e^{\alpha_2(d/2)}}{1 + \left(\frac{\alpha_2 - \alpha_1}{\alpha_2 + \alpha_1}\right)e^{\alpha_2(d-D)}} \quad \& \quad A'_2 = \frac{\cos(\kappa d/2)e^{-\alpha_2(d/2)}}{1 + \left(\frac{\alpha_2 + \alpha_1}{\alpha_2 - \alpha_1}\right)e^{\alpha_2(D-d)}} \qquad [A3b \& A3c]$$

And reveals the following expressions for the amplitude co-efficients for the odd modes.

$$A_1 = \frac{2\left(\frac{\alpha_2}{\alpha_2 + \alpha_1}\right)\sin(\kappa d/2)e^{\alpha_2(d-D)/2}e^{\alpha_1(D/2)}}{1 + \left(\frac{\alpha_2 - \alpha_1}{\alpha_2 + \alpha_1}\right)e^{\alpha_2(d-D)}} \qquad [A4a]$$

$$A_2 = \frac{\sin(\kappa d/2)e^{\alpha_2(d/2)}}{1 + \left(\frac{\alpha_2 - \alpha_1}{\alpha_2 + \alpha_1}\right)e^{\alpha_2(d-D)}} \quad \& \quad A'_2 = \frac{\sin(\kappa d/2)e^{-\alpha_2(d/2)}}{1 + \left(\frac{\alpha_2 + \alpha_1}{\alpha_2 - \alpha_1}\right)e^{\alpha_2(D-d)}} \qquad [A4b \& A4c]$$

Considering the boundary conditions at $x=d/2$ again, substituting equations A3a-c and using the relationship $\tanh(u)= [e^{u}-e^{-u}]/[e^{u}+e^{-u}]$ gives the following guidance condition for even modes.

$$\tan(\kappa d/2)=\left(\frac{\alpha_1\alpha_2+\alpha_1^2\tanh[\alpha_2(D-d)/2]}{\kappa\alpha_2+\kappa\alpha_1\tanh[\alpha_2(D-d)/2]}\right) \quad \textit{TE even mode condition} \qquad [A5]$$

Doing the same for equations A4a-c gives the following guidance condition for odd modes

$$\cot(\kappa d/2)=\left(\frac{\alpha_1\alpha_2+\alpha_1^2\tanh[\alpha_2(D-d)/2]}{\kappa\alpha_2+\kappa\alpha_1\tanh[\alpha_2(D-d)/2]}\right) \quad \textit{TE odd mode condition} \qquad [A6]$$

Equations A5 and A6 can now be combined with equations A2a-c and solved to determine the mode characteristics of the TE modes in a five-layer planar waveguide (the TM modes can be determined by duality as in chapter 2).

Appendix B:

PUBLICATIONS

B1 Publications arising from work reported in this thesis

Refereed journal publications

E. Daran, D.P. Shepherd, **T. Bhutta** & C. Serrano, *"Laser operation of a Nd:LaF_3 thin film grown by molecular-beam epitaxy"*, Electronic Letters, Vol. 35, p. 398-400, (1999).

C.B.E. Gawith, **T. Bhutta**, D.P. Shepherd, P. Hua, J. Wang, G.W. Ross & P.G.R. Smith, *"Buried laser waveguides in neodymium-doped BK-7 by K^+-Na^+ ion-exchange across a direct-bonded interface"*, Applied Physics Letters, Vol. 75, No 24, p.3757-3759, (1999).

C.L. Bonner, **T. Bhutta**, D.P. Shepherd & A.C. Tropper, *"Double-clad structures and proximity coupling for diode-bar-pumped planar waveguide lasers"*, IEEE Journal of Quantum Electronics, Vol. 36, No. 2, p. 236-242, (2000).

S.J. Barrington, **T. Bhutta**, D.P. Shepherd & R.W. Eason, *"The effect of particulate density on performance of Nd:$Gd_3Ga_5O_{12}$ waveguide lasers grown by pulsed laser deposition"*, Optics Communications, Vol. 185, p. 145-152, (2000).

T. Bhutta, A.M. Chardon, D.P. Shepherd, E. Daran, C. Serrano & A. Munoz-Yague, *"Low phonon energy Nd:LaF_3 channel waveguide lasers fabricated by molecular beam epitaxy"*, IEEE Journal of Quantum Electronics, Vol. 37, No. 11, p. 1469-1477, (2001).

T. Bhutta, J.I. Mackenzie, D.P. Shepherd & R.J. Beach, *"Spatial dopant profiles for transverse-mode selection in multi-mode waveguides"*, Journal of the Optical Society of America B, Vol. 19, p. 1539-1543, (2002).

C.B.E. Gawith, A. Fu, **T. Bhutta**, P. Hua, D.P. Shepherd, E.R. Taylor, P.G.R. Smith, D. Milanese & M. Ferraris, *"Direct-UV-written buried channel waveguide lasers in direct-bonded intersubstrate ion-exchanged neodymium-doped germano-borosilicate glass"*, Applied Physics Letters, Vol. 81, No. 19, p. 3522-3524, (2002).

Conference publications

T. Bhutta, C.L. Bonner, D.P. Shepherd, A.C. Tropper, D.C. Hanna, *"Diode-bar-pumped planar waveguide lasers: double-clad structures and proximity coupling"*, QE-14 Manchester 6-9 Sep 1999 Paper 8-1 p. 69, (1999).

E. Daran, D.P. Shepherd, **T. Bhutta** & F. Lahoz, *"Nd:LaF_3 waveguide laser fabricated by molecular beam epitaxy"*,, CLEO '99 Baltimore 23-28 May 1999 CThD4, (1999).

C.L. Bonner, **T. Bhutta**, D.P. Shepherd, A.C. Tropper, D.C. Hanna & H.E. Meissner, *"Proximity-coupled, diode-bar-pumped, waveguide laser"*, CLEO '99 Baltimore 23-28 May 1999 CThD6, (1999).

C.B.E. Gawith, **T.Bhutta**, D.P. Shepherd, P. Hua, G.W. Ross, P.G.R. Smith & J. Wang, *"Ion-exchange across a direct-bonded interface"*, CLEO 2000 San Francisco 7-12 May 2000 CWK37, (2000).

T. Bhutta, D.P. Shepherd, C. Serrano & E. Daran, *"Nd:LaF_3 channel waveguide lasers fabricated by molecular beam epitaxy"*, CLEO/Europe Nice 10-15 Sep 2000 CTuM8, (2000).

A. Chardon, E. Daran, **T. Bhutta**, D.P. Shepherd & A. Munoz-Yague, *"Rare-earth-doped LaF_3 waveguide laser devices"*, MIOMD 2001 Montpellier 2-3 Apr 2001 Y-3, (2001).

C.B.E. Gawith, A. Fu, **T. Bhutta**, D.P. Shepherd, E.R. Taylor, P.G.R. Smith, D. Milanese & M.Ferraris, *"Single-mode UV-written buried channel waveguide lasers in direct-bonded neodymium-doped SGBN"*, CLEO 2002 Long Beach, California 19-24 May 2002 CTuK53, (2002).

B2 Other publications

T. Bhutta, R.P. Salathe, D.P. Shepherd, R.W. Eason & M. Pollnau, *"Ti-sapphire planar waveguide coherent broadband emitter"*, CLEO 2001 Baltimore 6-11 May 2001 CFH5, (2001).

M. Pollnau, R.P. Salathe, **T. Bhutta**, D.P. Shepherd & R.W. Eason, *"Continuous-wave broadband emitter based on a transition-metal-ion doped waveguide"*, Optics Letters, Vol. 26, p. 283-285, (2001).

ACKNOWLEDGEMENTS